eXPRESS Polymer Letters Vol.4, No.8 (2010) 455
Available online at www.expresspolymlett.com
DOI: 10.3144/expresspolymlett.2010.57

Preface

E. C. Muniz[1], *E. F. Lucas*[2*]

[1]Department of Chemistry, Maringá State University, Av. Colombo, 5790 - 87020900, Maringá, Brazil
[2]Institute of Macromolecules, Federal University of Rio de Janeiro, Av. Horacio Macedo, 2030 - 21941598, Rio de Janeiro, Brazil

Dear Readers,

You are reading the Special Issue of ***eXPRESS Polymer Letters*** devoted to 10th Brazilian Polymer Congress (10th CBPol). The CBPol has been occurring since 1991, at every 2 years, as a regular meeting of Brazilian community that has been attracting people from other countries. The 10th Brazilian Polymer Congress was held in Foz do Iguassu, Brazil, in October 13–17, 2009 and was attended by 1,026 professors, researchers, students, and professionals. The subjects were distributed in parallel sessions comprising: (1) Composites and nanocomposites; (2) Degradation and recycling; (3) Biopolymers; (4) Structure and properties; (5) Characterization techniques and standardization; (6) Polymeric biomaterials; (7) Synthesis and process of polymerization; (8) Polymer blends; (9) Technological development; (10) Special applications; and (11) Technical lectures. A total of 9 invited lectures, 22 key-notes, 122 oral presentations and 721 posters were presented by participants from 15 countries. During the Forum, about 260 participants have attended short courses on the following subjects: (1) Experimental design and optimization applied to polymeric materials; (2) Premature failure on polymers; (3) Composites of polymers with vegetal fibers; (4) Emulsion polymerization. The conference was organized by The Brazilian Polymer Association (ABPol). Professor/researchers from academy and industries constituted the organizing committee.

The invited lectures covered: the future of additive for plastic reinforcing; the effect of crystallizing process on morphology and polymers properties; synergistic effect on epoxy nanocomposites by incorporation of inorganic nanoparticles; self assemblies on glyco-hybrid block copolymers; characterization of MIP by solid state and suspended state NMR; hydrogels for protein delivery and tissue engineering; interactions in macromolecule-metal complexes; and an overview on encapsulation of inorganic particles. As the winner of ABPol – Prof. Eloisa Mano award, Prof. M. A.-De Paoli told about his contribution to the polymer field in the last 30 years.

To celebrate the 10th Edition of CBPol, representative articles which have been presented during the Conference are being published in this Special Issue because of high accessibility of ***eXPRESS Polymer Letters*** by several readers and by the great acceptance of this journal by the international scientific community. On behalf of the Organizing Committee of 10th CBPol we would like to thank the sponsors and all participants for their presence and support for the success of the 10th CBPol.

In 2011, the Brazilian Polymer Association will be organizing the 11st Edition of the Brazilian Polymer Congress. The conference will be held in Sao Paulo (province), in October, and we would like to invite all ***eXPRESS Polymer Letters*** readers to take part in it. More details will be given at www.abpol.com.br.

Sincerely yours,

Prof. E. C. Muniz and E. F. Lucas

*Corresponding author, e-mail: elucas@ima.ufrj.br

eXPRESS Polymer Letters Vol.4, No.8 (2010) 456–464
Available online at www.expresspolymlett.com
DOI: 10.3144/expresspolymlett.2010.58

Effect of the preparation method on the drug loading of alginate-chitosan microspheres

F. O. M. S. Abreu[1*], *M. M. C. Forte*[2] , *T. B. L. Kist*[3] *L. P. Honaiser*[3]

[1]Laboratory of Biopolymers/ Analytical and Physical-Chemistry Department, Federal University of Ceará-UFC, Fortaleza-CE, Brazil
[2]Laboratory of Polymeric Materials/Engineering School, PO Box 15.010, Federal University of Rio Grande do Sul (UFRGS), Porto Alegre-RS, Brazil
[3]Laboratory of Analytical Methods/Bioscience Institute, Federal University of Rio Grande do Sul-UFRGS, Porto Alegre-RS, Brazil

Received 13 January 2010; accepted in revised form 4 March 2010

Abstract. Alginate-chitosan (ALG-CHI) microspheres obtained by polyelectrolyte complexation are pH-sensitive, bio-compatible and adhesive, and are excellent candidates for the delivery of drugs, proteins and peptides in the human body. A wide variety of methods for the production of these polymeric complexes has been provided. The water-in-oil emulsion is a complex production method, but generally enhances the control of particle size and particle size distribution of the microspheres, extremely necessary for obtaining repeatable controlled release behavior. In this work, a novel and facile water-in-oil emulsion method for the ALG-CHI polyelectrolyte complexes is discussed. The method proposed produced ALG-CHI microspheres with improved morphology and enhanced drug loading in comparison with the aqueous medium method. The drug loading in the water-in-oil emulsion was over 30% higher than in the aqueous medium, an indication that the new method proposed the common drug leaching during the microspheres' preparation is avoided, being an interesting alternative to encapsulate drugs of hydrophilic nature.

Keywords: *biodegradable polymers, polymer gels, microspheres, chitosan, drug loading*

1. Introduction

Alginate-chitosan hydrogels (ALG-CHI) have been proposed as drug delivery system in the past decade, due to their attractive combination of pH-sensitivity, bio-compatibility and adhesiveness, requiring relative mild gelation conditions for the network formation [1]. A great deal of processes was developed for these hydrogels' production in the last few years [2]. One of the limitations of these hydrogels is the drug leaching during their preparation [3] which can be reduced by controlling the reactions conditions [4–7]. In a previous work [8] several ALG-CHI formulations were statistically investigated in aqueous medium in order to modulate and control the polyelectrolyte complexation and subsequently the hydrogel properties. In another report, the influence of the introduction of some carboxylic groups on chitosan was studied and the effects on the formation of polymer complexes with ALG at pH 4 and 6 [9]. In both reports, microspheres were obtained with high yield, low particle size and desirable swelling ability required in the intestinal media for promising drug release. Emulsion methods have been proposed in order to increase the encapsulation efficiency of drugs using low water solubility polymers [10–12].

Gel bead system based on calcium alginate and chitosan were successfully produced in oil-in-water

*Corresponding author, e-mail: flaviamonteiroabreu@gmail.com

emulsion for oral delivery of allyl isothiocyanate [10]. Hydrogel microspheres of chitosan crosslinked with glutaraldehyde with uniform-size have been produced by a membrane emulsification technique [11], and a water-in-oil (W/O) emulsion coalescence technique was proposed for the production of CHI particles using vegetable oil [12]. Both methods generated microspheres with enhanced control of particle size and particle size distribution, which are important for repeatable controlled release behavior [11, 12]. Despite some different water-in-oil methods have been used to produce microspheres [13–16], they have not been utilized for the preparation of ALG-CHI microspheres to enhance the encapsulation of water-soluble drugs.

Ionic and covalent crosslinkers can be added to the ALG-CHI system for improving the properties. Calcium chloride is frequently used as an ionic crosslinker in ALG-CHI systems [7–9, 11] causing a reduction in the hydrogel porosity [17]. Among the covalent crosslinkers, there are some reports for chitosan nanoparticles crosslinked with glutaraldeyde [13, 18] and genipin [19, 20]. Genipin is a natural covalent crosslinker that presents very low toxicity in comparison with conventional crosslinkers and can present promising results in the reinforcement of ALG-CHI based microspheres [20].

In this work, a novel W/O emulsion method was designed for ALG-CHI microspheres' preparation using two types of crosslinker, calcium ions and genipin, and two types of surfactant agents with a view to increase the drug loading of some model drugs. The properties of the ALG-CHI particles produced in emulsion by different methods were compared with those obtained by the aqueous method.

2. Experimental

2.1. Materials

Alginic acid sodium salt (~250 mPa·s viscosity at 25°C 1 wt%, 64.4 kDa) and polyvinyl pirrolidone (40 kDa) was purchased from Sigma. Low molecular weight Chitosan (90% deacetylated, 6.68 kDa) was purchased from Aldrich. Calcium chloride and polyvinyl alcohol (86.5–89.5% hydrolyzed, 30–70 kDa) were purchased from Synth. Genipin was purchased from Challenge Bioproducts. Fluorescein salt was supplied by Synth, lisinopril and fluorescein isothiocianate were supplied by Sigma. All reagents were analytical grades and were used as received.

2.2. Microspheres preparation

ALG-CHI microspheres were produced in W/O emulsion, testing two types of surfactant and two types of crosslinker, resulting in four different formulations in emulsion. Also ALG-CHI microspheres were produced in aqueous medium, as described in earlier work [8], for comparison of properties. Polymer complexes were prepared using appropriate proportions, in order to obtain hydrogels with polymer ratio ALG:CHI = 35:65, condition previously optimized in previous articles [8, 9]. The model drugs were added using a mass ratio Polymer:Drug of 5:1, condition optimized prior the design. Six formulations were produced in triplicate, the conditions are shown in Table 1.

Aqueous solution of ALG (1% w/v) were prepared and diluted to a final concentration of 0.2% w/v using distilled water. CHI solution (1% w/v) were dissolved in an acetic acid solution with pH = 3, and further diluted to (0.2% w/v) with distilled water. ALG-CHI–Ca^{+2} microspheres were prepared by placing the solution of CHI 0.2% and ALG 0.2% in separate tubes and adding the 2 mM $CaCl_2$ solution into the tube with CHI solution and homogenized. The surfactant powder was added in each tube in a 1.5% w/v concentration and homogenized in an ultrasonic bath for 25 min. Both tubes were carefully added to a vessel containing mineral oil in a volume ratio 6:1 mineral oil: aqueous phase. The mixture was vigorously sonicated with an ultrasonic probe for 3 min producing a stable emulsion, and then replaced in the ultrasonic bath for additional 20 min. The emulsion was centrifuged at 3500 rpm for 30 min for aqueous and oil-phase

Table 1. Formulations used for production of ALG-CHI microparticles in W/O emulsion and aqueous method

Formulations	Preparation method	Surfactant type	Crosslinker type
1-AQ/Ca	Aqueous	–	$CaCl_2$
2-AQ/gen	Aqueous	–	Genipin
3-EM/PVA/Ca	Emulsion	PVA	$CaCl_2$
4-EM/PVA/Gen	Emulsion	PVA	Genipin
5-EM/PVP/Ca	Emulsion	PVP	$CaCl_2$
6-EM/PVP/Gen	Emulsion	PVP	Genipin

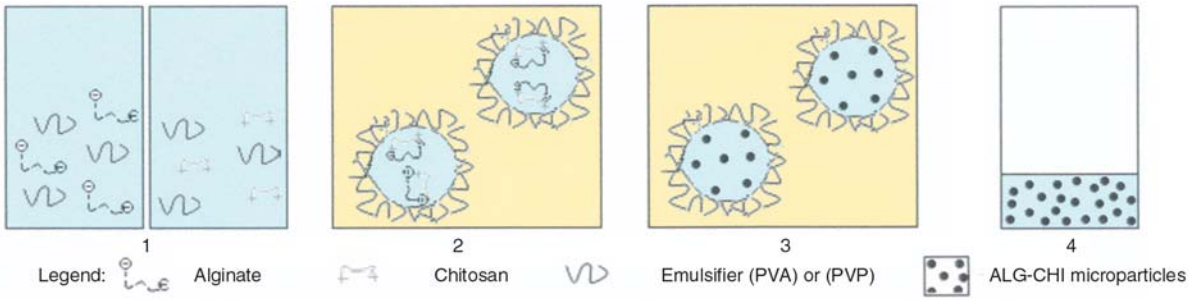

Figure 1. Schematic representation of ALG-CHI particles preparation by W/O emulsion method. Step 1: Aqueous solution having ALG, CHI and surfactant; Step 2: Stable water-in-oil emulsion; Step 3: ALG-CHI particles in the water-in-oil emulsion micelles; Step 4: ALG-CHI particles separated in the aqueous phase.

separation, than the aqueous-phase was again centrifuged and the solid obtained was lyophilized. The preparation of the microspheres ALG-CHI-genipin was similar; the genipin solution (0.1% w/w) was added in the tube containing ALG, and there was no addition of $CaCl_2$ in the system. ALG-CHI microspheres loaded with the models drugs fluorescein or lisinopril labeled with FITC were prepared by adding the model drugs in the tube containing the CHI solution and homogenized. Figure 1 shows a schematic representation of the components in all steps of the ALG-CHI nanoparticles preparation by the water-in-oil method.

2.3. Microspheres characterization

Hydrogel samples were dried and then sputter-coated with gold for Scanning Electron Microscope (SEM) characterization in a Jeol JSM 5800 microscope, using an acceleration voltage of 5 kV. The morphology was investigated through Fluorescence Optical microscope (OM) (Leitz Wetzlar). The loading and the encapsulation efficiency were determined by UV/VIS spectroscopy, at 489 and 499 nm, in a MICRONAL-Brazil spectrometer (model B582) as following: a 10 mg sample was crushed in ethanol and its concentration was calculated using a calibration curve obtained from samples of pure fluorescein at 489 nm and lisinopril labeled with fluorescein isothiocianate (FITC) at 499 nm at certain concentration range. All analysis was replicated twice.

The encapsulation efficiency (*EE*) was evaluated for fluorescein as model drug and for lisinopril labeled with FITC as shown by Equation (1):

$$\%EE = \frac{M}{M_0} \cdot 100 \quad (1)$$

where M is the amount of drug in loaded sample, as determined from the calibration curve and M_0 is the initial drug amount added to the complex.

3. Results and discussion

ALG-CHI microspheres were prepared from 0.2 wt% polymer solution having the polymer mass ratio ALG/CHI = 35/65. These conditions were chosen due to good particle stability and properties reported previously [8, 9], where hydrogels presented higher yield and lower swelling degree. In a previous study, it was seen that CHI based microspheres prepared at aqueous medium showed low encapsulation efficiency of hydrophilic drugs (unpublished results). This could be related to the drug highly hydrophilic character, which present stronger interaction between drug-solvent (water) than the electrostatic interactions between drug-microspheres. In this work, microspheres with controlled morphology were produced by emulsion method and by aqueous method, using two types of crosslinker and surfactant, focusing in differences in the morphology and drug distribution pattern, aiming at encapsulation efficiency optimization.

3.1. Morphology

The morphology of the ALG-CHI microspheres was observed through SEM, as shown in Figure 2. The ALG-CHI hydrogel particles showed spherical shape and the average particle size and particles size distribution varied according to the preparation method, in aqueous medium or W/O emulsion, and to the crosslinker type, genipin or $CaCl_2$. In general, there was an increase in the regularity of the particles shape when genipin was used as crosslinker agent, as revealed by the SEM micrographs Fig-

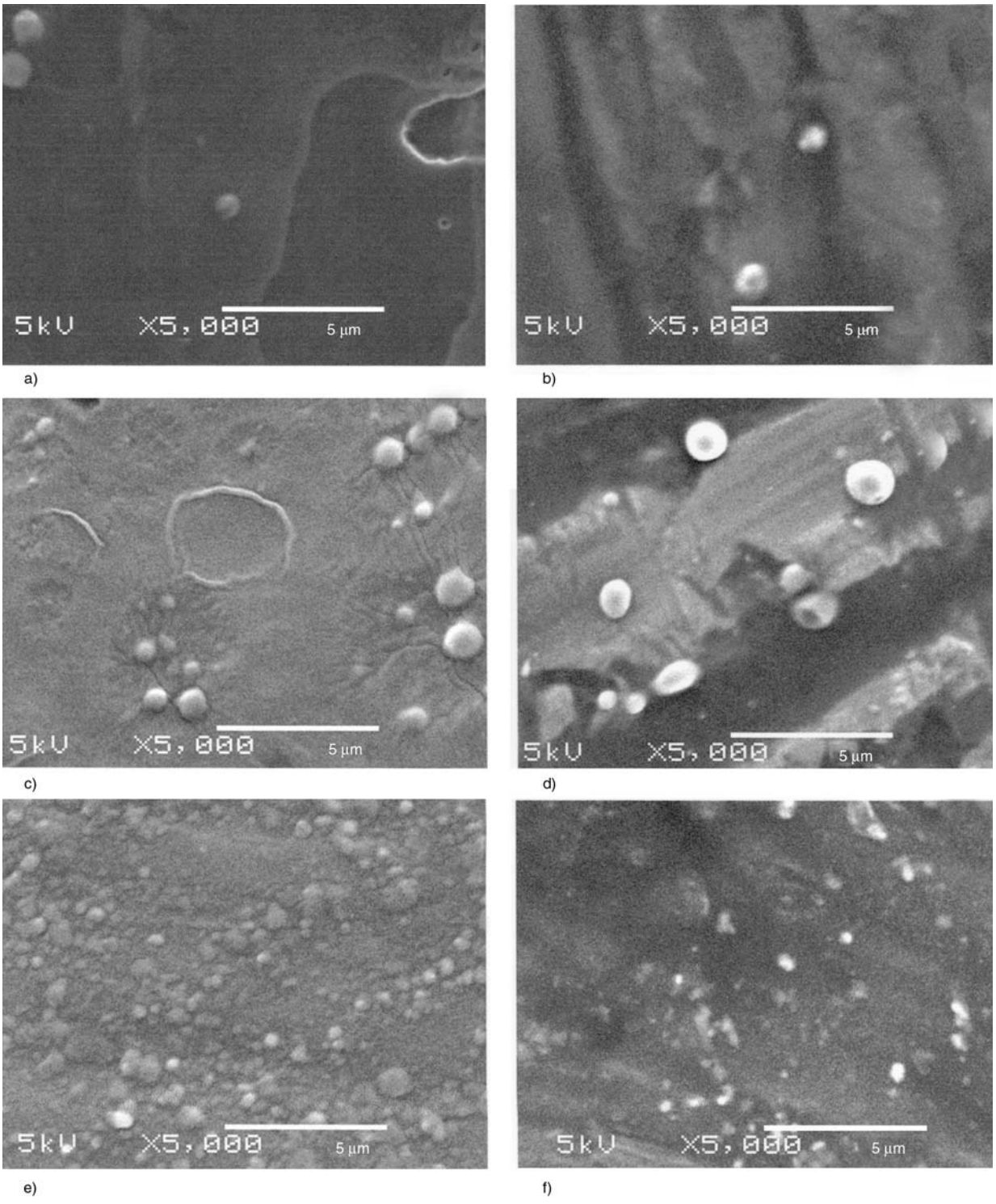

Figure 2. SEM micrograph images of ALG-CHI microparticles obtained using $CaCl_2$ as croslinker: by aqueous method with $CaCl_2$ (a) and with genipin (b), and by W/O emulsion method using PVA with genipin (c) and with $CaCl_2$ (d) and using PVP with Genipin (e) and with $CaCl_2$ (f)

ure 2a, 2c and 2e. ALG-CHI particles produced in W/O emulsion with PVA using both crosslinker agents presented a more spherical shape and regular structure, revealed by the SEM micrographs Figure 2c and 2d.

Figure 3 shows OM micrographs of ALG-CHI microspheres obtained by aqueous and emulsion method. Microspheres produced through the former method were more irregular in shape and there was a tendency to form agglomerates (Figure 3a

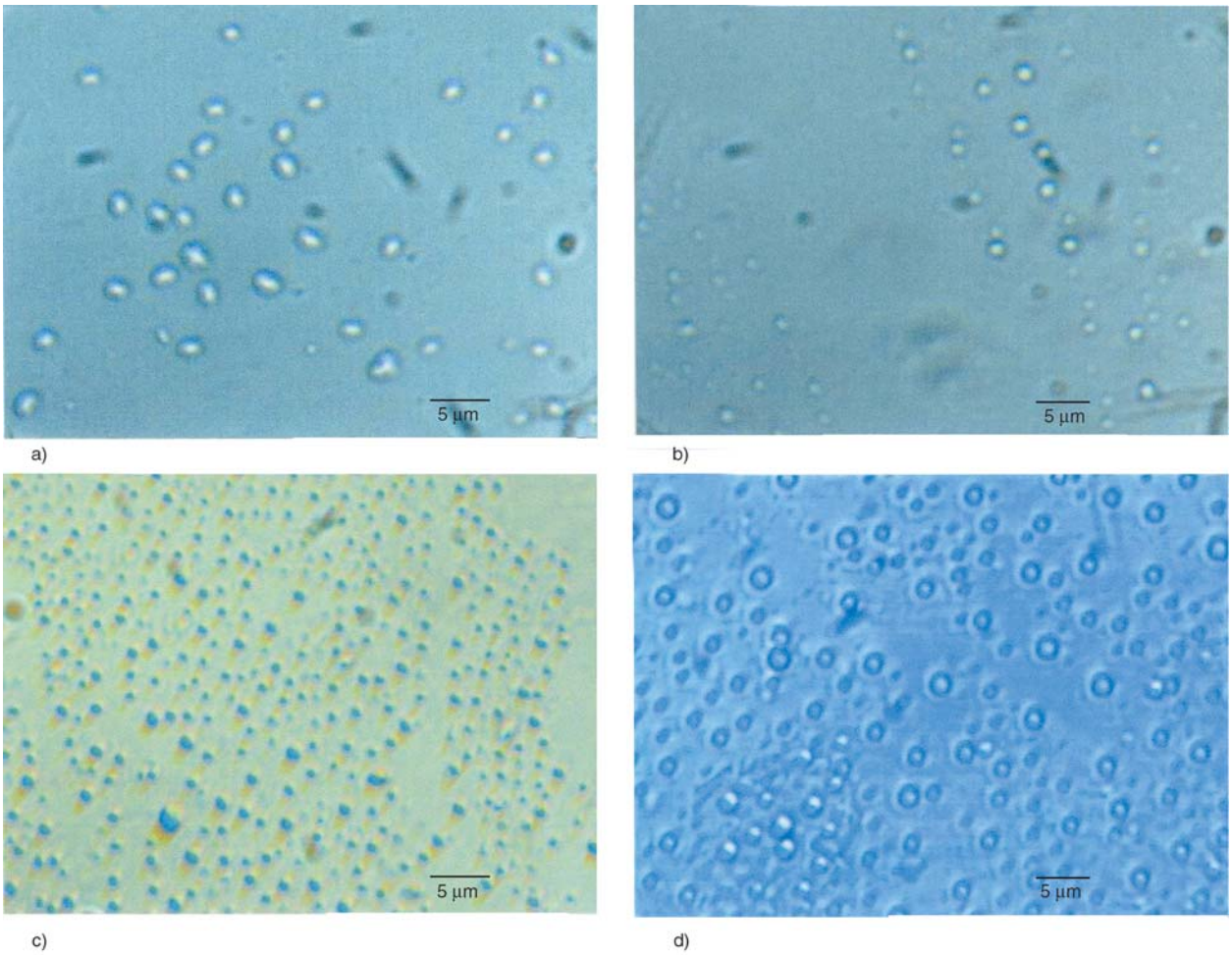

Figure 3. MO micrograph images of ALG-CHI microparticles obtained in aqueous medium with genipin (a) and with $CaCl_2$ (b), and by W/O emulsion method using PVA with genipin (c) and PVP with $CaCl_2$ (d)

and 3b). The particle agglomeration in the aqueous method is possibly caused by the formation of inter-aggregate complexes between the ALG carboxylic chains in the hydrogel induced by Ca^{+2}. This is in accordance with Zhu *et al.* [21] results, in which the agglomeration effect was observed for carboxymethyl-chitosan aqueous solutions in presence of metallic ions. This agglomeration that occurs simply by electrostatic interactions between the ions and the polymers may lead to the formation of microparticles with irregular morphology and higher polydispersity. On the other hand, microspheres prepared through the emulsion method presented uniform size with self-avoiding particles (Figure 3c and 3d), being potentially more adequate for drug delivery. The emulsion method, due to the ALG-CHI particles arrangement inside the droplets, may prevent the formation of inter-aggregated complex caused by electrostatic interactions. Studies regarding the preparation of microparticles by emulsion were conducted by others; Kofuji *et al.* [12] reported chitosan microparticles chelated by metallic produced by emulsion technique with irregular morphology and rough surface; on the other hand, Wang *et al.* [13] obtained chitosan microparticles with excellent size control and smooth surface by a innovative membrane emulsification technique. Table 2 shows the average particle size of ALG-CHI microspheres. The average particle size of the ALG-CHI microspheres corresponds to the average diameter measured on fifty

Table 2. Encapsulation efficiency and average particle size of ALG-CHI microparticles obtained in different formulations

Formulations	Encapsulation efficiency [%]		Particle size [µm]
	Fluorescein	Lisinopril	
1-AQ/Ca	38±15	45±12	1.3±0.6
2-AQ/gen	50±12	60±9	1.6±0.9
3-EM/PVA/Ca	83±10	80±8	0.5±0.3
4-EM/PVA/Gen	77±8	86±7	0.8±1
5-EM/PVP/Ca	78±4	74±9	0.7±0.3
6-EM/PVP/Gen	29±16	37±10	0.6±0.2

particles from each batch. It can be seen from the average diameter values that the particles size varied according to the preparation method and composition used. Microparticles produced by the W/O emulsion method were smaller having narrower particle size distribution than those produced by the aqueous method. Chitosan microparticles chelated by a metal ion obtained by emulsion coalescence technique in vegetal oil presented uniform size with low polidispersity [12]. Some data on emulsion methods report particles having broad size range, due to the use of high-speed blenders and high pressure homogenizers which involves mechanical shear force to reduce the size of the emulsion droplets and forms polydisperse particles [15]. However, the formulations produced by emulsion method with PVP as surfactant presented lower polydispersity than those produced with PVA and equivalent polydispersity to those produced by aqueous medium method. PVP perhaps exhibits better stabilizing effect, where the adsorption of the polymer in the droplets surface avoids the coagulation and consequently the agglomeration of droplets. On the other hand, PVA presents higher molecular weight than PVP (30–70 and 40 kDa, respectively) and higher affinity to the ALG-CHI polymers. In this sense, different segments of a single PVA macromolecule may absorb simultaneously on two or more droplets, leading to an attractive force which results in droplets aggregation, with consequently higher particle size and high polidispersity.

3.2. Encapsulation efficiency

Using 2% of loading of the drug models, the encapsulation efficiency was determined using a calibration curve in a UV-visible spectrometer, as described earlier. The calibration curves for fluorescein and for lisinopril labeled with FITC are in Figure 4. The correlation between absorbance and concentration for fluorescein and lisinopril are given respectively by the Equations (2) and (3):

$$y = 0.035x - 0.004, \qquad R^2 = 0.998 \tag{2}$$

$$y = 0.0204x - 0.0715, \qquad R^2 = 0.992 \tag{3}$$

The curves presented excellent linearity for low and high drug concentration, with a correlation factor R^2 >0.99. The model drug's concentrations were

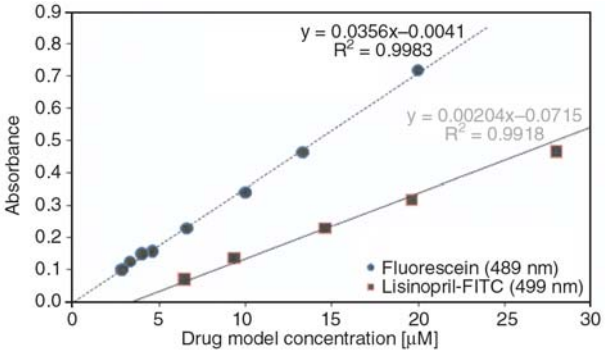

Figure 4. Calibration curve for fluorescein and lisionpril labeled with Isothiocianate

calculated using Equations (2) and (3) and the encapsulation efficiency values for each system produced were calculated using Equation (1), as shown in Table 2. Comparing the encapsulation efficiency (*EE*) values is observed that particles produced in aqueous medium presented relatively low *EE* in comparison with the majority of the *EE* values of the microspheres obtained by W/O emulsion method, which successfully entrapped over 70% of lisinopril and fluorescein. The *EE* of lisinopril-FITC was higher or equivalent than fluorescein, probably due to the lower hydrophilic character which may cause lower drug leaching. Genipin was more effective as crosslinker than Ca^{+2} for ALG-CHI microparticles loaded with lisinopril produced by aqueous method and also by W/O emulsion with PVA. In particular, there was a notable increase of 15% in the encapsulation efficiency of lisinopril when genipin was used instead of $CaCl_2$ in the hydrogel preparation through the aqueous method. As previously reported [19], controlled release rates of indomethacin from ALG-CHI particles were achieved by increasing the genipin content in the hydrogel due to a higher crosslinking density. In fact, the genipin content can be manipulated in order to control the chitosan crosslink density [20]. On the other hand, when $CaCl_2$ was used as crosslinking agent using the W/O emulsion method the surfactant type did not have strong influence in the efficiency of both model drugs, and the formulations presented high *EE* values for both drugs. An analysis of the surfactant effect in the *EE* shows that it with PVA it was achieved the highest values of encapsulation efficiency for both drugs and using both types of crosslinker. Despite the fact that PVA has formed particles with higher polidispersity, depending

upon the application of the delivery system, it might be desirable to achieve high *EE* values with a decrease of the control of the size.

Figure 5 shows the lisinopril-FITC encapsulation and distribution within the particles investigated by Fluorescence Optical microcopy (FOM). It is evidenced in the lisinopril-FITC-ALG-CHI microspheres micrographs that the distribution pattern varied according to the preparation method and crosslinker type. In aqueous medium, the drug dispersion was favored by replacing $CaCl_2$ with genipin (Figure 5a and 5b, respectively) also corroborated by the *EE* values. In Figure 5c and 5d the homogeneous dispersion of the drug is shown inside the ALG-CHI microspheres produced through the W/O emulsion method. Particularly, the surfactant seems to affect the encapsulation efficiency of ALG-CHI particles crosslinked with genipin. The reported mechanism for genipin-chitosan crosslinking reaction is a nucleophilic attack of chitosan amino groups in the dihydropiran ring of genipin [20]. A high loss of hydrogen ions from protonated amino groups to the carboxylic groups favors the nucleophilicity of amino groups, which in turn may increase the CHI crosslinking density [20]. In the case of the microspheres here reported, the residual carboxylic groups (25%) in the PVA molecules may favor the chitosan deprotonation, which facilitates the amino nucleophilic attack, increases the crosslinking density and consequently the encapsu-

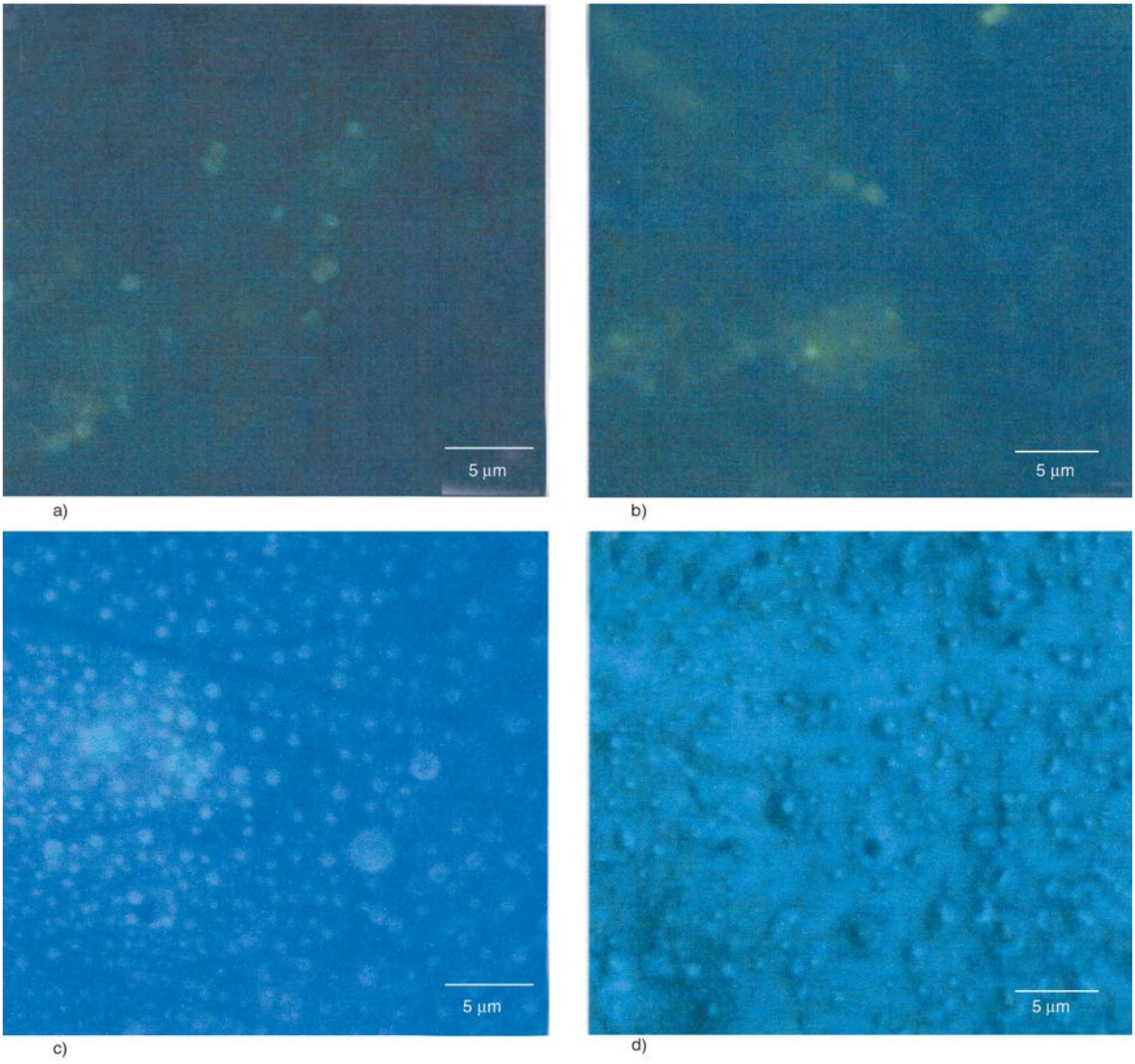

Figure 5. FOM micrograph images for drug distribution pattern. ALG-CHI microparticles obtained in aqueous medium with $CaCl_2$ (a) and with genipin (b), and by W/O emulsion method using PVA with $CaCl_2$ (c) and PVP with genipin (c)

lation efficiency (85% for the system EM/PVA/Gen loaded with lisinopril). On the other hand, in the case of the ionic crosslinker (calcium chloride), PVP and PVA were a good surfactant for the W/O system and the average *EE* was around 75%.

In summary, ALG-CHI microspheres produced in W/O emulsion with PVA as surfactant using both types of crosslinker presented highly spherical particles with acceptable size distribution for a variety of delivery systems. On the other hand, the emulsion system ALG-CHI–Ca^{+2} using PVP as crosslinker presented spherical particles with lower polidispersity, desirable for some specific applications. In addition, those particles formed self-avoided domains, avoiding aggregation. Moreover, these particles presented higher encapsulation efficiency reaching values up to 75% than those produced in aqueous medium.

4. Conclusions

Different methods for production of ALG-CHI microspheres were tested in order to increase the encapsulation efficiency and optimize the morphology. Regarding the crosslinker type, genipin increased significantly the *EE* of microspheres produced in aqueous medium. It was observed that the emulsion method in general was more efficient to encapsulate the model drugs than the aqueous method. Moreover, ALG-CHI microspheres produced in emulsion using PVA as surfactant presented highly spherical particles with acceptable size distribution, and the emulsion system ALG-CHI–Ca^{+2} using PVP as crosslinker presented lower particle size with higher size control, desirable for some specific applications. Those particles formed self-avoided domains, avoiding aggregation and higher encapsulation efficiency reaching values up to 75%, indicating that the emulsion method is a promising route to encapsulate hydrophilic drugs.

Acknowledgements

The authors thank the Governmental Agencies CNPq and CAPES for the financial support to this work and to Dr. Hamid Elassari (France) for the exchange of ideas.

References

[1] Berger J., Reist M., Mayer J. M., Felt O., Peppas N. A., Gurny R.: Structure and interactions in covalently and ionically crosslinked chitosan hydrogels for biomedical applications. European Journal of Pharmaceutics and Biopharmaceutics, **57**, 19–34 (2004). DOI: 10.1016/S0939-6411(03)00161-9

[2] Sinha V. R., Singla A. K., Wadhawan S., Kaushik R., Kumria R., Bansal K., Dhawan S.: Chitosan microspheres as a potential carrier for drugs. International Journal of Pharmaceutics, **274**, 1–33 (2004). DOI: 10.1016/j.ijpharm.2003.12.026

[3] George M., Abraham T. E.: Polyionic hydrocolloids for the intestinal delivery of protein drugs: Alginate and chitosan- A review. Journal of Controlled Release, **114**, 1–14 (2006). DOI: 10.1016/j.jconrel.2006.04.017

[4] De S., Robinson D.: Polymer relationships during preparation of chitosan-alginate and poly-l-lysine-alginate nanospheres. Journal of Controlled Release, **89**, 101–112 (2003). DOI: 10.1016/S0168-3659(03)00098-1

[5] Ribeiro A. J., Silva C., Ferreira D., Veiga A.: Chitosan-reinforced alginate microspheres obtained through the emulsification/internal gelation technique. European Journal of Pharmaceutical Science, **25**, 31–40 (2005). DOI: 10.1016/j.ejps.2005.01.016

[6] Wittaya-areekul S., Kruenate J., Prahsarn E. C.: Preparation and in vitro evaluation of mucoadhesive properties of alginate/chitosan microparticles containing prednisolone. International Journal of Pharmaceutics, **312**, 113–118 (2006). DOI: 10.1016/j.ijpharm.2006.01.003

[7] Alsarra I. A., Betigeri S. S., Zhang H., Evans B. A., Neau S. H.: Molecular weight and degree of deacetylation effects on lipase-loaded chitosan bead characteristics. Biomaterials, **23**, 3637–3644 (2002). DOI: 10.1016/S0142-9612(02)00096-0

[8] Abreu F. O. M. S., Bianchini C., Forte M. M. C., Kist T. B. L.: Influence of the composition and preparation method on the morphology and swelling behavior of alginate-chitosan hydrogels. Carbohydrate Polymers, **74**, 283–289 (2008). DOI: 10.1016/j.carbpol.2008.02.017

[9] Abreu F. O. M. S., Bianchini C., Kist T. B. L., Forte M. M. C.: Preparation and properties of core-shell alginate-carboxymethylchitosan hydrogels. Polymer International, **58**, 1267–1274 (2009). DOI: 10.1002/pi.2657

[10] Kim W-T., Chung H., Shin I-S., Yam K. L., Chung D.: Characterization of calcium alginate and chitosan-treated calcium alginate gel beads entrapping allyl isothiocyanate. Carbohydrate Polymers, **71**, 566–573 (2008). DOI: 10.1016/j.carbpol.2007.06.028

[11] Wang L-Y., Ma G-H., Su Z-G.: Preparation of uniform sized chitosan microspheres by membrane emulsification technique and application as a carrier of protein drug. Journal of Controlled Release, **106**, 62–75 (2005).
DOI: 10.1016/j.jconrel.2005.04.005

[12] Kofuji K., Qian C-J., Murata Y., Kawashima S.: Preparation of chitosan microparticles by water-in-vegetable oil emulsion coalescence technique. Reactive and Functional Polymers, **62**, 77–83 (2005).
DOI: 10.1016/j.reactfunctpolym.2004.09.002

[13] Wang L-Y., Gu Y-H., Zhou Q-Z., Ma G-H., Wan Y-H., Su Z-G.: Preparation and characterization of uniform-sized chitosan microspheres containing insulin by membrane emulsification and a two-step solidification process. Colloids and Surfaces B: Biointerfaces, **50**, 126–135 (2006).
DOI: 10.1016/j.colsurfb.2006.05.006

[14] Zhi J., Wang Y., Lu Y., Ma J., Luo G.: In situ preparation of magnetic chitosan/Fe_3O_4 composite nanoparticles in tiny pools of water-in-oil microemulsion. Reactive and Functional Polymers, **66**, 1552–1558 (2006).
DOI: 10.1016/j.reactfunctpolym.2006.05.006

[15] Liu G., Shao L., Ge F., Chen J.: Preparation of ultrafine chitosan particles by reverse microemulsion. China Particuology, **5**, 384–390 (2007).
DOI: 10.1016/j.cpart.2007.08.002

[16] Hamidi M., Azadi A., Rafiei P.: Hydrogel nanoparticles in drug delivery. Advanced Drug Delivery Reviews, **60**, 1638–1649 (2008).
DOI: 10.1016/j.addr.2008.08.002

[17] Gaserod O., Smidsrod O., Skjak-Braek G.: Microcapsules of alginate-chitosan-I: A quantitative study of the interaction between alginate and chitosan. Biomaterials, **19**, 1815–1825 (1998).
DOI: 10.1016/S0142-9612(98)00073-8

[18] Banerjee T., Mitra S., Singh A. K., Sharma R. K., Maitr A.: Preparation, characterization and biodistribution of ultrafine chitosan nanoparticles. International Journal of Pharmaceutics, **243**, 93–105 (2002).
DOI: 10.1016/S0378-5173(02)00267-3

[19] Moura M. J., Figueiredo M. M., Gil M. H.: Rheological study of genipin cross-linked chitosan hydrogels. Biomacromolecules, **8**, 3823–3829 (2007).
DOI: 10.1021/bm700762w

[20] Mi F-L., Sung H-W., Shyu S-S.: Drug release from chitosan-alginate complex beads reinforced by a naturally occurring cross-linking agent. Carbohydrate Polymers, **48**, 61–72 (2002).
DOI: 10.1016/S0144-8617(01)00212-0

[21] Zhu A., Dai S., Li L., Zhao F.: Salt effects on aggregation of *O*-carboxymethylchitosan in aqueous solution. Colloids and Surfaces B: Biointerfaces, **47**, 20–28 (2006).
DOI: 10.1016/j.colsurfb.2005.11.020

eXPRESS Polymer Letters Vol.4, No.8 (2010) 465–473
Available online at www.expresspolymlett.com
DOI: 10.3144/expresspolymlett.2010.59

Chemical, morphological and mechanical analysis of sisal fiber-reinforced recycled high-density polyethylene composites

S. L. Fávaro[1], T. A. Ganzerli[1], A. G. V. de Carvalho Neto[1], O. R. R. F. da Silva[2], E. Radovanovic[1]*

[1]Universidade Estadual de Maringá, Departamento de Química, Grupo de Materiais Poliméricos e Compósitos, Av. Colombo 5790, 87020-900, Maringá, Paraná, Brazil
[2]Embrapa Algodão, Rua Osvaldo Cruz, 1143, 58107-720, Campina Grande, Paraíba, Brazil

Received 12 January 2010; accepted in revised form 16 March 2010

Abstract. Natural fibers are widely used as plastic composite material reinforcements. In this work, composites of post-consumer high-density polyethylene (HDPE) reinforced with sisal fibers were prepared. PE and sisal fibers were chemically modified to improve their compatibilities, try to increase the hydrophobic character of the sisal fiber and hydrophilic character HDPE. Sisal was mercerized with a NaOH solution and acetylated and the PE was oxidized with $KMnO_4$ solution. The chemically modified fibers were characterized by Fourier Transformed Infrared Spectroscopy (FTIR) and ^{13}C Nuclear Magnetic Resonance Spectroscopy (^{13}C NMR). The composites were prepared by extrusion of modified and unmodified materials containing either 5 or 10 wt% fibers. The morphology of the obtained materials was evaluated by SEM. The fiber chemical modification improves it adhesion with matrix, but not benefit were obtained with HDPE oxidation. Flexural and impact tests demonstrated that the composites prepared with modified sisal fibers and unmodified PE present improved mechanical performance compared to pure PE.

Keywords: *polymer composites, recycling, surface treatments, sisal fibers, recycled polyethylene*

1. Introduction

The increasing use of polymeric materials can be observed in our daily life, in uncounted consumer goods around us. However, the production and use of plastics has a range of environmental impacts. Plastics production requires significant quantities of resources, primarily fossil fuels, both as a raw material and to deliver energy for the manufacturing process. The disposal of plastics products also contributes significantly to their environmental impact. Because most plastics are non-degradable, they take a long time to break down, possibly up to hundreds of years. With more and more plastics products, particularly plastics packaging, being disposed of soon after their purchase, the landfill space required by plastics waste is a growing concern. Thereby, the interest on recycled materials developed from post-consumer polymers has gained an increasing attention. The largest fraction of polymers wastes consist of polyolefins, such as polyethylene (PE) and polypropylene (PP) [1], therefore recycling is an alternative destination for these materials. However, to obtain products from recycled material may be necessary specific properties that are not present in original plastic [2]. The environment friendly alternative way to the modification of some properties of polymers is the utilization of natural fibers forming composite materials, and this area presented a crescent development in the last 20 years [3]. The natural fibers, besides pre-

*Corresponding author, e-mail: eradovanovic@uem.br

senting many advantages in relation to synthetic fibers (low cost, renewability, biodegradability, abundance), could also present better mechanical performance from its composites than the ones obtained with synthetic fibers, for instance, the glass fibers [3–5]. Thus, natural fibers, such as fibers of wood, jute, kenaf, hemp, sisal, pineapple, rice husk, etc, have successfully been applied to improve mechanical properties of plastic composites [6–12].

Among natural fibers, sisal is one of the most used in the world, and Brazil is one of the biggest producers. The exceptional mechanical characteristics of sisal are already making its application in automotive industry and civil construction possible [13, 14].

However, like any other hydrophilic lignocellulosic fiber used as reinforcement of hydrophobic plastic in composites, the relatively poor compatibility between them is the barrier to obtain good results. Then, coupling agents are generally used to modify the fiber-matrix interface and thereby enhance the fiber-matrix adhesion [3, 15].

In this article, mechanical and morphological properties of composites, prepared from a post-consumer high density polyethylene (PE) as matrix and sisal fibers as reinforcement phase were studied.

2. Experimental section

2.1. Composite preparation

2.1.1. Recycled polyethylene surface modification

The recycled high-density polyethylene was obtained from Plaspet Polymer Recycling Industry – Maringá – PR – Brazil. The polymer was previously hand-separated from other polymers, washed with water, and cut in ~1.5 mm diameter pellets on site. Before surface modification in laboratory, the polyethylene pellets were washed again and dried at 60°C for 8 h. Surface modification conditions were previously determined [16]: the pellets were immersed in a $KMnO_4$, (Nuclear, Brazil), 0.25 mol·l^{-1}, and solution in HCl (Nuclear, Brazil), 0.50 mol·l^{-1} acidic medium at 25°C for 8 h. Hence, the oxidized polyethylene will be labeled PEox and the untreated polymer, PE.

2.1.2. Sisal fibers surface modification

The sisal fiber, namely *Agave Sisalana* variety coming from state of Bahia – Brazil, was kindly supplied by Embrapa Algodão. Sisal was cut between 0.5 and 1.0 cm of length. Previously to the composite preparation, the sisal was washed with distilled water at 80°C for 1 h and dried in oven at 100°C for 5 h. Sisal mercerization was conducted by keeping it in 10 wt% NaOH solution at room temperature for 3 h. After mercerization, the sisal was rinsed with water to remove the soda excess until pH ~7 was reached and dried in oven at 100°C for 3 h. After this, the sisal was acetylated as follows: the fibers were immersed in pure acetic acid at room temperature for 1 h, then removed and immersed in acetic anhydride acidified with 0.1 wt% sulfuric acid for 5 min at room temperature. Finally, the samples were rinsed with water until pH ~7.0 was reached and dried at 100°C for 5 h. The acetylated sisal fibers were labeled Sac, the mercerized ones were labeled Sm, and the unmodified fibers were labeled S.

2.1.3. Extrusion

The sisal fibers (modified and unmodified) were incorporated into PE (and PEox) at 5 and 10 wt%. The components were mixed in a lab-made monoscrew extruder with a 25/700 mm (diameter/length) screw L/D = 28. The cylinder temperature profile was adjusted to 110, 155 and 185°C for the three heating zones with an average rotation of 40 rpm for all formulations. After extruding, the material was water-cooled down to room temperature.

2.1.4. Injection moulding

The mechanical test specimens were obtained by injection moulding in a Pavan Zanet 100 t injection machine with a 42 mm diameter screw at 180°C and injection pressure of 35 bar. The composites prepared were labeled using the representation as in the example: PEox/Sac10, where PEox represents the oxidized polyethylene matrix with 10 wt% of acetylated sisal fibers as reinforcement.

2.2. Characterization techniques

2.2.1. Water contact angle

The water contact angle in the sessile drop method was measured with contact angle meter Cam Micro, Tantec, USA. Each contact angle value was taken as an average value of five different measurements in different parts of two samples fabricated under the same experimental conditions.

2.2.2. Infrared spectroscopy (FTIR-HATR)

IR spectra of the polymer and sisal fibers were recorded in a FTIR- Pike Miracle ATR, Digilab Scimitar Series using Horizontal Attenuated Totally Reflectance Fourier Transformed Infrared spectroscopy technique, FTIR-HATR, using a FTIR-BOMEM-100 Spectrometer, Canada. The FTIR-HATR technique works by passing a radiation beam through a crystal made of a high-refractive index infrared-transmitting material, which is then totally internally reflected at the surface. The sample is brought in contact with the totally reflecting surface of the ATR crystal; the evanescent wave is attenuated in regions of the infrared spectrum where the sample absorbs energy. Each spectrum represents 128 co-added scans rationed against a reference spectrum obtained by recording 128 co-added scans of an empty HATR cell.

2.2.3. ^{13}C Magic Angle Spinning Nuclear Magnetic Resonance Spectroscopy (^{13}C MAS NMR)

^{13}C MAS NMR spectra of sisal were recorded in a Varian Mercury Plus BB 300 MHz spectrometer, USA, operating at 75.34 MHz for ^{13}C with contact time of 1 ms and recycle time of 20 s, and 128 scans for the signal accumulation.

2.2.4. Scanning electron microscopy (SEM)

The sisal fibers and the composites were observed using a Shimadzu SS 550 Superscan scanning electron microscope, Japan. The samples were gold coated by sputtering technique and observed under different magnifications. Composite fracture surface analyses were performed after immersing the materials in liquid nitrogen for 10 min.

2.2.5. Tensile testing

The composite tensile strength and modulus assays were performed according to the ASTM D-638 test method. The samples were submitted to tensile tests in an EMIC DL 2000 machine (Brazil) at a constant cross-speed of 50 mm/min. Tensile properties were determined for eight samples of each composition.

2.2.6. Flexural testing

The composite flexural strength and modulus were determined, in an EMIC DL 2000 machine (Brazil), using the three-point bending test method following the ASTM D-790-00 A test method. A span of 63 mm was used in a 5 kN load cell. The load was placed midway between the supports. The crosshead speed applied was 20 mm/min. The flexural properties were determined for eight samples of each composition.

2.2.7. Izod impact testing

The notched Izod impact strength tests were conducted according to ASTM D 256-00 A at room temperature in an EMIC-Al testing machine (Brazil) using a 5.4-J hammer. Each value obtained represented the average of five samples.

3. Results and discussion

Table 1 shows the chemical compositions of sisal fibers [17]. The length of sisal is between 1.0 and 1.5 cm and the diameter is about 100–300 μm [18]. The fiber is actually a bundle of hollow sub-fibers. The fibrillar-like structures of fibers can be observed in the fracture image SEM (Figure 1A). Over these structures (Figure 1B) was observed the presence of impurities, composed by parenchymatous cells and others constituents of the fiber as lignin, hemicelluloses and waxes. After alkaline treatment of sisal fibers was observed the extraction of these surface constituents [19] (Figure 1C). Therefore, the exposition of hydroxyl groups

Table 1. The chemical compositions of sisal fibers

Cellulose	Hemi-celluloses	Lignin	Ash
(% by weight)			
43–56	21–24	7–9	0.6–1.1

$$\text{cellulose-OH} + \text{NaOH} \rightarrow \text{cellulose-ONa} + H_2O + \text{impurites} \quad (1)$$

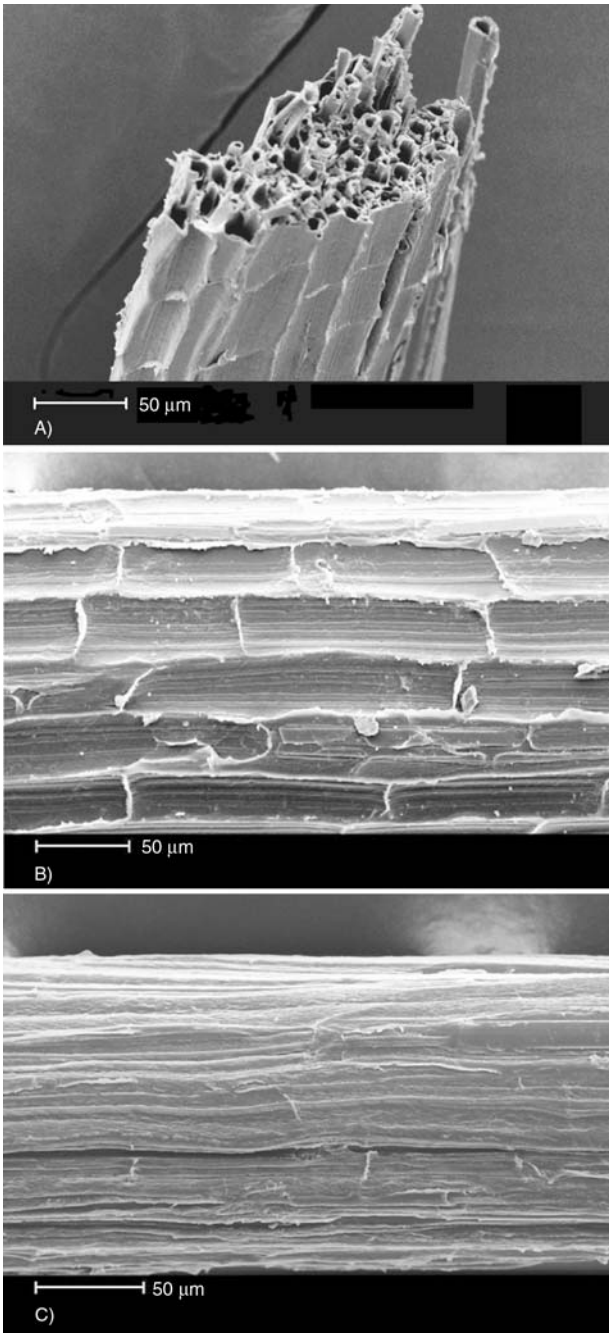

Figure 1. Sisal fiber SEM micrographs: fibrillar structure in fracture image (A), unmodified (B) and mercerized (C) fiber surface images

(Equation (1)) of cellulose microfibers occurred and this treatment should improve the acetylation process of all hydroxyl groups present in the cellulose structure (carbons 2, 3 and 6 in Figure 2) in the acetylating reaction.

The FTIR spectra of S (A), Sm (B), and Sac (C) are shown in Figure 3. Compared with the curve of unmodified sisal, the spectra of mercerized and acetylated cellulose have several differences. After the mercerization process, the bands at 1730 and 1245 cm^{-1}, attributed to the stretching vibrations of C=O and C–O groups, respectively, disappeared. These kinds of groups are present in lignin and hemicelluloses structures. After acetylating reaction, new acetyl groups were added to cellulose, as indicated in curve C, with the vibrations at 1740 cm^{-1} (–C=O) and 1240 cm^{-1} (C–O). The spectrum of unmodified cellulose shows an absorption peak at 1375 cm^{-1} attributed to the –C–H bending vibration. After esterification, the added contribution of the acetyl (–C–CH_3) stretching vibration intensifies this absorption peak [20, 21].

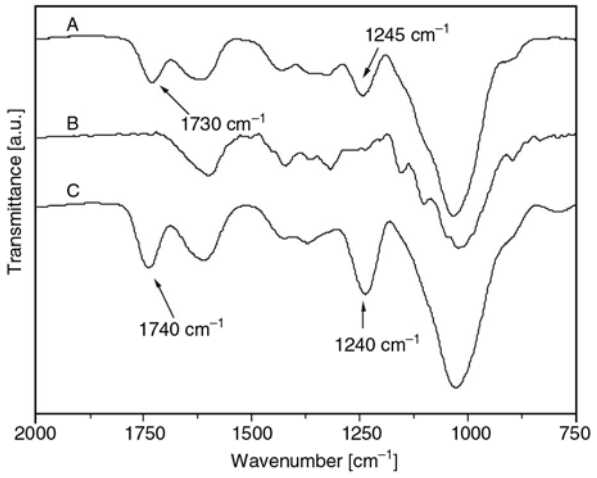

Figure 3. Sisal fibers FTIR-HATR spectra: unmodified (A), mercerized (B), and acetylated (C)

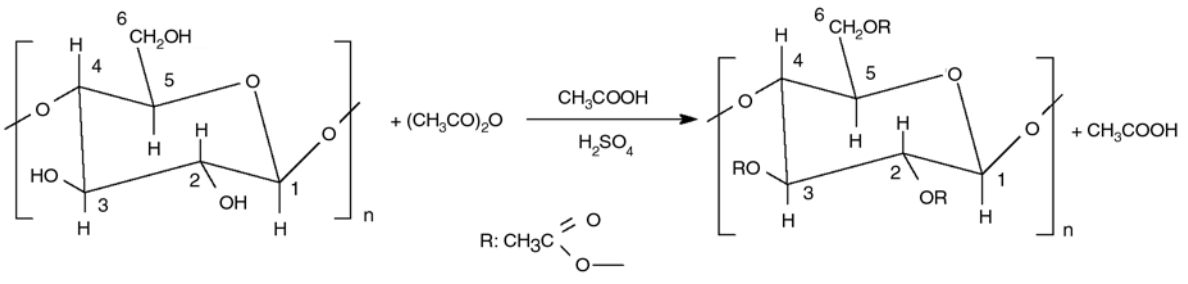

Figure 2. Hydroxyl groups in the cellulose structure

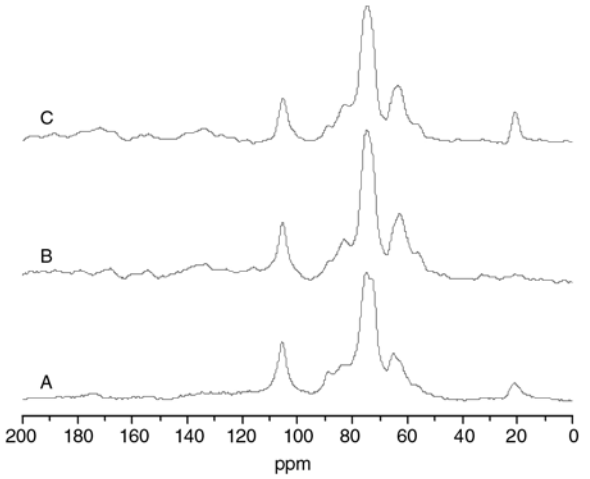

Figure 4. Sisal fibers ^{13}C MAS solid-state NMR spectra: unmodified (A), mercerized (B), and acetylated (C)

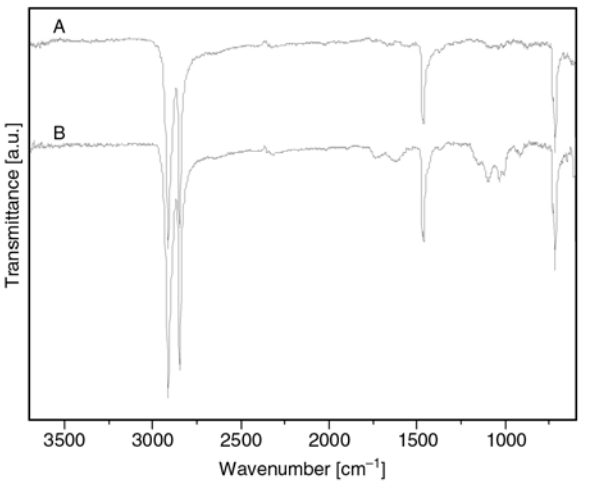

Figure 5. FTIR-HATR spectra of PE (A) and PEox (B)

The mercerization and acetylation reactions of sisal cellulose were also studied by solid-state ^{13}C MAS NMR spectroscopy. The NMR spectra of S (A), Sm (B), and Sac (C) samples are shown in Figure 4. In spectrum A, all noticeable signals of the carbohydrate moiety carbon atoms occur between 50 and 110 ppm. The signal at 21 ppm is assigned to the CH_3 carbon of the hemicellulose acetyl groups. The signals at 105 ppm (C-1), 89 ppm (C-4 of crystalline cellulose), 84 ppm (C-4 of amorphous cellulose), 75 ppm (C-5), 73 ppm (C-2 and C-3), and 64 ppm (C-6) have all been reported before [22]. The intensity of C-4 signal at 89 ppm of crystalline cellulose decreased comparatively to the signal at 84 ppm, as shown by the comparison of spectrum A to spectra B and C. The C-6 signal in A shifted from 64 to 62 ppm in B and C. These changes may indicate that the crystalline structure of cellulose was partially disrupted by the break of α-cellulose hydrogen bonds by the mercerization and acetylation reactions [23]. The degree of substitution (DS) obtained by acetylation in Sac was 0.90 (substitution of 30% in the 3 OH groups of each cellulose monomer). This value was obtained by area deconvolution of the peak at 21 ppm in spectrum C attributed to the $–CH_3$ of the acetyl group generated by the acetylation reaction and related to the deconvoluted area of the peak at 105 ppm (C-1).

Figure 5 shows the FTIR HATR spectra of PE and polyethylene samples oxidized with $KMnO_4$/HCl (PEox). The absorption peaks at 2916, 2848, 1463, and 719 cm^{-1} in A are attributed to methylene nonsymmetric stretching vibration, methylene symmetric stretching vibration, methylene nonsymmetric changing angle vibration, and methylene swing in plane vibration, respectively. The main changes involving oxidized (spectrum B) and untreated polymers, occurred between 1730 and 1650 cm^{-1} and between 1100 and 1000 cm^{-1}, are attributed to different C=O and C–O groups, respectively, created on the polyethylene surface by the $KMnO_4$/HCl solution treatment. The increase in the absorption peak intensities at 1645 and 909 cm^{-1} in the FTIR spectrum may indicates the formation of unsaturated vinyl groups, as already described by other authors [24, 25]. The oxidation process decreased the polyethylene surface water contact angle in the sessile drop measurements, varying from 92.4° in PE to 60.0° in PEox, which decreased the polymer surface hydrophobicity, but did not changed the bulk characteristics [16].

The tensile properties of PE, PEox and composites with 5 and 10 wt% of either S or Sac are depicted in Figure 6. A gradual decrease in the tensile strength was observed to PE/sisal composites comparatively to that of the pure polymer matrix. The composites with modified PEox and S or Sac presented the lowest tensile strength values. PE/S10 presented values near to the tensile strength value of pure PE. The decrease in the composite tensile strength values may be explained by dewetting effect. The fiber/matrix boundary region stress concentrates around the reinforcement particle. Consequently, the fiber-matrix interaction weakens up, thus, probably leading to debonding at the boundary region. Moreover, the addition of sisal to the polymer matrix increases the tensile modulus significantly

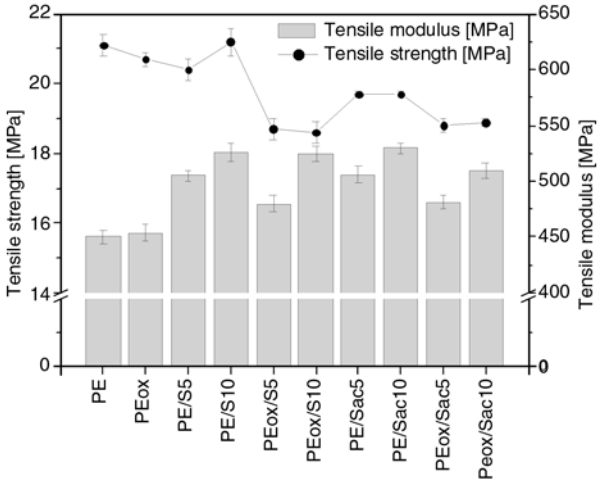

Figure 6. Tensile properties of PE, PEox, PE/sisal and PEox/sisal composites

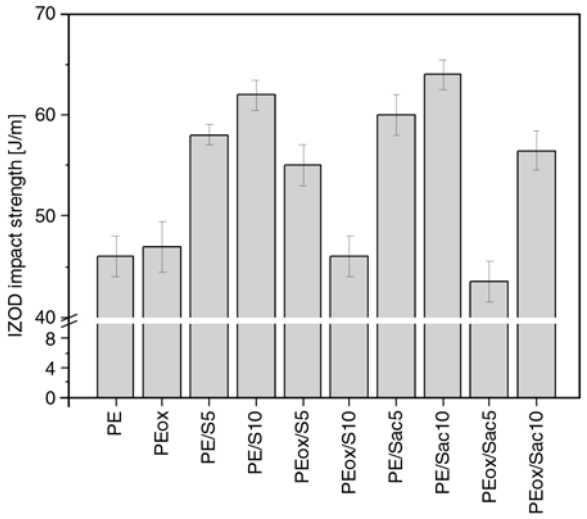

Figure 8. Izod impact properties of of PE, PEox, PE/sisal and PEox/sisal composites

from almost 450 GPa for PE to approximately 520 GPa for PE/S10, PE/Sac10, PEox/S and PEox/S10, an increase of 16%. Among composites, those with 5% of reinforcement presented the lowest tensile modulus values.

The flexural properties of PE and four different composites reinforced with either 5 or 10 wt% sisal fibers are shown in Figure 7. The flexural strength of PE/S5 and PE/S10 was improved by approximately 10 and 15%, respectively. As already observed in the tensile measurements, the flexural strength values of composites containing PEox decreased when compared with those of composites with the same quantity of reinforcement, for instance, the composite PE/S10 presented values near to 25 MPa, but the composite with the same quantity of fibers and matrix oxidized (PEox/S10) presents values around 22 MPa. This result could

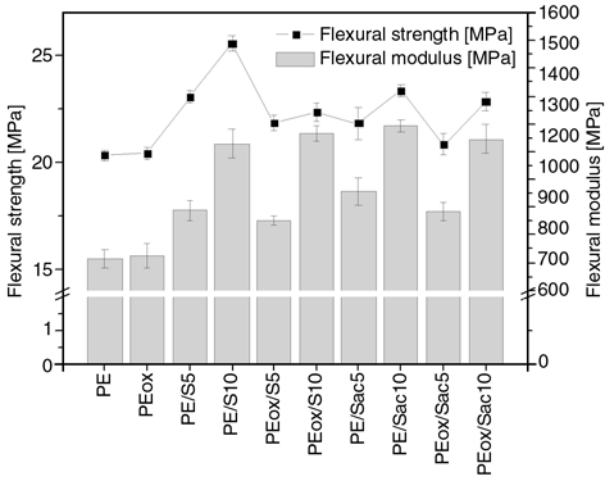

Figure 7. Flexural properties of PE, PEox, PE/sisal and PEox/sisal composites

be explained by the absence of phase compatibility between sisal fibers and polymer surface after chemical modification. The flexural modulus increased significantly (c.a. 55%) in all composites with 10% of reinforcement.

The Izod impact tests were conducted on notched specimens at room temperature. Figure 8 shows the Izod impact tests of two different compositions of sisal-polyethylene composites. Relative to the pure PE Izod impact strength, the value of acetylated sisal composite (PE/Sac10) is 40% higher, and the composites with modified matrix (PEox/S and PEox/Sac) presented the lower values.

Figures 9 show the photomicrographs of the polyethylene – sisal composites with 10 wt% fibers. The samples were fractured in liquid nitrogen prior to observation with scanning electron microscopy (SEM). In the micrographs presented in Figures 9A of composite PE/S10 it is possible to observe the nonexistence of phase adherence, which the fiber pullout at the fracture. An increase in adhesion between the phases occurs in the composites prepared with one of the modified materials. For composite PE/Sac10, it is possible to observe a high adhesion between the inside of the modified sisal fibers and the unmodified matrix. The modification of polymer also increases the adhesion between the materials (Figure 9C) (absence of pullout), however this behavior is not homogeneous, being that the composites also presents regions of not adherence (Figure 9D). Probably during the composites extrusion process occurred an increase in the mobility of the HDPE chains and the softening of

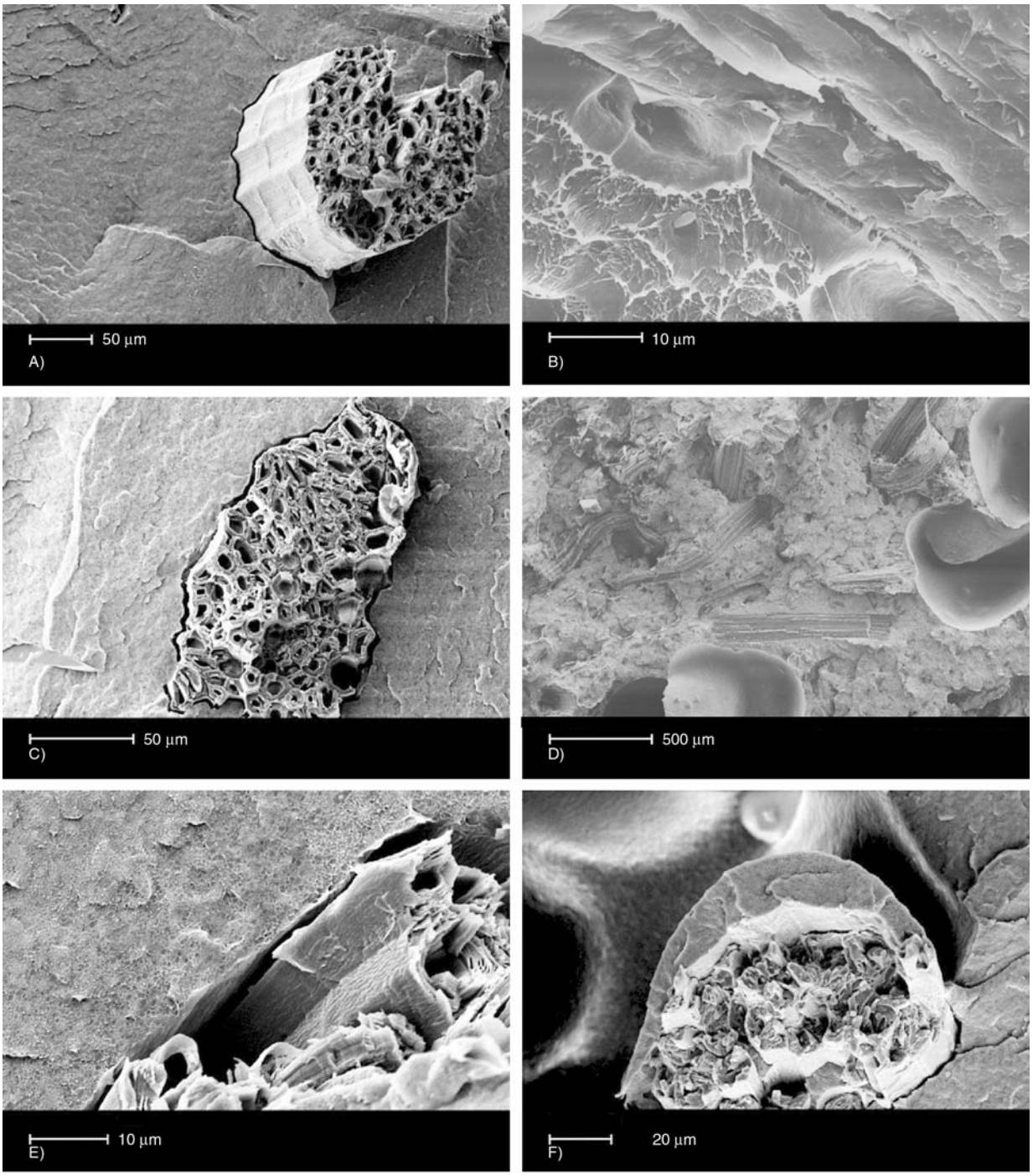

Figure 9. SEM micrographs of composites: PE/S10 (A), PE/Sac10 (B), PEox/S10 (C) and (D), PEox/Sac10 (E) and (F)

polymer, thus, in the end of the extrusion process the fibers could be in contact not only with the oxidized surface polymer, but also with parts not oxidized (bulk). Consequently, the modification of polyethylene surface did not improve mechanical properties of composites. Figures 9E and 9F display the photomicrographs of composite PEox/Sac10. They show two opposite situations: a significant interfacial interaction between the fiber inside and the matrix, which prevents the fiber pullout at the fracture (Figure 9F), and fiber pullout between nonadhered phases (Figure 9E). The interface adhesion allows stress transfer from the matrix to the fiber and accounts for the superior tensile and flexural modulus of the composites. However, other micrographs (not shown here) show that phase nonadherance predominates in PEox/Sac10, which explains its poor mechanical properties. Nonadherance probably predominates due to the increased in the hydrophilic character of the polymer surface, in

opposition to the increased hydrophobic character of the sisal fiber surface, related to the acetyl groups that were added to cellulose. The high fiber/polymer adhesion presented in Figure 9E probably occurred in an unmodified polymer region, such as the inner part of the polymer film.

4. Conclusions

Unmodified and oxidized recycled HDPE composites reinforced with unmodified and acetylated sisal fiber were fabricated by extrusion and injection molding. The acetylated sisal fibers were characterized by FTIR, solid-state ^{13}C MAS NMR and SEM. The latter was changed by acetylation with a degree of substitution (DS) of 0.90. The mechanical, chemical, and morphological aspects of different composite compositions (polymer/fiber) were studied. The incorporation of sisal fibers into the PE matrix increased appreciably the tensile and flexural modulus of the composite prepared with 10 wt% of acetylated sisal fiber and unmodified polyethylene matrix. This composite presented an increase of 40% in impact strength comparatively to values obtained to pure HDPE. SEM photomicrographs demonstrated the interfacial interaction between acetylated sisal fibers and unmodified PE. The modification of PE did not improve its interaction with modified and unmodified fibers, which explains the poor mechanical properties of its composites.

Acknowledgements

S. L. Fávaro is grateful to CAPES (Brazil) for her master fellowship. The authors wish to thank CNPq and SETI – Fundação Araucária for the financial support and to COMCAP/UEM for scanning electron microscopy images.

References

[1] Cavalieri F., Padella F.: Development of composite materials by mechanochemical treatment of post-consumer plastic waste. Waste Manage, **22**, 913–916 (2002).
DOI: 10.1016/S0956-053X(02)00084-3

[2] Dullius J., Ruecker C., Oliveira V., Ligabue R., Einloft S.: Chemical recycling of post-consumer PET: Alkyd resins synthesis. Progress in Organic Coatings, **57**, 123–127 (2006).
DOI: 10.1016/j.porgcoat.2006.07.004

[3] Panthapulakkal S., Law S., Sain M.: Enhancement of processability of rice husk filled high-density polyethylene composite profiles. Journal of Thermoplastic Composite Materials, **18**, 445–458 (2005).
DOI: 10.1177/0892705705054398

[4] García D., López J., Balart R., Ruseckaite R. A., Stefani P. M.: Composites based on sintering rice husk-waste tire rubber mixtures. Materials and Design, **28**, 2234–2238 (2007).
DOI: 10.1016/j.matdes.2006.06.001

[5] Kim H-S., Yang H-S., Kim H-J., Park H-J.: Thermogravimetric analysis of rice husk flour filled thermoplastic polymer composites. Journal of Thermal Analysis and Calorimetry, **76**, 395–404 (2004).
DOI: 10.1023/B:JTAN.0000028020.02657.9b

[6] Sgriccia N., Hawley M. C.: Thermal, morphological, and electrical characterization of microwave processed natural fiber composites. Composites Science and Technology, **67**, 1986–1991 (2007).
DOI: 10.1016/j.compscitech.2006.07.031

[7] Bullions T. A., Hoffman D., Gillespie R. A., Price-O'Brien J., Loos A. C.: Contributions of feather fibers and various cellulose fibers to the mechanical properties of polypropylene matrix composites. Composites Science and Technology, **66**, 102–114 (2006).
DOI: 10.1016/j.compscitech.2005.03.017

[8] Wollerdorfer M., Bader H.: Influence of natural fibres on the mechanical properties of biodegradable polymers. Industrial Crops and Products, **8**, 105–112 (1998).
DOI: 10.1016/S0926-6690(97)10015-2

[9] Fávaro S. L., Lopes M. S., de Carvalho Neto A. G. V., Santana R. R., Radovanovic R.: Chemical, morphological, and mechanical analysis of rice husk/post-consumer polyethylene composites. Composites Part A: Applied Science and Manufacturing, **41**, 154–160 (2010).
DOI: 10.1016/j.compositesa.2009.09.021

[10] Sreekumar P. A., Thomas S. P., Saiter J. M., Joseph K., Unnikrishnan G., Thomas S.: Effect of fiber surface modification on the mechanical and water absorption characteristics of sisal/polyester composites fabricated by resin transfer molding. Composites Part A: Applied Science and Manufacturing, **40**, 1777–1784 (2009).
DOI: 10.1016/j.compositesa.2009.08.013

[11] Angelini L. G., Lazzeri A., Levita G., Fontanelli D., Bozzi C.: Ramie (*Boehmeria nivea* (L.) Gaud.) and spanish broom (*Spartium junceum* L.) fibres for composite materials: Agronomical aspects, morphology and mechanical properties. Industrial Crops and Products, **11**, 145–161 (2000).
DOI: 10.1016/S0926-6690(99)00059-X

[12] Megiatto J. D., Silva C. G., Ramires E., Frollini E.: Thermoset matrix reinforced with sisal fibers: Effect of the cure cycle on the properties of the biobased composite. Polymer Testing, **28**, 793–800 (2009).
DOI: 10.1016/j.polymertesting.2009.07.001

[13] Bourmaud A., Baley C.: Rigidity analysis of polypropylene/vegetal fibre composites after recycling. Polymer Degradation and Stability, **94**, 297–305 (2009).
DOI: 10.1016/j.polymdegradstab.2008.12.010

[14] Suppakarn N., Jarukumjorn K.: Mechanical properties and flammability of sisal/PP composites: Effect of flame retardant type and content. Composites Part B: Engineering, **40**, 613–618 (2009).
DOI: 10.1016/j.compositesb.2009.04.005

[15] Dhakal H. N., Zhang Z. Y., Richardson M. O. W.: Effect of water absorption on the mechanical properties of hemp fibre reinforced unsaturated polyester composites. Composites Science and Technology, **67**, 1674–1683 (2007).
DOI: 10.1016/j.compscitech.2006.06.019

[16] Fávaro S. L., Rubira A. F., Muniz E. C., Radovanovic E.: Surface modification of HDPE, PP, and PET films with $KMnO_4$/HCl solutions. Polymer Degradation and Stability, **92**, 1219–1226 (2007).
DOI: 10.1016/j.polymdegradstab.2007.04.005

[17] Li Y., Mai Y-W., Ye L.: Sisal fibre and its composites: A review of recent developments. Composites Science and Technology, **60**, 2037–2055 (2000).
DOI: 10.1016/S0266-3538(00)00101-9

[18] Bisanda E. T. N., Ansell M. P.: The effect of silane treatment on the mechanical and physical properties of sisal-epoxy composites. Composites Science and Technology, **41**, 165–178 (1991).
DOI: 10.1016/0266-3538(91)90026-L

[19] Sreekala M. S., Kumaran M. G., Thomas S.: Oil palm fibers: Morphology, chemical composition, surface modification, and mechanical properties. Journal of Applied Polymer Science, **66**, 821–835 (1997).
DOI: 10.1002/(SICI)1097-4628(19971031)66:5<821::AID-APP2>3.0.CO;2-X

[20] Lu X., Zhang M. Q., Rong M. Z., Shi G., Yang G. C.: Self-reinforced melt processable composites of sisal. Composites Science and Technology, **63**, 177–186 (2003).
DOI: 10.1016/S0266-3538(02)00204-X

[21] Bower D. I., Maddams W. F.: The vibrational spectroscopy of polymers. Cambridge University Press, Cambridge (1989).

[22] Martins M. A., Forato L. A., Mattoso L. H. C., Colnago L. A.: A solid state ^{13}C high resolution NMR study of raw and chemically treated sisal fibers. Carbohydrate Polymer, **64**, 127–133 (2006).
DOI: 10.1016/j.carbpol.2005.10.034

[23] Maunu S. L.: NMR studies of wood and wood products. Progress in Nuclear Magnetic Resonance Spectroscopy, **40**, 151–174 (2002).
DOI: 10.1016/S0079-6565(01)00041-3

[24] Wu Q., Qu B., Xu Y., Wu Q.: Surface photo-oxidation and photostabilization of photocross-linked polyethylene. Polymer Degradation and Stability, **68**, 97–102 (2000).
DOI: 10.1016/S0141-3910(99)00171-8

[25] Torikai A., Takeuchi A., Nagaya S., Fueki K.: Photodegradation of polyethylene: Effect of cross linking on the oxygenated products and mechanical properties. Polymer Photochemistry, **7**, 199–211 (1986).
DOI: 10.1016/0144-2880(86)90027-8

eXPRESS Polymer Letters Vol.4, No.8 (2010) 474–479
Available online at www.expresspolymlett.com
DOI: 10.3144/expresspolymlett.2010.60

Influence of polymer and surfactant on the aphrons characteristics: Evaluation of fluid invasion controlling

J. J. F. Cardoso[1], *L. S. Spinelli*[1*], *V. Monteiro*[2], *R. Lomba*[2], *E. F. Lucas*[1]

[1]Federal University of Rio de Janeiro, Institute of Macromolecules, Technological Center, Bl. J, Ilha do Fundão, Rio de Janeiro, Brazil
[2]Petrobras Research Center (CENPES), Ilha do Fundão, Q. 9, Rio de Janeiro, Brazil

Received 13 January 2010; accepted in revised form 16 March 2010

Abstract. Aphrons fluids are being studied for application in oil well drilling operation. These fluids consist, basically, of polymer and surfactant, which act as thickening agent and microbubbles producer, respectively. The specific function of aphrons is to act in the filtrate reduction of oil reservoirs presenting low pressure and depleted zones. The aphrons characteristics were evaluated as a function of type and concentration of polymer (xanthan gum-XG and partially hydrolyzed polyacrylamide-PHPA) and surfactant: anionic (*Blue Streak*®, sodium dodecyl sulfate-SDS) and nonionic (polyoxide-based copolymer). Through characterization results (size/size distribution of microbubbles, density and air content) and performance evaluation in the invasion controlling, it was possible to conclude that aphrons fluids prepared with SDS, at an optimal concentration but independent of the polymer type, showed better performance, and such result is related to relatively higher average diameter and broader size distribution of microbubbles, besides the low density and high air content, in the range evaluated in this study.

Keywords: *industrial applications, surfactant, aphrons, drilling fluids*

1. Introduction

Drilling of oil wells occurs by using drilling fluids to remove rock fragments as the drilling progresses [1]. Traditionally drilling muds are classified according to the base used to prepare them, which are air, water or oil. Most drilling operations in the world use water-based fluids, due to their low toxicity. Nevertheless, these have some disadvantages that can be overcome by the use of oil-based fluids [2].

Polymers, such as partially hydrolyzed polyacrylamide (PHPA), poly(vinyl acetate-co-maleic anhydride) (PVAMA), xanthan gum (XG) and carboxymethylcellulose (CMC), are applied in the preparation of drilling fluids to act as thickeners, filter loss reducers, clay swelling inhibitors, drag reduction agents, lubricants and dispersants [3–5].

Technology of aphrons-based drilling fluids (structured air microbubbles) was developed in the end of nineteen's. The potential of aphrons as components of drilling fluids rests in their ability to reduce the invasion of the fluid in the rock and to minimize the damages to the formation, due to their high power to seal off depleted zones [6].

According to Sebba, aphrons are colloidal dispersions containing microbubbles of 10–100 μm in diameter, whose cores can be composed of a gas, liquid or emulsion encapsulated by various layers of surfactants. The term colloidal is related to the small size of bubbles, despite the dimensions are not in fact at colloids range (1 nm–1 μm) [7, 8].

The encapsulating film protects the aphrons, from a thick film that presents as one a bilayer: the innermost layer contains surfactants whose hydrophobic

*Corresponding author, e-mail: spinelli@ima.ufrj.br

groups are inside the core and hydrophilic groups that are outside it. The external layer (protective layer) has surfactants whose hydrophobic and hydrophilic groups are arranged in the opposite order [8].

Aphrons and regulars foams are instable thermodynamically and, therefore, coalesce as a function of time. The principle of aphrons stability is based mainly on their structure (that is composed by multiples layers of surfactants around of the core), moreover electrostatic interactions or steric repulsions, when using ionic or nonionic surfactants, respectively [7]. The main characteristics of aphrons are also related to structure, such as: large interfacial area in relation to volume, due to the small size of bubbles, and high stability. Usually aphrons are characterized by size and size distribution of microbubbles using microscopy techniques and image analysis, besides others that evaluate their structure by layers thickness and number and microbubbles aggregation [9–11].

The acting mechanism of aphrons fluids during well drilling has been proposed in the literature; when aphrons penetrate the depleted zone, the difference between internal and external pressure causes them to expand, favoring the aggregation of bubbles which results in a micro-environment of bubbles that seal off the depleted formation. This generates enough energy to prevent the invasion of fluids, or filtrate, into the depleted zone. Moreover, there is no formation of filter cake, which reduces the possibility of drilling equipment gets stuck in the well and also mitigates corrosion problems [12].

In spite of the mechanism of aphrons has been ascribed in the literature, there is not enough information about the influence of fluid composition on the microbubbles structure. In a previous work we have presented results about synthetic-based aphrons [13]. This work aims to evaluate the influence of type and concentration of polymer and surfactant on water-based aphrons production and their characteristics of microbubbles size, microbubbles size distribution, density and air content, beyond evaluating their performance as invasion controlling as drilling fluids.

2. Experimental section

2.1. Materials

It was used two types of polymers: xanthan gum of molar mass of $2.0 \cdot 10^6$, Kelco Oil Field Group (Houston, USA), and partially hydrolyzed polyacrylamide (PHPA) of molar mass in the range of 1.0 to $1.2 \cdot 10^7$ and hydrolysis degree of 25%, SNF Floerger (Andrézieux, France). The surfactants used were *Blue Streak*® (commercial) and sodium dodecyl sulfate (SDS) from Vetec Fine Chemical (Rio de Janeiro, Brazil), and the monofunctional branched copolymer of poly(ethylene oxide-b-propylene oxide) (PEO-PPO), named L10, from Dow Chemical (São Paulo, Brazil). Magnesium oxide was used as pH controller and glutaraldehyde, supplied by Poland Chemical (Rio de Janeiro, Brazil), as biocide.

2.2. Preparation of aphrons fluids

Aphrons were prepared in two stages. The first one corresponds to the production of base drilling fluid, with a simple formulation, which contains distillated and deionized water, polymer, magnesium oxide and biocide. This formulation was prepared in a mixer (Hamilton Beach Brands, Washington, USA). The second stage is constituted of the incorporation of the microbubbles in the fresh prepared base fluid by mixing surfactant, stirring in the same mixer and using a filter press (Fann Instrument Company, Houston, USA), without filtering element, under 1.38 MPa (200 psi) of differential pressure [14].

These two thickener polymers (XG and PHPA) were used at 11.4 kg/m^3 (the concentration normally used in drilling fluids of petroleum and gas industry), 5.7 and 22.8 kg/m^3, which correspond to the half and the double of the reference concentration, respectively [15]. The surfactants concentrations were 2.0, 4.0 and 20.0 kg/m^3 for *Blue Streak*® and L10, and 4.0, 8.0 and 20.0 kg/m^3 for SDS. Such concentration values were depending on the respective critical micellar concentrations (CMC). The magnesium oxide and glutaraldehyde concentrations were kept constant at 2.0 kg/m^3 each.

2.3. Fluids characterization

The aphrons fluids were characterized in terms of:
- Size and number of microbubbles, by analyses of images using an optical microscope (Olympus SZH10, Center Valley, USA) with the program Size Meter 1.1;
- Density, by conventional method that uses the ratio between mass and total volume occupied by the fluid;
- Air content, using a compressibility test that is related to the compressed volume of the aphrons fluid, taking in account the air volume that suffers compression, when applying the same pressure in both cases.
- Viscosity, using the rheometer AR 2000 (TA Instruments, New Castle, USA), with parallel plates, at room temperature.

2.4. Evaluation of the performance as a filtrate controller

The performance test was carried out using a procedure adapted from Petrobras N-2607 standard. First, a ceramic filter disk (Fann Instrument Company, Houston, USA) with pore diameter of 10 μm was saturated in water to remove the air from the pores. Then, the fluid was passed through the filter cell containing the disk under a differential pressure of 0.69 MPa (100 psi). The mass of fluid expelled from the filter press per unit of time was determined. This procedure was applied to the aphrons and their respective base fluids. These results allowed determining the normalized mass flow, which is the ratio between the fluid flow and the maximum flow that is obtained when passing water through the filter disk. The normalized mass flow values were plotted as a function of time.

3. Results and discussion

3.1. Characterization of the aphrons fluids

The aphron fluids were characterized by optical microscopy to visualize the microbubbles. The number, size and size distribution of the microbubbles were determined by using the Size Meter 1.1 program. In general the results showed that the diameter of the aphrons produced with xanthan gum varied from 70 to 164 μm, while those produced with PHPA had smaller average diameters,

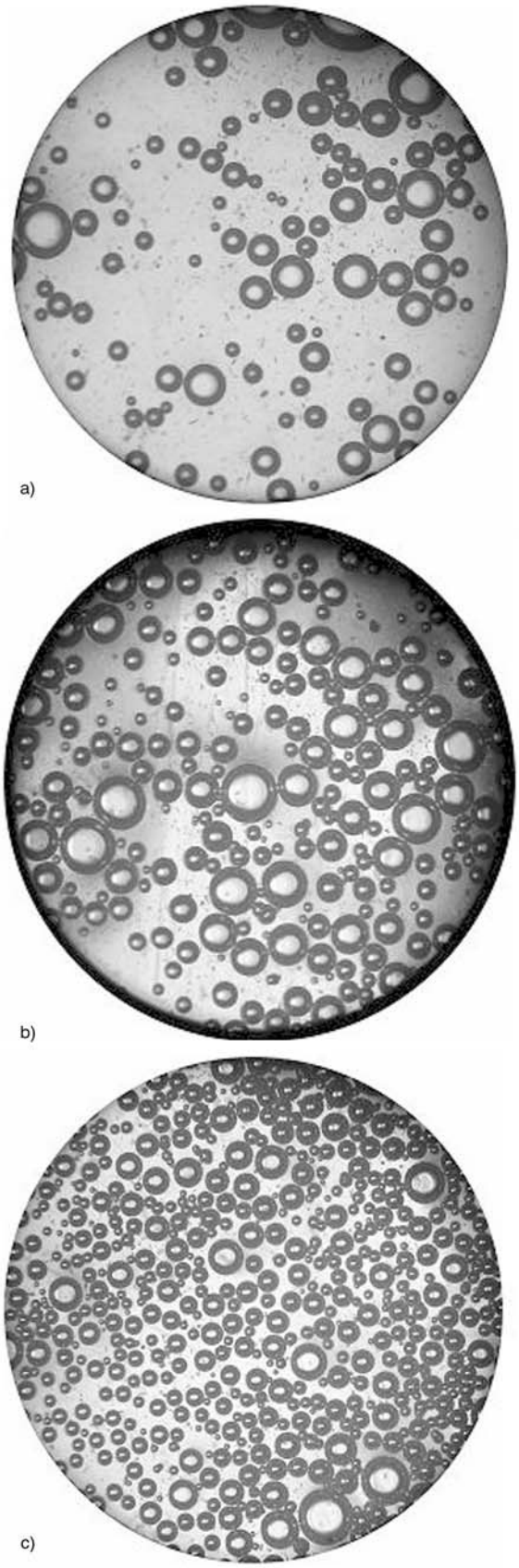

Figure 1. Micrographies of aphrons fluids obtained with xanthan gum at 5.7 kg/m^3, using *Blue Streak*® surfactant at (a) 2.0 kg/m^3, (b) 4.0 kg/m^3 and (c) 20.0 kg/m^3

ranging from 47 to 117 μm. However, the number of bubbles increased and their size decreased with increasing surfactant concentration, independent of the type of polymer added. Figure 1 shows the micrographs of the fluids containing xanthan gum at a concentration of 11.4 kg/m^3 using *Blue Streak*® as surfactant.

The correlation between the surfactant concentration and microbubble diameter was better observed in fluids containing low polymer concentration (5.7 kg/m^3), since the system presents lower viscosity.

The number of microbubbles increased with increasing surfactant concentration when using both *Blue Streak*® and SDS. In the latter case this increase was more pronounced when using xanthan gum as the polymer. With one exception, for PHPA-based fluids, the number of microbubbles declined when the SDS concentration was 20 kg/m^3.

The density of the aphrons produced with xanthan gum declined more rapidly than those prepared with PHPA as the surfactant concentration increased. These results can be related to the volume of incorporated air, because we found that aphrons produced with the anionic surfactants (*Blue Streak*® and SDS) had similar levels of incorporated air, greater than the level of the aphrons produced with the nonionic surfactant (L10) for fluids containing the two types of polymers. These results are coherent with the density results, i.e., systems prepared with nonionic surfactants are denser.

The viscosity analyses (Figure 2) showed that when xanthan gum was used, the aphron fluids were more viscous than their respective base fluids, for all the surfactant concentrations tested. For aphrons fluids produced using PHPA, the viscosity in relation to the base fluid only increased for the highest surfactant concentrations (4.0 and 20.0 kg/m^3). At lower shear rates, there was a slight dependence of the viscosity on the concentration of the surfactant used. The highest viscosity was obtained for the intermediate surfactant concentration. These results suggest there is an optimal surfactant concentration for production of aphrons fluids with controlled viscosities.

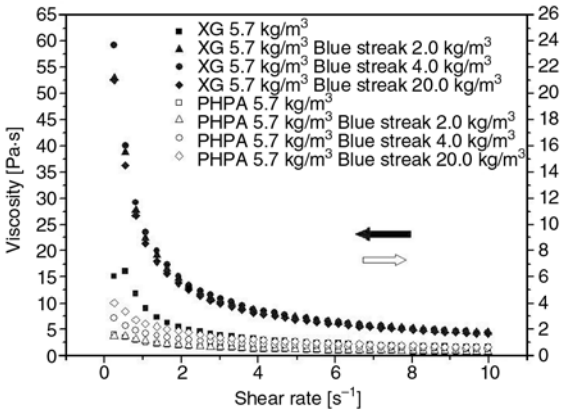

Figure 2. Viscosity against shear rate of base fluids (APX and APP) and aphrons fluids (APX B and APP B) produced with 5.7 kg/m^3 of xanthan gum (APX) or PHPA (APP) and different concentrations of *Blue Streak*® (2, 4 and 20 kg/m^3)

3.2. Evaluation of the base and aphron fluids as filtrate reducers

We performed tests with the base fluids and aphrons fluids at a pressure of 0.69 MPa (100 psi), using disks with a pore size of 10 μm. The fluids prepared with xanthan gum at the lowest concentrations (5.7 and 11.4 kg/m^3), using both anionic and nonionic surfactants, did not perform well in reducing filtrate. On the contrary, the presence of microbubbles in these systems caused higher flows through the porous disk in relation to the corresponding base fluid. On the other hand, the aphron fluids with the highest concentration of xanthan gum (22.8 kg/m^3), using both SDS and L10, had structures able to significantly reduce the filtrate flow in relation to the respective base fluid, since this system had a high number of microbubbles with greater average diameter, wider size distribution, lower density and higher volume of incorporated air.

For the PHPA-base fluids, the system with the lowest polymer concentration performed best, due to the fact that its microbubbles had the same characteristics as those produced with a high concentration of xanthan gum. Nevertheless, for the systems formed specifically with L10, increasing the concentration of this surfactant from 2.0 to 4.0 kg/m^3 significantly improved its performance as a filtrate reducer. However, at the highest concentration tested (20.0 kg/m^3), the aphrons had very high normalized mass flow rates, meaning they did not function as a filtrate reducing fluid.

Based on the aphron fluids' characteristics, the average bubble diameter appears to influence their performance. In other words, within the size range of the microbubbles formed, those with a wider size

Table 1. Percentage of filtrate reduction and characteristics of fluids containing xanthan gum and PHPA, respectively at 22.8 and 5.7 kg/m^3

Aphrons			Characteristics				Eficiency [%]	
Surfactant		Conc. [kg/m^3]	Average size of bubble [μm]	Size distribution of bubbles [μm]	Density [kg/m^3]	Air content [%]	Time [s]	
							15	60
Xanthane	–	–	–	–	–	–	–	–
	SDS	4.0	93	430	590	27.6	30.6	62.0
	SDS	8.0	113	390	450	68.9	40.4	100.0
	SDS	20.0	77	410	510	50.0	42.9	58.9
PHPA	–	–	–	–	–	–	–	–
	SDS	8.0	85	250	780	23.3	(a)	100.0
	L10	2.0	81	120	900	10.0	0.45	(a)
	L10	4.0	62	160	850	13.8	80.1	66.9
	L10	20.0	51	130	940	7.1	(a)	(b)

[a]The normalized rate of aphrons fluid presented above the rate of their base fluid, that causes the appearing of a negative efficiency
[b]In 22 seconds, all aphrons fluid had been passed by the disc

distribution more easily penetrate the pores and consequently perform better at reducing filtrate. The aphrons fluids that performed best were those produced with SDS as the surfactant, independent of the type of polymer used. However, the aphrons fluids produced with PHPA, using L10, were highly efficient in reducing filtrate at the start of the filtration process.

Table 1 shows the efficiency results (filtrate reduction percentage) for the best systems obtained, along with their characteristics. The aphrons fluids produced with L10 and SDS were slightly more efficient. The efficiency results are presented at two times, 15 and 60 seconds. These times are related to the start of the filtrate reduction test and the moment when the normalized flows tended to be constant.

Among these, the aphrons fluids with SDS were most efficient, in shorter analysis times, but in some cases (e.g., the aphrons with 11.4 kg/m^3 of PHPA and 8.0 kg/m^3 of SDS) they completely lost efficiency after 80 seconds, i.e., they attained the same flow rate as the corresponding base fluid.

The best performers among all the aphrons produced were the systems containing 5.7 kg/m^3 of PHPA and 8.0 kg/m^3 of SDS and containing 22.8 kg/m^3 of xanthan gum and 8.0 kg/m^3 of SDS. The second of these was efficient throughout the filtration process (15 s – 40.4% and 60 s – 100%). Thus, it should be tested in larger scale or with core samples from real reservoirs. This system has the advantage of very low density (450 kg/m^3), despite its relatively high polymer and surfactant concentrations (22.8 and 8.0 kg/m^3, respectively).

The existence of a possible correlation between a system's filtrate reduction performance and the characteristics of the aphrons determined in this study show that the relatively simple methods of evaluating properties utilized in this work for characterizing aphrons fluids can be used to predict their performance. However, the dynamic process of interaction of the fluid with the pores of the rock formation must be taken into consideration. However, this requires evaluation of the dynamic property of the fluid in relation to the pressure variance in the medium through which the bubbles move.

4. Conclusions

Both xanthan gum (XG) and partially hydrolyzed polyacrylamide (PHPA) performed well as viscosifiers in the production of aphron fluids. By using xanthan gum it was possible to obtain fluids with higher viscosities than those obtained with PHPA, at the same concentration, since the XG presents higher thickness performance than PHPA, due to its tendency to form molecular aggregates. In this case, the fluids presented lower densities and incorporated air volumes than that prepared with PHPA. In general, the size of the microbubbles decreased with increasing polymer concentration, probably due to the high viscosity of the fluids, which reduces the diffusion of the microbubbles in the medium. The tests with a ceramic disk with 10 μm pore size showed that fluids containing sodium dodecyl sulfate (SDS), at an optimal concentration, performed best in reducing filtrate, independent of the type of polymer used. This can be related to the

presence of microbubbles with larger average diameters and broader size distribution, besides the low density and high content of incorporated air. Aphrons fluids presenting good performance as filtrate reducer can be obtained by using different formulations, that is, varying kind and concentration of their constituents.

Acknowledgements

The authors acknowledge the financial support of Petrobras, the Coordinating Office for Improvement of University Researchers (CAPES), the National Council for Scientific and Technological Research (CNPq) and the National Petroleum Agency (ANP). The authors also thank Dow Chemical and Poland Chemical for supplying surfactants and biocide.

References

[1] Amorim L. V., Farias K. V., Viana J. D., Barbosa M. I. R., Pereira E., França K. B., Lira H. L., Ferreira H. C.: Water based drilling fluids. Part I: Effects of polymeric additives in the rheological properties (in Portuguese). Cerâmica, **51**, 128–138 (2005).
DOI: 10.1590/S0366-69132005000200010

[2] Lucas E. F., Mansur C. R. E., Spinelli L. S., Queirós Y. G. C.: Polymer science applied to petroleum production. Pure and Applied Chemistry, **81**, 473–494 (2009).
DOI: 10.1351/PAC-CON-08-07-21

[3] Thomas J. E.: Fundamentos da engenharia do petróleo. Editora Interciencia, Rio de Janeiro (2001).

[4] Amorim L. V., Barbosa M. I. R., Ferreira I. H. C.: Bentonite/polymer compound development to application in drilling fluids- Part 2 (in Portuguese). Revista Matéria, **13**, 209–219 (2008).
DOI: 10.1590/S1517-70762008000100026

[5] Sadiq R., Husain T., Veitch B., Bose N.: Evaluation of generic types of drilling fluid using a risk-based analytic hierarchy process. Environmental Management, **32**, 778–787 (2003).
DOI: 10.1007/s00267-003-0009-2

[6] Ivan C. D., Growcock F. B., Friedheim J. E.: Chemical and physical characterization of aphron-based drilling fluids. SPE International, 77445/1–77554/6 (2002).
DOI: 10.2118/77445-MS

[7] Jauregi P., Gilmour S., Varley J.: Characterisation of colloidal gas aphrons for subsequent use for protein recovery. Chemical Engineering Journal, **65**, 1–11 (1997).
DOI: 10.1016/S1385-8947(96)03154-3

[8] Jauregi P., Varley J.: Colloidal gas aphrons: Potential applications in biotechnology. Trends in Biotechnology, **17**, 389–395 (1999).
DOI: 10.1016/S0167-7799(99)01363-3

[9] Dai Y., Deng T.: Stabilization and characterization of colloidal gas aphron dispersions. Journal of Colloid and Interface Science, **261**, 360–365 (2003).
DOI: 10.1016/S0021-9797(03)00056-0

[10] Mansur E. H. A., Wang Y., Dai Y.: Removal of suspensions of fine particles from water by colloidal gas aphrons (CGA). Separation and Purification Technology, **48**, 71–77 (2006).
DOI: 10.1016/j.seppur.2005.07.022

[11] Fuda E., Jauregi P., Pyle D. L.: Recovery of lactoferrin and lactoperoxidase from sweet whey using colloidal gas aphrons (CGAs) generated from an anionic surfactant, AOT. Biotechnology Progress, **20**, 514–525 (2004).
DOI: 10.1021/bp034198d

[12] Brookey T., House R.: Aphron-containing well drilling and servicing fluids of enhanced stability. U.S. Patent 6422326, USA (2002).

[13] Spinelli L. S., Neto G. R., Freire L. F. A., Monteiro V., Lomba R., Michel R. C., Lucas E. F.: Synthetic-based aphrons: Correlation between properties and filtrate reduction performance. Colloid and Surface A: Physicochemical and Engineering Aspects, **353**, 57–63 (2010).
DOI: 10.1016/j.colsurfa.2009.10.017

[14] Growcoock F. B., Simon G. A., Rea A. B., Leonard R. S., Noello E., Castellan R.: Alternative aphron-based drilling fluid. in 'IADC/SPE Drilling Conference, Dallas, USA', 87134-MS (2004).
DOI: 10.2118/87134-MS

[15] Growcock F.: Enhanced wellbore stabilization and reservoir productivity with aphron drilling fluid technology. Final Report. MASI Technologies LLC, Houston (2005).

eXPRESS Polymer Letters Vol.4, No.8 (2010) 480–487
Available online at www.expresspolymlett.com
DOI: 10.3144/expresspolymlett.2010.61

Release of DNA from cryogel PVA-DNA membranes

A. J. M. Valente[1*], *S. M. A. Cruz*[1], *M.C. Morán*[1], *D. B. Murtinho*[1], *E. C. Muniz*[2], *M. G. Miguel*[1]

[1]Department of Chemistry, University of Coimbra, 3004-535 Coimbra, Portugal
[2]Grupo de Materiais Poliméricos e Compósitos, GMPC, Departamento de Química, Universidade Estadual de Maringá, 87020-900 – Maringá, PR, Brazil

Received 7 January 2010; accepted in revised form 17 March 2010

Abstract. Poly(vinyl alcohol) (PVA) hydrogels have been used for numerous biomedical and pharmaceutical applications, as a consequence of their non-toxic, non-carcinogenic and bioadhesive properties. In this communication the effect of different factors, such as type of electrolyte, ionic strength, temperature (ranging from 20 to 40°C) and cationic surfactants on the distribution coefficients (α) and release rate constants (k_R) of deoxyribonucleic acid (DNA) from PVA-DNA blend gel matrices (of a sheet shape), will be presented and discussed. The release kinetic constant and the distribution coefficient of DNA are quite sensitive to the surrounding matrix media (e.g., k_R ranges from $1.5 \cdot 10^{-8}$ to $4.7 \cdot 10^{-7}$ s^{-1}). The analysis of the temperature dependence on k_R shows that the activation energy for the DNA desorption to an aqueous solution is equal to 21.2 kJ/mol. These results constitute a step forward towards the design of controlled DNA release PVA-based devices.

Keywords: *polymer gels, polymers membranes, poly(vinyl alcohol), deoxyribonucleic acid, release kinetics*

1. Introduction

Hydrogels are polymeric materials with a three-dimensional network structure that can imbibe water, buffered or physiological solutions. Hydrogels show high water content, soft and rubbery consistency and low interfacial tension with water or biological fluids [1]. The ability of molecules of different size to diffuse into (drug loading), and out of (drug release) hydrogels, allows the use of hydrogels as delivery systems [2, 3].

In recent years, there has been considerable work performed in the development of cross-linked polymeric networks which are sensitive to their surrounding physiological environment and therefore will be desirable systems for site-specific drug-delivery [4–9].

Poly(vinyl alcohol) (PVA) is commonly used as a component to form hydrogels. PVA and its copolymers have been widely employed in controlled drug release systems [10]. PVA is hydrophilic and easily swells upon hydration [11]. Furthermore, PVA is non-toxic, non-carcinogenic, shows bioadhesive characteristics and is easily processed [12]. These properties make it ideal for biomedical uses, especially in drug delivery systems. PVA hydrogels can be cross-linked through the use of bifunctional agents, by using electron beam or γ-radiation, or by a 'freezing-thawing' process [13]. The later process addresses toxicity issues; furthermore, these physically cross-linked materials also exhibit higher mechanical strength and elasticity than PVA gels prepared by other methods [13]. Characterization and properties of the so-called PVA-based cryogels have been summarized by V. I. Lozinsky [14, 15].

Recently we have reported the encapsulation of deoxyribonucleic acid (DNA) into PVA hydrogels, obtained by a technique of repeated freezing and thawing [16]. The obtained cryogels were chemically and physically characterized, and show a good mechanical resistance and a white and opaque

*Corresponding author, e-mail: avalente@ci.uc.pt

appearance due to a heterogeneous porous structure. Furthermore, the encapsulated DNA molecules can be compacted or extended in the PVA matrix by tailoring the crystallinity degree of the PVA network.

In this paper the effect of different factors, such as electrolytes, ionic strength, cationic surfactants and temperature (ranging from 25 to 50°C) on the distribution coefficients (α) and release rate constants (k_R) of DNA from PVA-DNA blend gel matrices (of a sheet shape), will be presented and discussed. The kinetics of release will be evaluated by a reversible first-order kinetic law equation, developed by Reis *et al.* [17], based on the assumption that the release of a solute from a hydrogel is treated as a partition phenomenon.

2. Experimental

2.1. Reagents and materials

Poly(vinyl alcohol) (PVA) (molecular weight (M_w) 72 000, degree of polymerization ~1600, degree of hydrolysis 97.5–99.5 mol%) was supplied from Fluka (Steinheim, Germany). The sodium salt of deoxyribonucleic acid (DNA) from salmon testes of an average degree of polymerization of about 2000 base pairs was purchased from Sigma (Steinheim, Germany) and used as received. Sodium bromide, NaBr, (Merck, Darmstadt, Germany), sodium iodide, NaI (Merck, Darmstadt, Germany), sodium nitrate, $NaNO_3$ (Riedel-de Haën, Seelze, Germany), and sodium chloride, NaCl (Riedel-de Haën, Seelze, Germany) all of *pro analysis* grade, were used as received.

The fluorescence dye *N*,*N*,*N*′,*N*′-tetramethylacridine-3,6-diamine (acridine orange (AO)) was purchased from Molecular Probes (Invitrogen, Eugene, OR, USA).

These reagents were used without further purification. All solutions were prepared using Millipore-Q water.

2.2. Surfactant synthesis

The 1,12-dibromododecane (Aldrich, Steinheim, Germany), (10 mmol) was dissolved in 20–25 ml dry ethanol and 200 mmol of amine (triethylamine or an ethanolic solution of trimethylamine, 31–35%) were added. The reaction mixture was refluxed until the alkylbromide was consumed, usually 48 h, as monitored by TLC. The solvent and the excess amine were evaporated under reduced pressure and the residue was crystallized several times from the appropriate solvent or solvent mixtures.

Dodecane-1,12-bis(trimethylammonium bromide), $C_{12}Me_6$: Crystallized in ethanol, 93% yield.

Dodecane-1,12-bis(triethylammonium bromide), $C_{12}Et_6$: Crystallized in CH_2Cl_2/ethyl acetate, 85% yield.

2.3. Preparation of PVA-DNA gel matrices

A PVA solution of 14 wt% concentration was prepared by dissolving the appropriate amount of PVA into distilled water at 80°C under continuous stirring for three hours. An accurate amount of DNA (ca. 1% w/w), using a Scaltec SBC22 (Göttingen, Germany) balance with a resolution of ±0.01 mg, was added to 1 g of PVA solution, at room temperature, and mixed, under continuously stirring, during 4 hours. After that, the solution was casted into cylinder flasks and submitted to freezing for 12 hours at –20°C and, after that, thawed for 12 hours at +25°C. The cycles of freezing and thawing were repeated three times. After that, the blend gel membrane, of 2.20(±0.04) mm thickness – measured by a digimatic micrometer Mitutoyo (Kawasaki, Japan) with a resolution of 0.001 mm – shows a good mechanical resistance and a white and opaque appearance.

2.4. Desorption kinetics of DNA

DNA desorption kinetics were performed by immersing a PVA-DNA gel membrane sample (as it was synthesised) in 100 ml of liquid (water, salt or surfactant solution). Experiments have been carried out at 20°C. The effect of temperature on the release kinetics of DNA has been studied in the 20 to 40°C temperature range. In all experiments, temperature was kept constant by using a thermostatic bath Multistirrer 6 from Velp Scientifica (Milan, Italy). During DNA release experiments gel-containing solutions were stirred at ca. 220 rpm. At defined intervals, aliquots of the supernatant were collected. The amount of substance of DNA released from polymeric matrices, $n_{R,t}$, to the supernatant solution was determined by UV-vis spectrophotometry, by measuring the absorbance at 260 nm with a Jasco V-530 (Essex, UK) spectrophotome-

ter, and using the extinction coefficient of 6600 $M^{-1} \cdot cm^{-1}$ [18, 19].

2.5. Fluorescence microscopy

Freshly prepared membranes or supernatant solutions derived from the DNA release studies were stained with *N*,*N*,*N*′,*N*′-tetramethylacridine-3,6-diamine (acridine orange, AO), a nucleic acid selective fluorescent cationic dye, used to confirm the presence of DNA in the membranes. In addition, using AO, information about the secondary structure of the nucleic acid in the membranes has been obtained [20].

Stained samples were immediately examined with an Olympus BX51M (Hamburg, Germany) microscope equipped with a UV-mercury lamp (100W Ushio Olympus) and a filter set type MNIBA3 (470–495 nm excitation and 505 nm dichromatic mirror). The PVA-DNA membranes were observed using an Olympus 4×/0.10 objective lens (∞/–/FN22); supernatant solutions were observed using an Olympus 100×/1.30 oil-immersed objective lens (Hamburg, Germany).

Images were digitized on a computer through a video camera (Olympus digital camera DP70) and were analyzed with an image processor (Olympus DP Controller 2.1.1.176, Olympus DP Manager 2.1.1.158 – Olympus, Hamburg, Germany). All observations were carried out at 20°C.

Figure 1 shows modification on the surface morphology of PVA gel matrices in the absence and presence of DNA. It is possible to observe that DNA is distributed throughout all matrix, confirming the effectiveness of the mixing method.

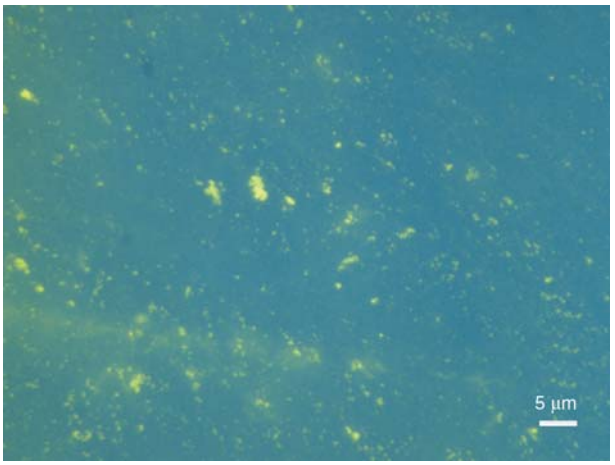

Figure 2. Fluorescence microscopy photograph of an aqueous supernatant solution of water in contact with PVA-DNA gel membrane

The secondary structure of DNA desorbed from PVA-DNA gel was also checked by fluorescence microscopy. Based on the observation of green or red fluorescence, acridine orange has been used to differentiate native, double-stranded DNA from denatured, single-stranded DNA [20]. Although the size of the observed objects suggests that the delivery of DNA is in the form of aggregates, no evidences of denaturation of DNA have been found (Figure 2).

3. Mathematical model

The quantification of the release kinetics of DNA has been done taking into account the initial and border conditions of a non-steady state diffusion transport occurring in a stirred solution of limited volume [21]. Recently, Reis *et al.* [17] developed a set of equations to model the release of dyes from

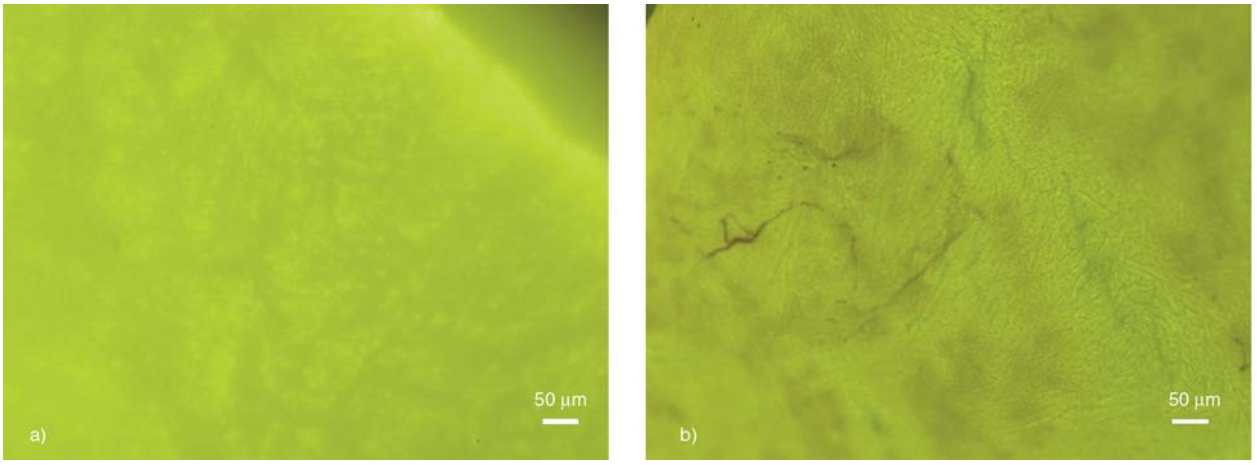

Figure 1. Fluorescence microscopy images for PVA blend matrix in the absence (a) and presence (b) of DNA

poly(*N*-isopropylacrylamide)–polyacrylamide taking into account the previous mentioned conditions, and treating the release of a solute from the gel as a partition phenomena, where the partitioning of such solute occurs between a solvent (or solution) phase and the hydrogel.

This behaviour can be quantified through the distribution coefficient, α, which characterizes the physical chemical affinity of the solute for both phases (Equation (1)):

$$\alpha = \frac{F_{R,\max}}{1 - F_{R,\max}} \tag{1}$$

where $F_{R,\max}$ is the maximum fraction of the released solute, and F_R is given by Equation (2):

$$F_R = \frac{C_{R,t}}{C_0} \tag{2}$$

where $C_{R,t}$ is the concentration of the solute released, at time t, and C_0 is the initial concentration of the loaded solute inside gel matrix.

When $t > 0$, the diffusion of the solute between the hydrogel and the solution phase occurs, and the process of release and absorption of solute occurs simultaneously.

Assuming a first order kinetic process, changes of solute concentration in solution at a given time t, can be expressed as Equation (3):

$$\frac{dC_{R,t}}{dt} = k_R(C_0 - C_{R,t}) - k_A(C_{R,0} - C_{A,t}) \tag{3}$$

where $C_{R,0}$ and $C_{R,t}$ are the concentration of the release solute at $t = 0$ and at time t, C_0 is the initial concentration of DNA in the gel and $C_{A,t}$ is the concentration of absorbed solute at specific time t. k_R and k_A are the rate constants for the release and absorption processes, respectively.

From the kinetic law equation, Equation (3), and taking into account considerations reported elsewhere [17], the release kinetics of DNA can be treated by using Equation (4):

$$F_R = F_{R,\max}\left(1 - e^{-(k_R / F_{R,\max})t}\right) \tag{4}$$

where $F_{R,\max} = C_{R,\max}/C_0$, and $C_{R,\max}$ is the maximum concentration of solute in solution released from the gel. By fitting Equation (4) to experimental data (e.g., Figure 3) it is possible to calculate the following parameters: $F_{R,\max}$ and k_R, and so to characterise the release not only in terms of kinetics, but also in terms of the partition coefficient.

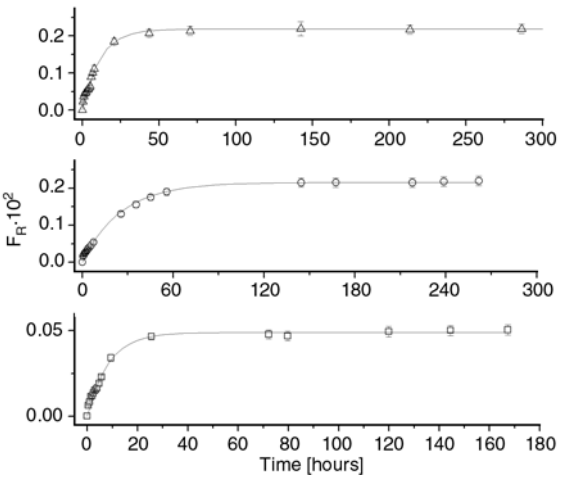

Figure 3. Desorption kinetics of DNA from PVA-DNA membranes to cationic surfactant solution: (□) C_{12}TAB, (o) $C_{12}Me_6$, (Δ) $C_{12}Et_6$. Solid lines represent the fraction of release DNA predicted by Equation (4).

It is worthwhile to note that the release of DNA, in all systems mentioned in this communication, follows a first-order kinetic law. The experimental data were analyzed using a nonlinear least-squares fitting procedure (Origin 8.0), using a 95% confidence level. The uncertainty in the fit of Equation (4) to the data is in general smaller than 5%.

4. Results and discussion

4.1. Effect of symmetrical and unsymmetrical electrolytes

Table 1 shows the effect of sodium salts on the distribution coefficient (α) and released rate constants (k_R) of DNA release from PVA-DNA gel membranes in different electrolyte media.

It is possible to observe that comparing the release of DNA to sodium salts, at a given concentration, there is a decrease of both α and k_R in the order: NaI > $NaNO_3$ > NaCl > NaBr. The order of anions does not differ much from that involved in their water structure modifying effects or of the Hofmeister series [22, 23]; that is, with the capacity of different aqueous solutions to solubilise DNA. Lozinsky *et al.* [24] have also reported that the reinforcing ability of the electrolyte with respect to the PVA cryogel strength has been shown to be in agreement with the position of these ions in the

Table 1. Values of different kinetic and equilibrium parameters for the release of DNA, from PVA cryogels, to different electrolyte solutions, at 25°C

	$\alpha/10^{-3}$	$k_R \cdot 10^{-7}$ [s^{-1}]
[NaI] [mM]		
10	4.7 (± 0.1)	4.8 (± 0.3)
25	4.6 (± 0.1)	1.33 (± 0.09)
50	3.33 (± 0.06)	1.07 (± 0.04)
[$NaNO_3$] [mM]		
10	3.43 (± 0.08)	1.92 (± 0.09)
25	3.31 (± 0.05)	1.19 (± 0.03)
50	2.51 (± 0.07)	4.66 (± 0.02)
[NaCl] [mM]		
10	2.81 (± 0.06)	1.27 (± 0.05)
25	2.54 (± 0.07)	0.66 (± 0.03)
50	2.08 (± 0.05)	0.40 (± 0.02)
[NaBr] [mM]		
10	2.37 (± 0.07)	0.83 (± 0.05)
25	2.24 (± 0.01)	0.462 (± 0.008)
50	1.05 (± 0.01)	0.128 (± 0.004)

Values inside brackets correspond to standard deviations.

lyotropic series. Among these salts, iodide solution has the strongest effect as water structure breaking, being the highest effective on the solubilisation of DNA [25]. Using similar arguments, NaBr is the less effective on the solubilisation of DNA in the aqueous phase [20]. We can hypothesise that such variation in the empirical sequence, when compared with the Hofmeister series, can be justified by the specific effect of bromide ions on the crystallinity of PVA and/or on the DNA structure. That is, the presence of bromide ions affects the PVA structure by decreasing its crystallinity due to the ability of NaBr as a hydrogen bond breaker [26]; consequently, it can be suggested that in more amorphous gels, due to the higher mobility of the PVA chains between the crystalline parts, DNA molecules evidenced stronger self interactions, generating aggregate structures and, thus, increasing the retention (α) of DNA inside the gel membrane. On the other hand, the effect of NaBr, on the DNA structure, in the gel membrane, is similar to that found by the addition of an azobenzene trimethylammonium bromide surfactant in DNA aqueous solution upon exposure to visible radiation [27]. Using the same arguments, the decrease in the rate constant of the DNA release with an increase of the retention degree can be attributed to a stabilization of DNA in the gel state. The last argument is also justified by the analysis of the effect of ionic strength on the partition coefficient and release rate constant of DNA from PVA membranes. The analysis of data (Table 1) suggests that an increase of the ionic strength leads to a higher retention of DNA inside gel, leading to an increase of DNA concentration gradient and, consequently, to a lower k_R. This can be justified by a salting-in phenomena [28], which contribute for a stabilization of the DNA inside the gel phase. Such stabilization occurs via aggregation of DNA. Consequently, the ability of DNA to diffuse out of gel decreases by steric hindrance [29] and/or by an increase of the resistance coefficient, which is a measure of the friction acting on a solute as it moves through a solvent (the friction acting on an aggregate is higher than that acting on a single molecule) [30].

4.2. Effect of temperature

The effect of temperature on the release of DNA from PVA-DNA gels to unbuffered water was evaluated at 20, 30, 37 and 40°C. Figure 4a, shows the temperature dependency of drug release. It can be seen that the release is temperature-dependent, and α and k_R increase by increasing temperature. It is interesting to note that the rate and distribution coefficients obtained for the release of DNA at 20°C in water is similar to those found for a solution of sodium nitrate 10 mM. With such results we can hypothesise that the delivery DNA mechanism is the same even in the absence of salt.

The temperature dependence of the rate constant, k_R, can be described by the Arrhenius relationship – Equation (5):

$$k_R = k_0 e^{-(E_a/RT)} \tag{5}$$

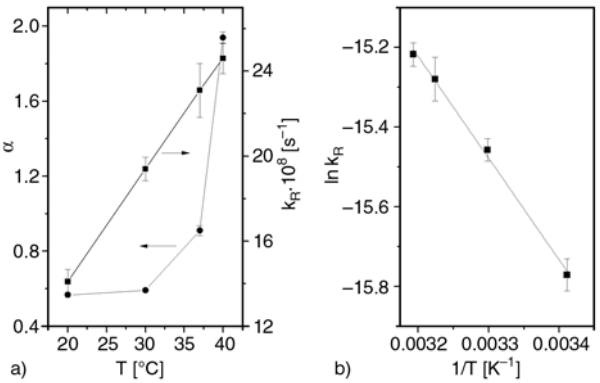

Figure 4. (a) Effect of temperature on the rate constants and distribution coefficients of DNA released from PVA-DNA membranes, (b) Arrhenius treatment of the temperature dependence of the rate constant, k_R

where k_0 is the preexponential factor, E_a is the activation energy, R is the universal gas constant, and T is the absolute temperature. One can determine the value of E_a from the slope of the linear relationship between ln$k$ and the reciprocal of absolute temperature as demonstrated in Figure 4b. It was found that E_a = 21.2(±0.8) kJ/mol. This value is in agreement with the previously reported activation energy for the mobility of DNA in cross-linked polyacrylamide slabs gels (ca. 16 kJ/mol for 700 bp DNA) [31].

4.3. Effect of cationic surfactants

Cationic surfactants interact strongly with DNA. Those interactions depend on the surfactant hydrophobic chain length, charge and headgroup [32, 33]. Figure 5 shows the effect of those factors on the release kinetics and distribution coefficient of DNA, from DNA-containing PVA gel matrices, to dodecyl-based cationic and di-cationic surfactants. All experiments have been carried out using surfactant solutions at pre-micelle concentrations.

The distribution coefficient of DNA in the presence of C_{12}TAB shows that almost all DNA is retained inside gel matrix (the cumulative DNA release is just 5%) [34]. The high retention of DNA inside cryogel, when in the presence of aqueous solutions of dodecyltrimethylammonium bromide, can be justified by the formation of a coating-like structure [35] on the PVA-DNA gel, formed as a consequence of strong interaction between the desorbed DNA and the sorbed surfactant. Upon surfactant charge increase the cumulative release of DNA also increase to around 20%. These values suggest that interaction between C_{12}TAB and DNA is much stronger than with di-cationic surfactants, as has been reported elsewhere [16]. On the other hand, there is no effect of the bulkiness head group, of the bolaamphiphile surfactants, on the distribution coefficients of DNA [33].

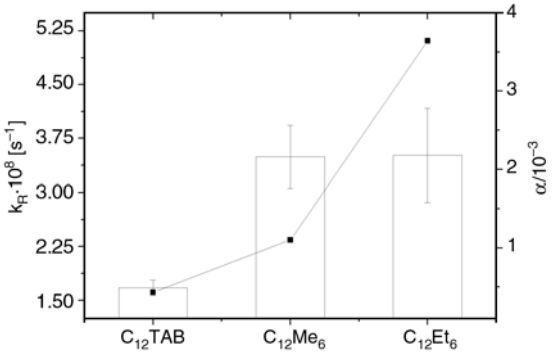

Figure 5. Distribution coefficients, α (columns), and rate constants, k_R (data points), for the release of DNA, from PVA-DNA membranes, to aqueous solutions of different surfactants at 20°C

However, it should be noted that the rate constants increase in the same order $k_R(C_{12}TAB) < k_R(C_{12}Me_6) < k_R(C_{12}Et_6)$, suggesting that the interactions between surfactants and DNA will affect the kinetics mechanism of release.

The main conclusion is that the release of DNA to a surfactant solution is quite sensitive to the balance between hydrophobic/hydrophilic and electrostatic interactions. Further studies have been carried out in order to have a deeper insight on such release mechanisms.

5. Conclusions

The kinetics and equilibrium properties of the release of DNA from PVA-DNA cryogel membranes to different solutions and temperatures have been studied. The first order kinetic law equation was found to be an excellent model to describe the experimental release data. The kinetics of release and the maximum amount of DNA desorbed are quite sensitive to the media where the PVA-DNA gel matrix is immersed. The rate of DNA release from PVA-DNA gels increased with increasing temperature with activation energy (E_a) of 21.2 kJ/mol.

Kinetic and equilibrium parameters show that it will be possible to control the release of DNA, which, coupled with the very good mechanical stability of these gel blends, are promising results for the further development of more appropriated PVA matrices, loaded with DNA, for biomedical and pharmaceutical applications. Furthermore, our results show that a simple method can provide useful experimental information on the importance of ion-ion correlation effects in electrolyte-containing DNA solutions.

Acknowledgements

We are grateful to Prof. Bjorn Lindman for his valuable comments on this paper. We thank FCT (Project PTDC/QUI/67962/2006) for financial support.

References

[1] Peppas N. A.: Hydrogels in medicine and pharmacy. vol I–III. CRC Press, Boca Raton (1986).

[2] Amsden B.: Solute diffusion within hydrogels. Mechanisms and models. Macromolecules, **31**, 8382–8395 (1998).
DOI: 10.1021/ma980765f

[3] Satish C. S., Satish K. P., Shivakumar H. G.: Hydrogels as controlled drug delivery systems: Synthesis, crosslinking, water and drug transport mechanism. Indian Journal of Pharmaceutical Sciences, **68**, 133–140 (2006).
DOI: 10.4103/0250-474X.25706

[4] Bayer C. L., Peppas N. A.: Advances in recognitive, conductive and responsive delivery systems. Journal of Controlled Release, **132**, 216–221 (2008).
DOI: 10.1016/j.jconrel.2008.06.021

[5] Leach J. B., Schmidt C. E.: Characterization of protein release from photocrosslinkable hyaluronic acid-polyethylene glycol hydrogel tissue engineering scaffolds. Biomaterials, **26**, 125–135 (2005).
DOI: 10.1016/j.biomaterials.2004.02.018

[6] del Valle E. M. M., Galan M. A., Carbonell R. G.: Drug delivery technologies: The way forward in the new decade. Industrial and Engineering Chemistry Research, **48**, 2475–2486 (2009).
DOI: 10.1021/ie800886m

[7] He C. L., Kim S. W., Lee D. S.: *In situ* gelling stimuli-sensitive block copolymer hydrogels for drug delivery. Journal of Controlled Release, **127**, 189–207 (2008).
DOI: 10.1016/j.jconrel.2008.01.005

[8] Oh J. K., Drumright R., Siegwart D. J., Matyjaszewski K.: The development of microgels/nanogels for drug delivery applications. Progress in Polymer Science, **33**, 448–477 (2008).
DOI: 10.1016/j.progpolymsci.2008.01.002

[9] Klouda L., Mikos A. G.: Thermoresponsive hydrogels in biomedical applications. European Journal of Pharmaceutics and Biopharmaceutics, **68**, 34–45 (2008).
DOI: 10.1016/j.ejpb.2007.02.025

[10] Juntanon K., Niamlang S., Rujiravanit R., Sirivat A.: Electrically controlled release of sulfosalicylic acid from crosslinked poly(vinyl alcohol) hydrogel. International Journal of Pharmaceutics, **356**, 1–11 (2008).
DOI: 10.1016/j.ijpharm.2007.12.023

[11] Patachia S., Valente A. J. M., Baciu C.: Effect of non-associated electrolyte solutions on the behaviour of poly(vinyl alcohol)-based hydrogels. European Polymer Journal, **43**, 460–467 (2007).
DOI: 10.1016/j.eurpolymj.2006.11.009

[12] DeMerlis C. C., Schoneker D. R.: Review of the oral toxicity of polyvinyl alcohol (PVA). Food and Chemical Toxicology, **41**, 319–326 (2003).
DOI: 10.1016/S0278-6915(02)00258-2

[13] Hassan C. M., Peppas N. A.: Structure and applications of poly(vinyl alcohol) hydrogels produced by conventional crosslinking or by freezing/thawing methods. Advances in Polymer Science, **153**, 37–65 (2000).
DOI: 10.1007/3-540-46414-X_2

[14] Lozinsky V. I.: Cryogels on the basis of natural and synthetic polymers: Preparation, properties and application. Russian Chemical Reviews, **71**, 489–511 (2002).
DOI: 10.1070/RC2002v071n06ABEH000720

[15] Lozinsky V. I.: Cryotropic gelation of poly(vinyl alcohol) solutions. Russian Chemical Reviews, **67**, 573–586 (1998).
DOI: 10.1070/RC1998v067n07ABEH000399

[16] Papancea A., Valente A. J. M., Miguel M. G., Lindman B.: PVA-DNA cryogel membranes: Characterization, swelling, and transport studies. Langmuir, **24**, 273–279 (2008).
DOI: 10.1021/la702639d

[17] Reis A. V., Guilherme M. R., Rubira A. F., Muniz E. C.: Mathematical model for the prediction of the overall profile of in vitro solute release from polymer networks. Journal of Colloid and Interface Science, **310**, 128–135 (2007).
DOI: 10.1016/j.jcis.2006.12.058

[18] Beach L., Schweitzer C., Scaiano J. C.: Direct determination of single-to-double stranded DNA ratio in solution using steady-state fluorescence measurements. Organic and Biomolecular Chemistry, **1**, 450–451 (2003).
DOI: 10.1039/b209284k

[19] Rosa M., Dias R., Miguel M. G., Lindman B.: DNA-cationic surfactant interactions are different for double- and single-stranded DNA. Biomacromolecules, **6**, 2164–2171 (2005).
DOI: 10.1021/bm050137n

[20] Morán M. C., Miguel M. G., Lindman B.: DNA gel particles. Soft Matter, (in press) (2010).
DOI: 10.1039/b923873e

[21] Crank J.: The mathematics of diffusion. Oxford University press, Oxford (1975).

[22] Lindman B., Forsen S., Forslind E.: Nuclear quadrupole relaxation of bromine-79 in aqueous solutions of quaternary ammonium bromides. The Journal of Physical Chemistry, **72**, 2805–2813 (1968).
DOI: 10.1021/j100854a020

[23] Marcus Y.: Effect of ions on the structure of water: Structure making and breaking. Chemical Reviews, **109**, 1346–1370 (2009).
DOI: 10.1021/cr8003828

[24] Lozinsky V. I., Domotenko L. V., Zubov A. L., Simenel I. A.: Study of cryostructuration of polymer systems. XII. Poly(vinyl alcohol) cryogels: Influence of low-molecular electrolytes. Journal of Applied Polymer Science, **61**, 1991–1998 (1996).
DOI: 10.1002/(SICI)1097-4628(19960912)61:11<1991::AID-APP13>3.0.CO;2-2

[25] Fortini M., Berti D., Baglioni P., Ninham B. W.: Specific anion effects on the aggregation properties of anionic nucleolipids. Current Opinion in Colloid and Interface Science, **9**, 168–172 (2004).
DOI: 10.1016/j.cocis.2004.05.025

[26] Paþachia S.: Blends based on poly(vinyl alcohol) and the products based on this polymer. in 'Handbook of polymer blends and composites' (eds.: Vasile C., Kulshreshtha A. K.) Rapra, Shawbury, 288–365 (2003).

[27] Le Ny A-L. M., Lee C. T.: Photoreversible DNA condensation using light-responsive surfactants. Journal of the American Chemical Society, **128**, 6400–6408 (2006).
DOI: 10.1021/ja0576738

[28] Baker J. P., Stephens D. R., Blanch H. W., Prausnitz J. M.: Swelling equilibria for acrylamide-based polyampholyte hydrogels. Macromolecules, **25**, 1955–1958 (1992).
DOI: 10.1021/ma00033a019

[29] Piai J. E., de Moura M. R., Rubira A. F., Muniz E. C.: Kinetic study of bovine serum albumin (BSA) released from alginate-Ca^{2+}/PNIPAAm hydrogels. Macromolecular Symposia, **266**, 108–113 (2008).
DOI: 10.1002/masy.200850620

[30] Valente A. J. M., Polishchuk A. Y., Burrows H. D., Miguel M. G., Lobo V. M. M.: Sorption/diffusion behaviour of anionic surfactants in polyacrylamide hydrogels: From experiment to modelling. European Polymer Journal, **39**, 1855–1865 (2003).
DOI: 10.1016/S0014-3057(03)00108-3

[31] Djouadi Z., Bottani S., Duval M-A., Siebert R., Tricoire H., Valentin L.: Mobility and activation energy of single-stranded DNA in denaturing cross-linked polyacrylamide slab gels. Journal of Chromatography A, **894**, 231–239 (2000).
DOI: 10.1016/S0021-9673(00)00700-7

[32] Dias R. S., Lindman B., Miguel M. G.: Compaction and decompaction of DNA in the presence of catanionic amphiphile mixtures. The Journal of Physical Chemistry B, **106**, 12608–12612 (2002).
DOI: 10.1021/jp020392r

[33] Dias R. S., Magno L. M., Valente A. J. M., Das D., Das P. K., Maiti S., Miguel M. G., Lindman B.: Interaction between DNA and cationic surfactants: Effect of DNA conformation and surfactant headgroup. The Journal of Physical Chemistry B, **112**, 14446–14452 (2008).
DOI: 10.1021/jp8027935

[34] Morán M. C., Miguel M. G., Lindman B.: Surfactant-DNA gel particles: Formation and release characteristics. Biomacromolecules, **8**, 3886–3892 (2007).
DOI: 10.1021/bm700850z

[35] Morán M. C., Miguel M. G., Lindman B.: DNA gel particles: Particle preparation and release characteristics. Langmuir, **23**, 6478–6481 (2007).
DOI: 10.1021/la700672e

eXPRESS Polymer Letters Vol.4, No.8 (2010) 488–499
Available online at www.expresspolymlett.com
DOI: 10.3144/expresspolymlett.2010.62

Polymer-polymer miscibility in PEO/cationic starch and PEO/hydrophobic starch blends

A. G. B. Pereira[1*], *A. T. Paulino*[2], *A. F. Rubira*[1], *E. C. Muniz*[1]

[1]Grupo de Materiais Poliméricos e Compósitos, GMPC – Departamento de Química Universidade Estadual de Maringá – Av. Colombo 5790 - 87020-900, Maringá, Paraná, Brazil
[2]Departamento de Engenharia de Sistemas Químicos – Faculdade de Engenharia Química. Universidade Estadual de Campinas – Av. Albert Einstein 500, Campinas, São Paulo, Brazil

Received 18 January 2010; accepted in revised form 22 March 2010

Abstract. The main purposes were evaluating the influence of different starches on the miscibility with Poly(ethylene oxide) (PEO) and their effects on the spherulite growth rate. Polymer-polymer miscibility in PEO/cationic starch and PEO/hydrophobic starch blends consisting of different w/w ratios (100/0, 95/05, 90/10, 80/20, 70/30, 65/35 and 60/40) was investigated. This analysis was based on the depression in the equilibrium melting temperature (T_m^0). By treating the data of thermal analysis (Differential Scanning Calorimetry – DSC) with Nishi-Wang equation, a positive value (0.68) was found for the interaction parameter of PEO/cationic starch. For PEO/hydrophobic starch blends, a negative value (–0.63) was obtained for the interaction parameter. The results suggested that PEO/cationic starch system should be immiscible. However, the system PEO/hydrophobic starch was considered to be miscible in the whole range of studied compositions. Through optical microscopy analysis, it was concluded that the spherulite growth rate is significantly affected by changing the amount and the type of starch as well.

Keywords: *polymer blends and alloys, PEO/starch blends, PEO/starch miscibility, PEO/starch spherulite growth rate, biopolymer*

1. Introduction

Blending of polymers is an interesting route for producing new materials, basically due to economics aspects [1]. The miscibility between the polymers is a very important factor in the development of polymer blends [1, 2]. Considering the low entropy associated to the polymers mixture, ΔS_m, the miscibility between the components of a polymer blend is mainly driven by the enthalpy of mixing, ΔH_m. Thus, effects that decrease ΔH_m will favor to the miscibility due to the decrease of the Gibbs energy of mixture, ΔG_m. In the light of this, attractive interactions among side groups or polymer segments are, in most of the cases, responsible for polymer-polymer miscibility.

Different techniques have been used for evaluating the miscibility, for example, thermal analysis through determination of the glass transition temperature (T_g) [3–5], microscopy (Optical Microscopy – OM, Scanning Electronic Microscopy – SEM, Atomic Force Microscopy – AFM, Transmission Electronic Microscopy – TEM, and so on) [5–8] and spectroscopy (Fourier Transform Infrared – FTIR-Image, Raman-Image, Nuclear Magnetic Resonance – NMR, and so on) [9–12].

The presence of an amorphous (or slightly crystalline) component affects the crystallization process of the other polymer component significantly. When a given system is miscible, the equilibrium melting temperature (T_m^0) is expected to be lower

*Corresponding author, e-mail: guilebasso@hotmail.com

than that for the pure crystallizable component. T_m^0 is the melting temperature for a perfect crystal when it presents same chemical potential of the surrounding liquid phase. The mixing of an amorphous (or slightly crystalline) polymer with a highly crystallizable one forming a polymer blend allows the new chemical potential of the liquid phase to be lower than that of the crystalline phase and, therefore, the equality of the chemical potentials of the liquid and the crystalline phases will be settled at lower temperature [13]. In this way, when the polymer blend consists of a crystallizable polymer and an amorphous polymer, the depression in equilibrium melting temperature (T_m^0) may be used for evaluating the polymer-polymer interaction parameter (χ_{12}) and thus the system miscibility [14].

Starch is a polysaccharide constituted by portions of amylose (linear) and amylopectin (branched) usually in a ratio of 20%:80%, respectively [15, 16]. Often, it comes from vegetables such as cassava, corn, wheat, among others. Taking into account its interesting properties such as biodegradability [17, 18], biocompatibility [19], availability and low costs [18], starch has been extensively studied as drug delivery system [20–22], cell culture scaffolds in tissue engineering [23, 24], papermakers [25], adhesives [26], polymer blends and composites [27–29], and others. In general, chemical modifications (grafting) and physical mixture (blending) [30] are some strategies employed in order to overcome limitations such as immiscibility with unlike polymers, unsatisfactory mechanical properties and degradation at low temperature [31].

Poly(ethylene oxide) (PEO), a semi-crystalline synthetic polymer, has the general molecular structure $(CH_2CH_2O)_n$. Due to its biocompatibility and low toxicity, the FDA has approved its use in many biomedical devices [32], including drug delivery systems [33, 34], tissue replacement and scaffolds [35–37], and surface coatings for the inhibition of protein and/or cell adsorption [38–41].

PEO/starch blends present great potential applications mainly in the biomedical field, like scaffolds for cell culture and tissue engineering [42–44]. This work is devoted to investigate the miscibility and crystallization rates of starches (cationic and hydrophobic) with PEO in different weight ratios and crystallization temperatures. Differential scanning calorimetry (DSC) was applied to evaluate the T_m^0 values and thermal behavior of system, by considering the miscibility as response. The spherulites growth rates were analyzed by the use of an optical polarized microscopy. The determination of miscibility was based on the evaluation of equilibrium melting point depression through the Nishi-Wang equation [14].

2. Experimental

2.1. Materials

PEO (Aldrich 18,199-4, M_v: 200 kg/mol). Hydrophobic starch, 9.4 mol% ethyl groups substituted on hydroxyl. Cationic starch, 5.8 mol% with quaternary ammonium salts substituted on hydroxyl. The modified starches are commercial samples gently donated by Lorenz Company (Cianorte, Brazil). The unmodified starch was donated by Impal S.A. (São Tomé, Brazil). All reagents were used without further purification. ^{1}H NMR was used for the determination of the degree of substitution on both modified starches. The value of molar mass of cationic starch is $12 \cdot 10^3$ kg·mol^{-1}, hydrophobic starch is $3.7 \cdot 10^3$ kg·mol^{-1}, and the unmodified starch is $5.4 \cdot 10^3$ kg·mol^{-1}, determined by Gel permeation chromatography/Size exclusion chromatrography (GPC/SEC) as described in the next section.

2.2. Sample preparation

Films of PEO and PEO/starch blends at w/w ratios of 95/05; 90/10; 80/20; 70/30; 65/35; and 60/40 were obtained as follows: for each blend ratio the desired amount of starch was solubilized in distilled water at 80°C, after the cooling of the starch solution the needed quantity of PEO was added to form a final aqueous solution of 5% w/v. Then, films of the different blends were obtained by casting at room temperature. The films were dried for 3 days (ambient conditions, ~25°C, 1 atm) followed by 24 h under vacuum at room temperature (ca. 25°C). The thicknesses of films were around 120 μm.

2.3. Crystallization of pure PEO and PEO/starch blends

The samples were crystallized in the absence of light and under reduced pressure in an aluminum

oven specially constructed for this purpose. The temperature of the system was controlled by a thermo-bath with ±0.1°C of precision. The samples (PEO and blends) were heated up to the molten state (~70°C) and kept at this temperature for 5 min to erase the thermal history. Then, the samples were quickly cooled to a desired crystallization temperature, T_C, and left at that temperature for 1 h. Each sample was crystallized with T_C ranging from 42 to 60°C. The T_C was increased in steps of 3°C.

2.4. DSC analysis

The DSC analysis was carried out in a calorimeter (Shimadzu, Model DSC 50, Japan) at a heating rate of 10°C·min^{-1} under a nitrogen stream of 10 ml·min^{-1}. For the pure PEO and a fixed blend ratio, the DSC curve was run after the sample has been treated at a desired T_C for 1 h. The value of melting point temperature, T_m, was estimated from melting peak, by applying the first derivative method. For the pure PEO and for each PEO/starch blend, the equilibrium melting temperature (T_m^0) was evaluated by using the Hoffman-Weeks plots [45], and the miscibility of the system was accessed based on the interaction parameter value (χ_{12}), which was evaluated by applying the Nishi-Wang equation [14].

2.5. Spherulites growth rate

The spherulites growth rates of pure PEO and PEO/starch blends were measured by the use of a polarized optical microscope equipped with a digital camera connected to a computer. Then, real-time images of crystallizing-events were recorded. The temperature of the sample (T_C) was controlled by a hot-stage (Micro-Química, model MQSDCT-3, Brazil) coupled to the microscope. For a given crystal growing at fixed T_C, the spherulite sizes were calculated, as a function of crystallization time, directly from the stored images, using a screen monitor. PEO spherulites growth rates were obtained from the linear dependence of spherulite size as a function of time at a fixed T_C. Triplicates were made for each blend at each T_C.

2.6. Evaluation of the molar mass of starch by GPC/SEC

Aqueous solutions of starch (0.5 w/v%) were prepared under 24 h of stirring of at 80°C. After, the solutions were diluted with distilled water until a final concentration of 0.25 (w/v%) and then filtered using cotton.

The molar masses of the starches were determined by gel permeation chromatography (GPC, some times also referred to as size exclusion chromatography, SEC) technique using equipment from Varian Inc. Scientific Instruments (USA) at room temperature and a Linear Ultrahydrogel (7.8 mm× 300 mm) chromatographic column and a flow rate of 0.5 ml·min^{-1}. Differential refractometer was used as detector. Pullulan with molar masses ranging from 1 to 100 kg·mol^{-1} were used as references while $NaNO_3$ (0.1 mol·l^{-1}) was used as eluent for building the calibration curve. Straight line dependence of molar mass (M) as a function of elution volume was obtained, fitted by the Equation (1):

$$\log(M) = -0.9273\, V_e + 12.55 \quad (1)$$

where M is the averaged M_n of the standard Pullulan, and V_e is the eluted volume.

2.7. Characterization of the cationic and the hydrophobic starches by FTIR, ^{1}HNMR, ^{13}CNMR and wide angle X-ray scattering (WAXS)

The characterization of the commercial samples of starches was performed by the use of FTIR, NMR spectroscopies and WAXS.

Fourier-transform infrared (FTIR) spectrum of each type of starch was obtained from a FTIR spectrophotometer (Bomem, model MB-100, Canada). The powder polymer was compressed with KBr powder into a tablet sample before the analysis. The spectra were obtained in the wave number range of 400–4000 cm^{-1} with resolution of 2 cm^{-1} by collecting 64 scans.

^{1}H and ^{13}C NMR spectra were obtained through a 300 MHz Varian model Mercury Plus BB spectrometer (USA) using DMSO-$_{d6}$ as solvent (10% wt.v).

Wide-angle X-ray (WAXS) diffraction patterns were obtained using a SHIMADZU XRD-6000 diffractometer (Japan) (40 kV, 30 mA, CuK_α) in the diffraction angle (2θ) ranging from 3 to 60° at a rate of $3°\cdot min^{-1}$.

3. Results and discussion

Miscibility results of PEO/unmodified starch system using the depression of T_m^0 through the Nishi-Wang equation were recently published by our group [46]. So, comparative discussion of the results of this work with those with PEO/unmodified starch will be done in the following sections.

3.1. Characterization of the cationic and the hydrophobic starches

In order to verify the effects of side groups on cationic and the hydrophobic starches introduced through industrial process (due to being commercial samples) on different properties investigated in this work, FTIR, ^1H and ^{13}C NMR spectra and WAXS profiles of such modified starches were obtained and compared to the respective unmodified starch, for the sake of comparison.

The chemical modification of starch generally occurs by the grafting of functional groups, mainly by the substitution of the hydrogen atom of the hydroxyl groups [47]. For the preparation of cationic starch, a common way is by the introduction of ammonium salts in the backbone of starch [48]. In the case of hydrophobic starch, the groups to be grafted to the starch chain are normally hydrocarbon chains [49].

Figure 1 shows the FTIR spectra obtained for cationic, hydrophobic and unmodified starches. The spectra presented almost the same profile. The characteristic vibrational modes that appear at 1451, 1121 and 1017 cm^{-1} were attributed to C–O stretching of the unhydroglucose units. A broad band at 3414 cm^{-1} was attributed to O–H vibration. The band at 2926 cm^{-1} is typical of C–H vibration. The more significant difference among them is related to the hydrophobic starch, in which the C–O–C and C–O–H vibrational mode (in the range

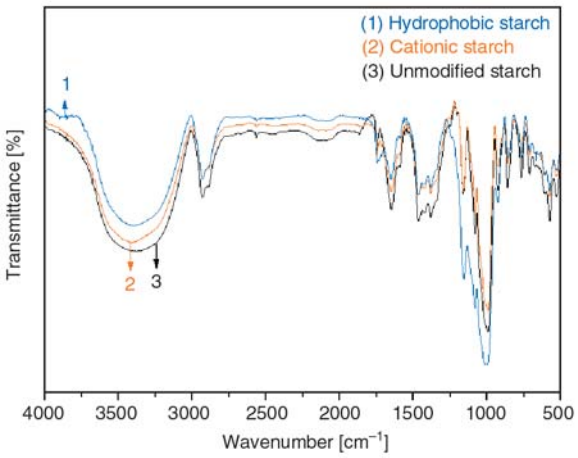

Figure 1. FTIR spectra for unmodified, cationic and hydrophobic starches

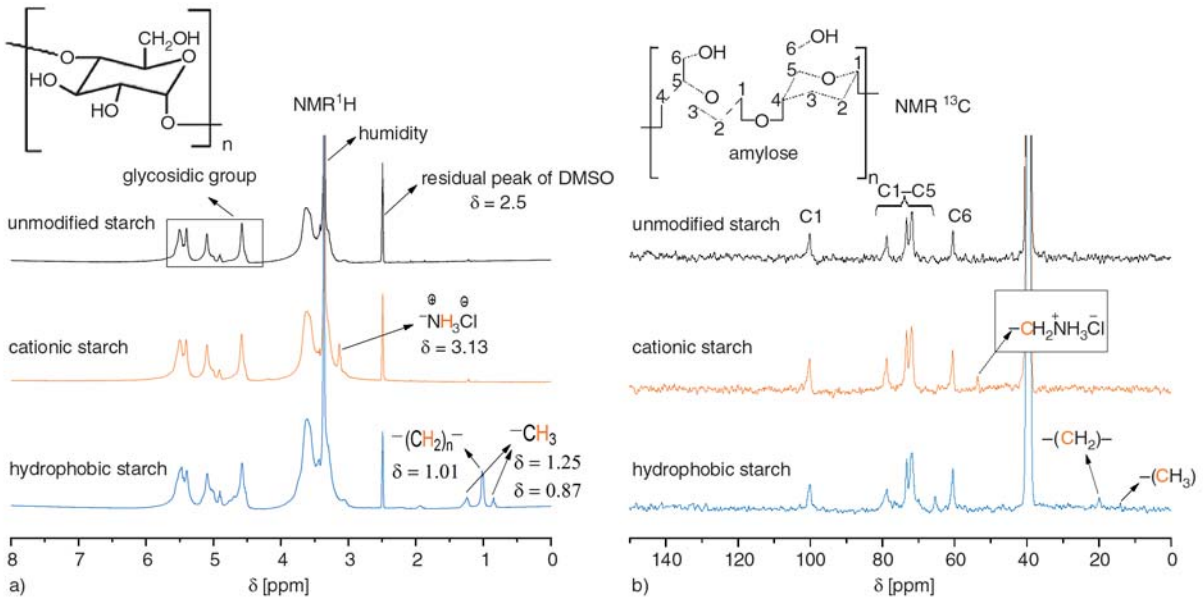

Figure 2. Nuclear Resonance magnetic of unmodified starch, cationic starch and hydrophobic starch a) ^1H NMR and b) ^{13}C NMR

of 1300–950 cm^{-1}) presented a higher intensity compared to the other starches.

^{1}H and ^{13}C NMR spectra obtained from starches (unmodified, cationic and hydrophobic) are presented in Figure 2a and 2b, respectively. From those spectra it is possible to point out that the starches are chemically different. The presence of the peak at δ = 3.13 on the ^{1}H NMR cationic starch spectrum was observed. Such signal was assigned to hydrogen atoms bonded to nitrogen atom, confirming the presence of ammonium salt on the polymer chains of cationic starch. It was also confirmed by the presence of the ^{13}C peak at ca. δ = 52 which was attributed to carbon atom bonded to nitrogen.

In the case of hydrophobic starch, the signals on ^{1}H NMR spectrum at δ = 1.01 (–CH_2–), δ = 1.25 and δ = 0.87 (–CH_3) indicate the presence of hydrocarbon side groups in the starch polymer chains that was also confirmed by the ^{13}C peaks at ca. δ = 12.5 and δ = 20 attributed to –CH_2– and –CH_3 groups. Nevertheless, the hydrocarbon chains should not be longer, due the fact that the integration of those peaks is very small in relation to the other peaks.

Although the NMR analysis showed the chemical groups grafted in the both cationic and hydrophobic starch chains, such fact is not clear in the FTIR spectra, suggesting that the degree of modification should be low, as confirmed by the calculus of modification from the ^{1}H NMR spectra.

Figure 3 presents the WAXS patterns for modified and unmodified starches. It is appropriate to notice that those starches do not present any well resolved peak; otherwise the curves are in halo form, suggesting that the starches comprise structure with a very low degree of crystallinity, and for that reason in this work they were considered as amorphous.

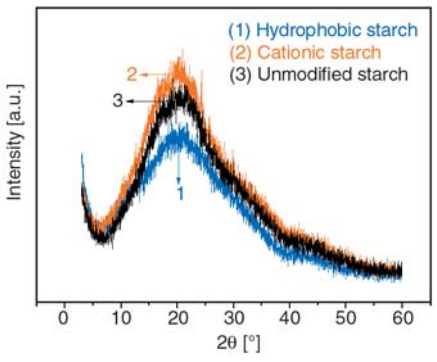

Figure 3. WAXS patterns for different starches (unmodified, cationic and hydrophobic)

3.2. Thermal analysis from DSC data

Thermograms were obtained for pure PEO and for several PEO/starch blends after being crystallized at given crystallization temperatures (T_C, ranging from 42 to 60°C). The non-equilibrium melting temperature value (T_m) was determined through the inflection point of the first derivative of the melting peak, as previously discussed [46].

According to Hoffman and Weeks approach [14, 45, 50], the melting temperature of an ensemble of crystals that: i) is large enough to neglect surface effects; ii) is in equilibrium with the liquid phase; and iii) presents perfection degree of crystallinity consistent with the minimum free energy, is defined as equilibrium melting temperature, T_m^0. Due to the high molar mass of polymers, their crystals are, in general, small and also display elevated density of defects. In this sense, the crystallization temperature (T_C) has a great influence on T_m, which one commonly is lower than T_m^0.

After all the DSC runs for pure PEO and for a given the PEO/Starch blends were accomplished, the respective T_m^0 values were evaluated through the Hoffman-Weeks method [45] as showed in Figure 4, by applying the Equation (2):

$$T_m = \left(\frac{1}{\eta}\right)T_C + T_m^0\left(1-\frac{1}{\eta}\right) \tag{2}$$

where T_m is the non-equilibrium melting temperature, η is the lamellar thickness factor, which is the ratio of the lamellar thickness to the critical nucleus thickness in the crystallization process [45]. This equation means that the crystallization temperature (T_C) affects the melting point (T_m) of a polymer, mainly attributed to the dependence of polymer chains mobility on the temperature [50].

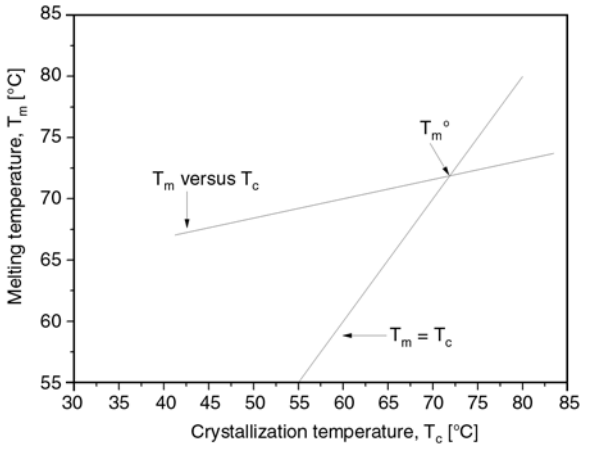

Figure 4. The equilibrium melting temperature (T_m^0) determination

As described in the introductory section, the depression in T_m^0 has been widely used to evaluate the miscibility of a polymer pair consisting of an amorphous and a crystalline component. Nishi and Wang [14] depicted the decrease of the T_m^0 in a crystalline polymer due to the presence of an amorphous miscible component and such depression can be predicted in through the Equation (3):

$$\frac{1}{T^0_{m_{PEO}}} - \frac{1}{T^0_{m_{Blend}}} = \frac{RV^u_{PEO}}{V^u_{starch}\Delta H^u_{PEO}} \cdot \left[\frac{\ln \phi_{PEO}}{m_{PEO}} + \left(\frac{1}{m_{PEO}} - \frac{1}{m_{starch}} \right) \phi_{starch} + \chi_{PEO,starch} \phi^2_{starch} \right] \quad (3)$$

where V_i^u is the molar volume of the repeating unit of the polymer; ΔH^u_{PEO} is the melting enthalpy of fully crystalline PEO; ϕ is the volume fraction; χ_{12} is the polymer-polymer interaction parameter; and m_i is the average-number of repeating unit of *i* component. The first and second terms (inside brackets) on the right side of equation refer to the entropy of mixing contribution for the decreasing of the equilibrium melting temperature, while the third term refers to the enthalpy share. Regarding macromolecules with high molar mass, the effect of the entropy is not remarkable and the depression in the melting temperature will be mainly of enthalpic nature, then the Equation (3) reduces into Equation (4):

$$\frac{1}{T^0_{m_{PEO}}} - \frac{1}{T^0_{m_{Blend}}} = \left(\frac{RV^u_{PEO}}{V^u_{starch}\Delta H^U_{PEO}} \right) \chi_{PEO,starch} \phi^2_{starch} \quad (4)$$

Based on Flory-Huggins theory, it can be shown that negatives values for the χ_{12} are correlated to existence of interactions between the polymers, thus resulting in the miscibility of the system.

So, after determination of the T_m^0 values for the blends, the evaluation of polymer-polymer interaction parameter and, consequently, the miscibility of the system were performed through the Nishi-Wang equation (Equation (4).

Figures 5 and 6 show the dependence of $1/T^0_{m_{PEO}} - 1/T^0_{m_{Blend}}$ to ϕ^2_{starch} for PEO/cationic starch and PEO/hydrophobic starch blends, respectively. The slope of the curve is related to the value of χ_{12}. Also, negative slope means that χ_{12} is negative-valued, then the system should be miscible. On the other hand, positive slope leads to positive values for χ_{12} suggesting immiscibility [51].

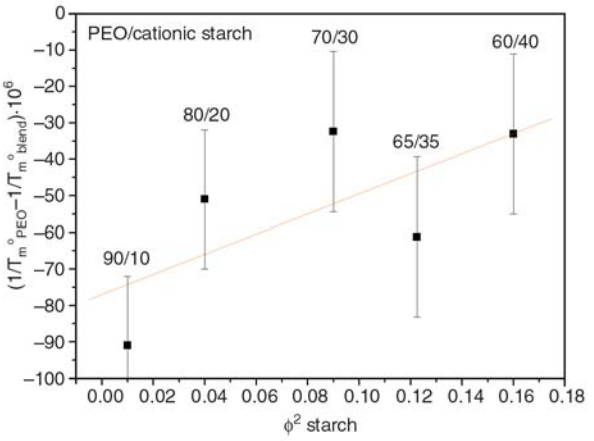

Figure 5. Dependence of $1/T^0_{m_{PEO}} - 1/T^0_{m_{Blend}}$ with ϕ^2_{starch} for PEO/cationic starch blends

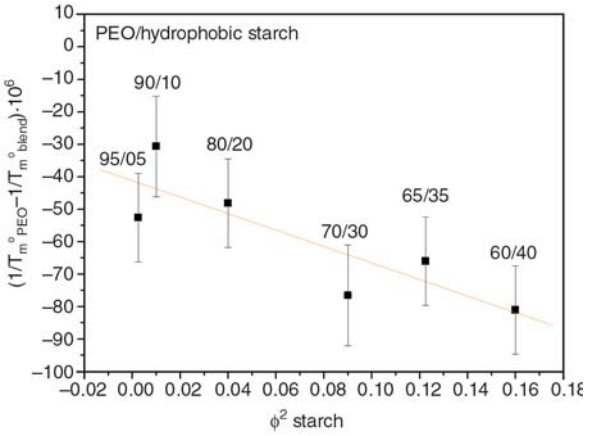

Figure 6. Dependence of $1/T^0_{m_{PEO}} - 1/T^0_{m_{Blend}}$ with ϕ^2_{starch} for PEO/hydrophobic starch blends

For PEO/cationic starch, the interaction parameter χ_{12} was determined as being 0.68. The following values were used for such evaluation:

$R = 8.314$ J·K^{-1}·mol^{-1},
$\Delta H_{PEO} = 7.6$ J·K^{-1}·mol^{-1},
$\Delta H^u_{PEO} = 40.3 \cdot 10^{-6}$ m^3·mol^{-1} and
$V^u_{starch} = 104.7 \cdot 10^{-6}$ m^3·mol^{-1}

obtained from the density $1.5 \cdot 10^3$ Kg·m^{-3} [52]. The blend ratio at 95/05 was not used for such to evaluating, due to the fact that there was an increase in T_m, when compared to the pure PEO. The positive value for χ_{12} indicated a complete immiscibility of the polymers.

In spite of the existence of errors associated to the measurement from Figure 6 in the same extension from Figure 5, the interaction parameter for *PEO/hydrophobic starch* was negative $\chi_{12} = -0.63$, indi-

cating that the system is miscible in the whole range of studied compositions.

According to the Nishi-Wang equation, χ_{12} should be independent of composition or of morphology upon determination of T_m^0 [14, 53]. This implies that the equation concerned could not completely fit the experimental data and the occurrence the intercept far from the origin has been reported [54]. Although the starches present only a low degree of modification, it seems that it is enough to induce difference on miscibility behavior with starch/PEO blends. Besides, an important factor that might have contributed to those behaviors is the different molar masses (not deeply studied in this work).

It is known the effect of the solvent on the miscibility of a polymer pair. For instance, PMMA/PVAc is miscible in chloroform at 30°C whereas in DMF, at the same temperature, the blend is immiscible [55].

Regarding PEO/starch blends, they were prepared by casting from aqueous solution. In the case of samples containing cationic starch the interaction water/starch should be favorable in relation to PEO/starch considering the high dielectric constant

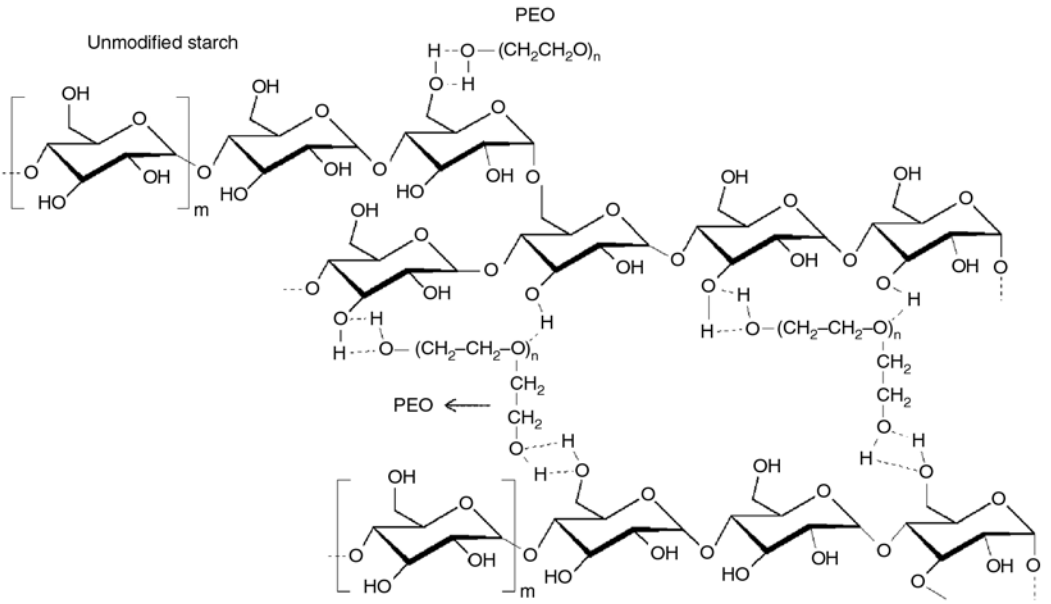

Figure 7. Possible interactions in unmodified starch/PEO

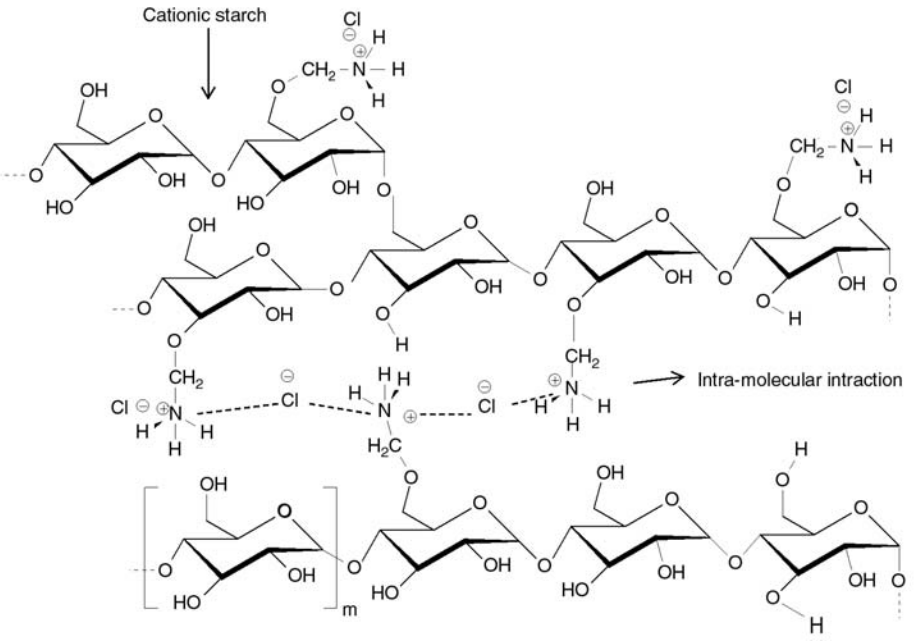

Figure 8. Possible interactions in cationic starch/PEO

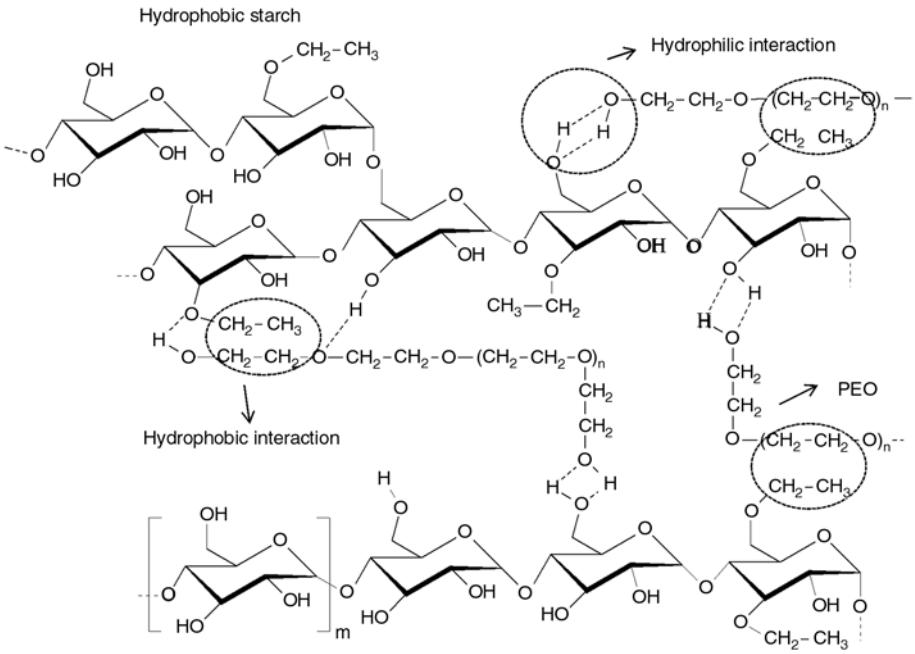

Figure 9. Possible interactions in hydrophobic starch/PEO

of water (ca. 78 at 20°C) [56]. After the drying process, the mobility of the starch chains is not enough to allow conformational changes in order to interact with PEO leading to miscible system. Also, the cationic groups grafted onto starch present intra-molecular interactions destroying the H-bonds between PEO and starch that it would probably occur if the starch was not modified.

Concerning blends with hydrophobic starch, the miscibility is understood as the synergy of two kinds of interactions, the hydrophilic H-bond interactions between hydroxyl groups of starch and oxygen atom of the ether group of PEO, and the hydrophobic interactions between the hydrophobic segments in the starch chain and the ethyl group present in the repeated units of PEO. The possible interactions between PEO and starches (unmodified, cationic and hydrophobic) are suggested in Figures 7–9.

3.3. Spherulites growth rates

The crystallization rates are dependent on the energy involved in the transport of the polymer chains towards to the growing crystals and also to the energy barrier for creation of secondary nuclei with a critical size [57]. These terms depend on the molecular characteristics of each component. For that reason, the crystallization rates become dependent on system-characterizing parameters, such as

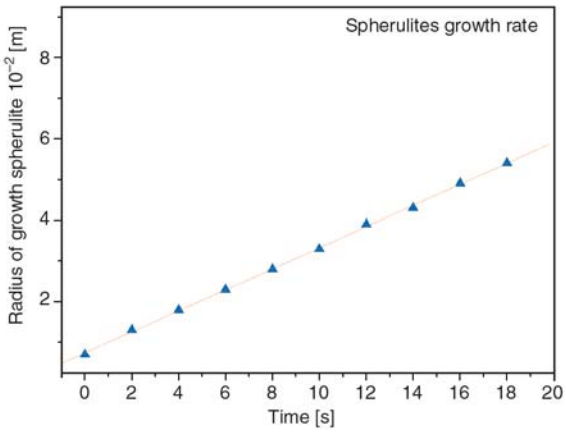

Figure 10. Dependence of isothermal radial growth rate of PEO as function of time (linear behavior)

T_C, T_g, T_m, and molar mass. The addition of a miscible amorphous component often causes the depression in the growth rate, owing the reduction of the melting temperature at equilibrium.

Figure 10 shows, in generic form, the time-dependent spherulite size at a defined T_C. The slope of the straight line is the spherulites growth rate for the respective blend ratio at a given T_C. It is important to notice that the isothermal spherulites growth presented linear dependence on time for all blend ratios.

When the radial growth rate for a given spherulite is plotted against the crystallization temperature (T_C), a maximum is observed. The temperature dependence spherulite growth rate is understood in terms of two competing process, the rate of molec-

ular transport in the melt (diffusion) which increases with temperature increasing, and the nucleation rate, which decreases with increasing temperature [57]. Diffusion is the prevailing factor at low temperatures, whereas at higher temperatures the nucleation rate is a dominant factor. When the T_C is close to T_g, the macromolecular mobility is drastically reduced and, therefore, the crystallization become slower. If T_C is close to T_m, it follows that the macromolecular mobility is high enough to avoid the crystallization and the nucleation rate would be extremely low [57].

Figure 11 refers to the dependence of the spherulites growth rate to the weight fraction of cationic starch at a given T_C. The spherulites growth rates in PEO/cationic starch remain almost invariable in the range from 80/20 to 60/40. However, for the ratios of 95/05 and 90/10, a considerable increase was observed in the spherulites growth rate, with respect to pure PEO. For instance, the spherulite growth rate for 95/05 ratio rate was twice higher than that observed for the pure PEO. Besides, only the 95/05 blend crystallizes at 59°C. The spherulite growth rate in the PEO/cationic starch blends is higher than that of pure PEO (with the exception of 65/35 and 60/40 ratios). This fact is another indicating that the blend ratios from 95/05 to 70/30 are immiscible, in agreement with the thermal analysis data. In this case, it may be inferred that cationic starch forms very small nucleus that would act as nucleation agents for the crystallization enhancing the spherulite growth rate.

Figure 12 refers to the dependence of the spherulites growth rate to the weight fraction of hydrophobic starch at a given T_C. In this case, the maximum

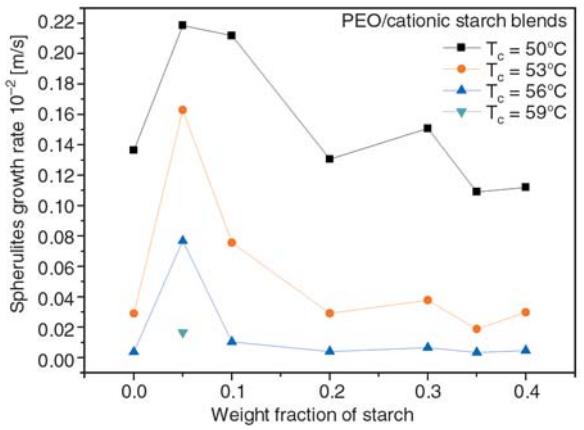

Figure 11. Spherulites growth rates as functions of weight fraction of starch for different ratios of PEO/cationic starch blends at a given T_C

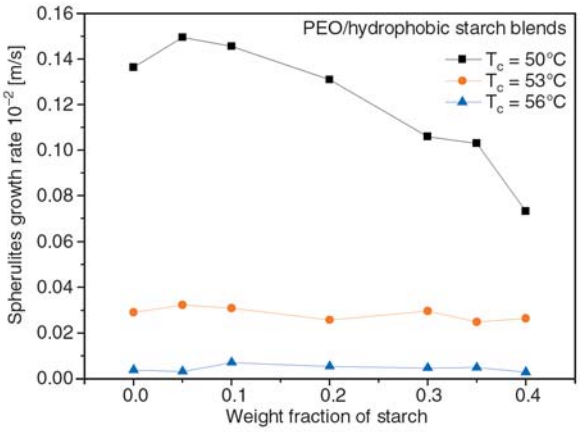

Figure 12. Spherulites growth rates as functions of weight fraction of starch for different ratios of PEO/hydrophobic starch blends at a given T_C

temperature in which the crystallization occurs was 56°C, independent on blend ratio. It may be observed that the crystallization rates do not change significantly for all the blend ratios at 53 and 56°C. Also, it was verified, for this system, a reduction in the crystallizations rates at T_C = 50°C with increasing amount of hydrophobic starch. At this temperature (T_C = 50°C), the spherulites growth rates of blends become practically equal to or lower than that of pure PEO. In the sense of the discussion above, the results would indicate polymer-polymer miscibility for PEO/hydrophobic starch. This would match with the results of miscibility from melting temperature depression analysis.

It should be emphasized that this kind of blends has great potential of application on the biomedical field, such as scaffolds for cell culture. The analyses of citotoxicity of those systems are in progress in our lab.

4. Conclusions

The miscibility and the spherulites growth rate in blends constituted by PEO and either cationic or hydrophobic starches were evaluated by using thermal analysis and optical microscopy. The PEO/cationic system was considered to be immiscible, based on the positive value for the interaction parameter, χ_{12}. This fact, in molecular level, was explained in terms of the solvent effect on the miscibility during the casting process. Also, the cationic groups grafted onto starch may present intramolecular interactions that would destroy the H-bonds, between PEO and starch, that probably occur in PEO/unmodified starch.

The hydrophobic starch was evaluated as miscible with the hydrophilic PEO, taking into account the negative value for interaction parameter, $\chi_{12} = -0.63$. It was pointed out that the small degree of substitution, the short hydrocarbon chain and the hydrophilic and hydrophobic interactions with PEO were responsible to the miscible behavior.

The understanding of the miscibility behavior of such systems (PEO/cationic starch and PEO/hydrophobic starch) maybe an interesting tool to evaluate the potential applications of those materials, mainly in the biomedical field such as scaffolds for cell culture.

References

[1] Sanchez I. C.: Bulk and interface thermodynamics of polymer alloys. Annual Review of Materials Science, **13**, 387–412 (1983).
DOI: 10.1146/annurev.ms.13.080183.002131

[2] Utracki L. A.: Polymer alloys and blends: Thermodynamic and rheology. Hanser, Munich (1989).

[3] Hu Y., Sato H., Zhang J., Noda I., Ozaki Y.: Crystallization behavior of poly(l-lactic acid) affected by the addition of a small amount of poly(3-hydroxybutyrate). Polymer, **49**, 4204–4210 (2008).
DOI: 10.1016/j.polymer.2008.07.031

[4] Haddadine-Rahmoun N., Amrani F., Arighi V., Cowie J. M. G.: Interpolymer complexation and thermal behaviour of poly(styrene-*co*-maleic acid)/poly(vinyl pyrrolidone) mixtures. Thermochimica Acta, **475**, 25–32 (2008).
DOI: 10.1016/j.tca.2008.06.013

[5] Reis K. C., Pereira J., Smith A. C., Carvalho C. W. P., Wellner N., Yakimets I.: Characterization of polyhydroxybutyrate-hydroxyvalerate (PHB-HV)/maize starch blend films. Journal of Food Engineering, **89**, 361–369 (2008).
DOI: 10.1016/j.jfoodeng.2008.04.022

[6] Pouteau C., Baumberger S., Cathala B., Dole P.: Lignin-polymer blends: Evaluation of compatibility by image analysis. Comptes Rendus Biologies, **327**, 935–943 (2004).
DOI: 10.1016/j.crvi.2004.08.008

[7] Zeng M., Sun X., Wang Y., Yao X., Xiao H., Wang B., Qi C.: Correlations between the free-volume properties and the miscibility of chitosan/polar polymers blends membranes. Radiation Physics and Chemistry, **77**, 1062–1068 (2008).
DOI: 10.1016/j.radphyschem.2008.01.008

[8] Girotto C., Cheyns D., Aernouts T., Banishoeib F., Lutsen L., Cleij T. J., Vanderzande D., Genoe J., Poortmans J., Heremans P.: Bulk heterojunction organic solar cells based on soluble poly(thienylene vinylene) derivatives. Organic Electronics, **9**, 740–746 (2008).
DOI: 10.1016/j.orgel.2008.05.014

[9] Moore J. A., Kaur S.: Blends of poly(amide-enaminonitrile) with poly(ethylene oxide), poly(4-vinylpyridine), and poly(*N*-vinylpyrrolidone). Macromolecules, **31**, 328–335 (1998).
DOI: 10.1021/ma9701548

[10] Meier R. J.: Vibrational spectrosopy: A 'vanishing' discipline? Chemical Society Reviews, **34**, 743–752 (2005).
DOI: 10.1039/b503880d

[11] Stuart B. H.: A Fourier transform Raman spectroscopy study of the crystallisation behaviour of a poly(ether ether ketone)/poly(ether sulphone) blend. Spectrochimica Acta Part A: Molecular and Biomolecular Spectroscopy, **53**, 107–110 (1997).
DOI: 10.1016/S1386-1425(97)83014-4

[12] Crispim E. G., Rubira A. F., Muniz E. C.: Solvent effects on the miscibility of PMMA/PVAc blends: II. Using two-dimensional NMR method, NOESY. Polymer, **41**, 933–945 (2000).
DOI: 10.1016/S0032-3861(99)00222-0

[13] Fadnis C., Illiger S. R., Rao K. P., Demappa T.: Miscibility studies of HPMC/PVA blends in water by viscosity, density, refractive index and ultrasonic velocity method. Carbohydrate Polymers, **74**, 779–782 (2008).
DOI: 10.1016/j.carbpol.2008.04.036

[14] Nishi T., Wang T. T.: Melting point depression and kinetic effects of cooling on crystallization in poly(vinylidene fluoride)-poly(methyl methacrylate) mixtures. Macromolecules, **8**, 909–915 (1975).
DOI: 10.1021/ma60048a040

[15] García-Alonso A., Jiménez-Escrig A., Martin-Carrón N. M., Bravo L., Calixto F. S.: Assessment of some parameters involved in the gelatinization and retrogration of starch. Food Chemistry, **66**, 181–187 (1999).
DOI: 10.1016/S0308-8146(98)00261-1

[16] Singh J., Kaur L., McCarthy O. J.: Factors influencing the physico-chemical, morphological, thermal and rheological properties of some chemically modified starches for food applications-A review. Food Hydrocolloids, **21**, 1–22 (2007).
DOI: 10.1016/j.foodhyd.2006.02.006

[17] Scott G.: 'Green' polymers. Polymer Degradation and Stability, **68**, 1–7 (2000).
DOI: 10.1016/S0141-3910(99)00182-2

[18] Wang X-L., Yang K-K., Wang Y-Z., Wang D-Y., Yang Z.: Crystallization and morphology of a novel biodegradable polymer system: Poly(1,4-dioxan-2-one)/starch blends. Acta Materialia, **52**, 4899–4905 (2004).
DOI: 10.1016/j.actamat.2004.06.044

[19] Mano J. F., Sousa R. A., Boesel L. F., Neves N. M., Reis R. L.: Bioinert, biodegradable and injectable polymeric matrix composites for hard tissue replacement: State of the art and recent developments. Composites Science and Technology, **64**, 789–817 (2004). DOI: 10.1016/j.compscitech.2003.09.001

[20] Vieira A. P., Ferreira P., Coelho J. F. J., Gil M. H.: Photocrosslinkable starch-based polymers for ophthalmologic drug delivery. International Journal of Biological Macromolecules, **43**, 325–332 (2008). DOI: 10.1016/j.ijbiomac.2008.06.002

[21] Mehyar G. F., Liu Z., Han J. H.: Dynamics of antimicrobial hydrogels in physiological saline. Carbohydrate Polymers, **74**, 92–98 (2008). DOI: 10.1016/j.carbpol.2008.01.023

[22] Sadeghi M., Hoosseinzadeh H.: Synthesis of starch-poly(sodium acrylate-co-acrylamide) superabsorbent hydrogel with salt and pH-responsiveness properties as a drug delivery system. Journal of Bioactive and Compatible Polymers, **23**, 381–404 (2008). DOI: 10.1177/0883911508093504

[23] Salgado A. J., Coutinho O. P., Reis R. L.: Novel starch-based scaffolds for bone tissue engineering: Cytotoxicity, cell culture, and protein expression. Tissue Engineering, **10**, 465–474 (2004). DOI: 10.1089/107632704323061825

[24] Mendes S. C., Reis R. L., Bovell Y. P., Cunha A. M., van Blitterswijk C. A., Bruijn J. D.: Biocompatibility testing of novel starch-based materials with potential application in orthopaedic surgery: A preliminary study. Biomaterials, **22**, 2057–2064 (2001). DOI: 10.1016/S0142-9612(00)00395-1

[25] Sohara A. K., Parmod K., Kansal P., Shishir S.: Effect of cationic starch and long fibered bamboo pulp on the double fold of recycled bagasse paper. Quarterly Journal of Indian Pulp and Paper Technical Journal, **20**, 179–184 (2008).

[26] Packhan D. E.: Adhesive technology and sustainability. International Journal of Adhesion and Adhesives, **29**, 248–252 (2009). DOI: 10.1016/j.ijadhadh.2008.06.002

[27] Mano J. F., Reis R. L.: Viscoelastic monitoring of starch-based biomaterials in simulated physiological conditions. Materials Science and Engineering A, **370**, 321–325 (2004). DOI: 10.1016/j.msea.2003.08.088

[28] Liao H. T., Wu C. S.: Preparation and characterization of ternary blends composed of polylactide, poly(ε-caprolactone) and starch. Materials Science and Engineering: A, **515**, 207–214 (2009). DOI: 10.1016/j.msea.2009.03.003

[29] Wu R-L., Wang X-L., Li F., Li H-Z., Wang Y-Z.: Green composite films prepared from cellulose, starch and lignin in room-temperature ionic liquid. Bioresource Technology, **100**, 2569–2574 (2009). DOI: 10.1016/j.biortech.2008.11.044

[30] Mano J. F., Koniarova D., Reis R. L.: Thermal properties of thermoplastic starch/synthetic polymer blends with potential biomedical applicability. Journal of Materials Science: Materials in Medicine, **14**, 127–135 (2003). DOI: 10.1023/A:1022015712170

[31] Hoffmann B., Volkmer E., Kokott A., Weber M., Hamisch S., Schieker M., Mutschler W., Ziegler G.: A new biodegradable bone wax substitute with the potential to be used as a bone filling material. Journal of Materials Chemistry, **17**, 4028–-4033 (2007). DOI: 10.1039/b707992n

[32] Lee K. Y., Yuk S. H.: Polymeric protein delivery systems. Progress in Polymer Science, **32**, 669–697 (2007). DOI: 10.1016/j.progpolymsci.2007.04.001

[33] Nagata M., Yamamoto Y.: Photoreversible poly(ethylene glycol)s with pendent coumarin group and their hydrogels. Reactive and Functional Polymers, **68**, 915–921 (2008). DOI: 10.1016/j.reactfunctpolym.2008.01.003

[34] Salmaso S., Semenzato A., Bersani S., Matricardi P., Rossi F., Caliceti P.: Cyclodextrin/PEG based hydrogels for multi-drug delivery. International Journal of Pharmaceutics, **345**, 42–50 (2007). DOI: 10.1016/j.ijpharm.2007.05.035

[35] Kuo Y-C., Ku I-N.: Cartilage regeneration by novel polyethylene oxide/chitin/chitosan scaffolds. Biomacromolecules, **9**, 2662–2669 (2008). DOI: 10.1021/bm800651r

[36] Reignier J., Huneault M. A.: Preparation of interconnected poly(ε-caprolactone) porous scaffolds by a combination of polymer and salt particulate leaching. Polymer, **47**, 4703–4717 (2006). DOI: 10.1016/j.polymer.2006.04.029

[37] Hou Q., Grijpma D. W., Feijen J.: Porous polymeric structures for tissue engineering prepared by a coagulation, compression moulding and salt leaching technique. Biomaterials, **24**, 1937–1947 (2003). DOI: 10.1016/S0142-9612(02)00562-8

[38] Bozukova D., Pagnoulle C., Pauw-Gillet M. C., Desbief S., Lazzaroni R., Ruth N., Jérome R., Jérome C.: Improved performances of intraocular lenses by poly(ethylene glycol) chemical coatings. Biomacromolecules, **8**, 2379–2383 (2007). DOI: 10.1021/bm0701649

[39] Chen H., Zhang Z., Chen Y., Brook M. A., Sheardown H.: Protein repellant silicone surfaces by covalent immobilization of poly(ethylene oxide). Biomaterials, **26**, 2391–2399 (2005). DOI: 10.1016/j.biomaterials.2004.07.068

[40] Unsworth L. D. Sheardown H., Brash J. L.: Polyethylene oxide surfaces of variable chain density by chemisorption of PEO-thiol on gold: Adsorption of proteins from plasma studied by radiolabelling and immunoblotting. Biomaterials, **26**, 5927–5933 (2005). DOI: 10.1016/j.biomaterials.2005.03.010

[41] Archambault J. G., Brash J. L.: Protein repellent polyurethane-urea surfaces by chemical grafting of hydroxyl-terminated poly(ethylene oxide): Effects of protein size and charge. Colloids and Surfaces B: Biointerfaces, **33**, 111–120 (2004).
DOI: 10.1016/j.colsurfb.2003.09.004

[42] Willerth S. M., Sakiyama-Elbert S. E.: Approaches to neural tissue engineering using scaffolds for drug delivery. Advanced Drug Delivery Reviews, **59**, 325–338 (2007).
DOI: 10.1016/j.addr.2007.03.014

[43] Popelka Š., Machová L., Rypácek F.: Adsorption of poly(ethylene oxide)-*block*-polylactide copolymers on polylactide as studied by ATR-FTIR spectroscopy. Journal of Colloid and Interface Science, **308**, 291–299 (2007).
DOI: 10.1016/j.jcis.2006.12.022

[44] Deitzel J. M., Keinmeyer J. D., Hirnonen J. K., Tan N. C. B.: Controlled deposition of electrospun poly(ethylene oxide) fibers. Polymer, **42**, 8163–8170 (2001).
DOI: 10.1016/S0032-3861(01)00336-6

[45] Hoffman J. D., Weeks J. J.: Melting process and the equilibrium melting temperature of polychlorotrifluoroethylene. Journal of Research of the National Bureau of Standards Section A: Physics and Chemistry, **66**, 13–28 (1962).

[46] Pereira A. G. B., Gouveia R. F., de Carvalho G. M., Rubira A. F., Muniz E. C.: Polymer blends based on PEO and starch: Miscibility and spherulite growth rate evaluated through DSC and optical microscopy. Materials Science and Engineering: C, **29**, 499–504 (2009).
DOI: 10.1016/j.msec.2008.09.009

[47] Wang P-X., Wu X-L., Hua X-D., Kun X., Ying T., Bing D-X., Bo L-W.: Preparation and characterization of cationic corn starch with a high degree of substitution in dioxane-THF-water media. Carbohydrate Research, **344**, 851–855 (2009).
DOI: 10.1016/j.carres.2009.02.023

[48] Baek K., Yang J. S., Kwon T. S., Yang J. W.: Cationic starch-enhanced ultrafiltration for Cr(VI) removal. Desalination, **206**, 245–250 (2007).
DOI: 10.1016/j.desal.2006.03.568

[49] Qiao L., Gu Q-M., Cheng H. N.: Enzyme-catalyzed synthesis of hydrophobically modified starch. Carbohydrate Polymers, **66**, 135–140 (2006).
DOI: 10.1016/j.carbpol.2006.02.033

[50] Coleman M. M., Painter P. C.: Hydrogen bonded polymer blends. Progress in Polymer Science, **20**, 1–59 (1995).
DOI: 10.1016/0079-6700(94)00038-4

[51] Rim P. B., Runt J. P.: Melting point depression in crystalline/compatible polymer blends. Macromolecules, **17**, 1520–1526 (1984).
DOI: 10.1021/ma00138a017

[52] Mark J. E.: Polymer data handbook. Oxford University Press, New York (1999).

[53] Chow T. S.: Miscible blends and block copolymers. Crystallization, melting and interaction. Macromolecules, **23**, 333–337 (1990).
DOI: 10.1021/ma00203a057

[54] Alfonso G. C., Russell T. P.: Kinetics of crystallization in semicrystalline/amorphous polymer mixtures. Macromolecules, **19**, 1143–1152 (1986).
DOI: 10.1021/ma00158a036

[55] Crispim E. G., Rubira A. F., Muniz E. C.: Solvent effects on the miscibility of poly(methyl methacrylate)/poly(vinyl acetate) blends: I: Using differential scanning calorimetry and viscometry techniques. Polymer, **40**, 5129–5135 (1999).
DOI: 10.1016/S0032-3861(98)00653-3

[56] Cabane B., Vuilleumier R.: The physics of liquid water. Comptes Rendus Geoscience, **337**, 159–171 (2005).
DOI: 10.1016/j.crte.2004.09.018

[57] Sperling L. H.: Introduction to physical polymer science. Wiley, Bethlehem (2006).

eXPRESS Polymer Letters Vol.4, No.8 (2010) 500–508
Available online at www.expresspolymlett.com
DOI: 10.3144/expresspolymlett.2010.63

Swelling of organoclays in styrene. Effect on flammability in polystyrene nanocomposites

L. Timochenco[1], V. G. Grassi[3], M. Dal Pizzol[3], J. M. Costa[2], L. G. Castellares[2], C. Sayer[1], R. A. F. Machado[1], P. H. H. Araújo[1]*

[1]Department of Chemical Engineering, Federal University of Santa Catarina, CEP 88040 900, Florianópolis SC, Brazil
[2]CENPES/PETROBRÁS R&D Center Rio de Janeiro RJ, Brazil
[3]Innova S/A Triunfo RS, Brazil

Received 14 January 2010; accepted in revised form 23 March 2010

Abstract. In this work the effect of the compatibility between organoclays and styrene on the flammability of polystyrene/clay nanocomposites obtained through *in situ* incorporation was investigated. The reactions were carried out by bulk polymerization. The compatibility between organoclays and styrene was inferred from swelling of the organoclay in styrene. The nanocomposites were characterized by X-ray diffraction and Transmission Electron Microscopy. The heat release rate was obtained by Cone Calorimeter and the nanocomposites were tested by UL94 horizontal burn test. Results showed that intercalated and partially exfoliated polystyrene/clay nanocomposites were obtained depending on the swelling behavior of the organoclay in styrene. The nanocomposites submitted to UL94 burning test presented a burning rate faster than the virgin polystyrene (PS), however an increase of the decomposition temperature and an accentuated decrease on the peak of heat release of the nanocomposites were also observed compared to virgin PS. These results indicate that PS/clay nanocomposites, either intercalated or partially exfoliated, reduced the flammability approximately by the same extent, although reduced the ignition resistance of the PS.

Keywords: *nanocomposites, flammability, polystyrene, organoclay, swelling*

1. Introduction

In situ incorporation is an effective route to obtain polystyrene/clay nanocomposites [1–10]. Nonetheless, the compatibility between monomer and organoclay is a critical factor in determining the microstructure of nanocomposites obtained through *in situ* incorporation [1]. A good compatibility between monomer and organoclay is fundamental to disperse the clay in the reaction medium, avoiding its agglomeration. In addition, the penetration of the monomer into the basal space of lamellae allows the entrance of oligomeric radicals and the consequent intercalation of lamellae with polymer. If the separation of the lamellae is high enough, delamination (exfoliation) occurs.

Liauw *et al*. [2] had measured the swelling volume and the viscosity of organoclays in toluene considering that the compatibility of organoclays with styrene can be considered in the same way as with toluene and therefore can be a predictor of state of clay dispersion within the resulting composite. Fu and Qutubuddin [1] determined the swelling behavior of organoclays in styrene comparing wettability and rheology measurements and observed that the organoclay prepared with a styryl group had the highest compatibility with styrene and formed exfoliated polystyrene nanocomposites while the organoclays that presented weaker interaction formed intercalated polystyrene nanocomposites after polymerization of styrene and organoclay

*Corresponding author, e-mail: pedro@enq.ufsc.br

mixtures. Similar results were observed by Arioli *et al.* [3] when comparing the swelling volume of organoclays in styrene. The higher the swelling volume the higher the degree of organoclay exfoliation in polymer matrix after polymerization of styrene in the presence of organoclay. The use of other solvent mixtures (tetrahydrofuran and water) resulted in different clay intercalation with styrene-vinylpyridine (SVP, 36.40 wt% styrene and 63.60 wt% 4-vinylpyridine) block copolymers in the *in situ* formation of polystyrene/clay nanocomposite and the most effective exfoliated nanocomposite, showed the highest thermal stability and the best dynamic mechanical responses [11]. The significant enhancement of both tensile and flexural strength in polymer/clay nanocomposites is usually attributed to the delaminated clay formation [12].

The good dispersion of clay produces a substantial improvement in fire performance in polymeric matrices such as polystyrene [10, 13–18] at least in terms of peak heat release rate (Peak HRR) accessed by cone calorimeter. The suggested mechanism by which clay nanocomposites reduce the heat release rate involves the formation of a char that serves as a barrier to both mass and energy transport [10]. According to Levchik and Weil [19] flame retardancy achieved with nanocomposites alone is not enough for the ignition resistance inferred by the UL-94 test and they suggest a better approach to combine the nanocomposite with another flame retardant, such that the nanocomposite provides the base reduction in flammability, and the secondary flame retardant provides the ignition resistance. Several papers [20–22] investigated the effect of the chemical and physical structure of polymer/clay interfaces on the flammability of polymer composites and nanocomposites. Some of these papers showed that the clay/polymer nanocomposite improved not only the cone calorimetry results, but the UL94 performance as well. One of the reasons is the increase of viscosity caused by clay that arrests the dripping of the polymer during burning which is reflected by the UL94 rating [21].

The objective of this work is to investigate the correlation of the compatibility between monomer and organoclay and the flammability properties of the polystyrene/clay nanocomposite obtained through *in situ* incorporation. To attain this objective, different organoclays were incorporated to the polymer matrix through styrene bulk polymerization. The compatibility between organoclays and styrene was inferred from swelling of the organoclay in styrene. The nanocomposites were characterized and the thermal stability and flammability were studied.

2. Material and methods

Styrene was provided by Innova S.A., Brazil, with a purity about 99.6% and inhibitor (p-terc-butilcatechol) concentration equal to 12 ppm. Benzoyl peroxide (BPO) with 75% of active oxygen P.A. grade (Elf Atochem Chemicals, USA) was used as initiator. The montmorillonite (MMT) containing exchangeable cations of primarily Na^+ was provided by Southern Clay Products, USA. The organoclays were prepared and supplied by Southern Clay (Cloisite 10A and Cloisite 15A), USA, and by SüdChemie (Nanofil 15), Germany. All reactants, including the clays, were used as received, without any previous treatment. The Cloisite 10A and Cloisite 15A clays were the SWy-1 montmorillonite modified by 2MBHT (dimethyl-benzyl-hydrogenated-tallow, quaternary ammonium) and 2M2HT (dimethyl-dihydrogenatedtallow, quaternary ammonium), respectively. The hydrogenated tallow was a mixture of ~65% of C18, ~30% of C16 and ~5% of C14 and the anion was the chloride. The Nanofil 15 clay was a montmorillonite modified with C18 chains (distearyl-dimethyl ammonium chloride).

2.1. Bulk polymerization

At first 3.0% of clay in relation to the total mass of polymer was dispersed in styrene (S) during two hours under vigorous stirring (1200 rpm) in a jacketed reactor at 25°C. This step was conducted to allow the dispersion and swelling of the clay with the styrene. After this initial dispersion step, the reactor temperature was raised up to 90°C and initiator (0.5% w/w related to the total mass of monomer) was added to the reaction medium. Reaction was kept at 90°C for 2 hours after which the reaction medium was transferred to an aluminum vessel and immersed in an oil bath with a gradual temperature increase (20°C/hour) up to 180°C, maintained for 2 additional hours. Nitrogen was fed to the reactor during the whole reaction to avoid inhibition by oxygen.

2.2. Characterization

The swelling volume of organoclays in styrene was measured using a 100 ml measuring cylinder. The sample (1.0 g) was sprinkled onto the styrene surface (100 ml) and it slowly fell to the bottom of the cylinder. The swelling volume was recorded after 24 h (a swelling equilibrium was reached by this time). XRD patterns of organoclays and polystyrene nanocomposites were obtained by using Philips X'Pert X-ray diffractometer, with a Cu tube source (wavelength λ of 1.54056 Å) operated at 1 kW. Transmission electron microscopy (TEM) images of polystyrene/layered silicate (clay) nanocomposites were obtained at 100 kV, with a JEOL electron microscope. The samples were ultramicrotomed with a diamond knife on a Leica Ultracut UCT microtome at room temperature to give 70 nm thick sections. The sections were transferred to carbon-coated Cu grids of 200 mesh. The contrast between the layered silicates and the polymer phase was sufficient for imaging, so no heavy metal staining of sections prior to imaging was required.

Thermogravimetric analyses (TGA) were conducted on a Shimadzu TGA-50 equipment, under inert atmosphere with a N_2 flux of 50 ml/min and heating rate of 10°C/min, until the final temperature, 600°C, was reached. The horizontal burning test UL94 [23] was conducted according to the ASTM D635 procedure [24]. The dimension of the standard bar samples were 125×13×3 mm. The flammability data reported here were the averages of five samples. Combustion behavior was assessed according to the ASTM E 1354 [25] procedure in a Fire Testing Technology (FTT) dual cone calorimeter apparatus. During the test, the materials were subjected to irradiated heat plus the feedback heat from the flame starting from the ignition of the volatile products (ignition time). The aim was to simulate the conditions likely to occur in a real fire [26]. The samples were irradiated at 35 kW/m^2, and the data were collected for the first 250 s, this being regarded as representative of the initial stage of a fire when it can still be stopped before becoming uncontrollable after flashover. The exhaust gas flow rate was 24 l/s. The heat released was calculated from the consumption of oxygen due to combustion. The analysis by cone calorimeter gives the ignition time (T_{ig}), the heat release rate (HRR) and its peak value (Peak HRR), the average value of heat release rate over the entire heat release rate curve for the material during combustion of the sample (Avg HRR) and the total heat release.

3. Results and discussion

Swelling tests were performed in order to characterize the organoclays in respect to their affinity towards styrene. The values of swelling of the three tested clays might be observed in Table 1. According to the results shown in Table 1, two samples (Nanofil 15 and Cloisite 15A) presented moderate swelling values, whereas clay Cloisite 10A presented the highest value. The naturally occurring Na-MMT did not swell in styrene. The higher the swelling volume, the higher the compatibility between the organoclay and styrene. All clays tested in this work were montmorillonite modified with quaternary ammonium salts. The salts used to modify the organophilicity of the clays Nanofil 15 and Cloisite 15A presented dimethyl-dehydrogenated-tallows, being the tallow of Cloisite 15A a mixture of ~65% of C18, ~30% of C16 and ~5% of C14 and the tallow of Nanofil 15 clay was composed by C18 chains. As the swelling value provides an information about the affinity of the clay towards the monomer, Cloisite 10A presented the higher swelling value as its quaternary ammonium salt was composed by a dimethyl-benzyl-hydrogenated-tallow that presents a high compatibility with styrene as observed before by other authors [1, 2]. Similar results were obtained by Fu and Qutubuddin [4] that observed that montmorillonite modified with vinylbenzyldodecyldimethyl ammonium chloride gave the highest styrene dispersion viscosity by a wide margin (more than 10 times), when compared to montmorillonite clays modified with quaternary ammonium salts featuring alkyl chains of C16 to C18. The high degree of styrene compatibility afforded by the styryl group of the quaternary ammonium salt illustrates the importance of matching monomer/polymer structure to that of the intercalant [2].

Table 1. Swelling volumes of Na-MMT and organoclays in Styrene at 25°C

Clay	ml clay/100 ml Sty
Na-MMT	–
Cloisite 10A	26
Cloisite 15A	12
Nanofil 15	15

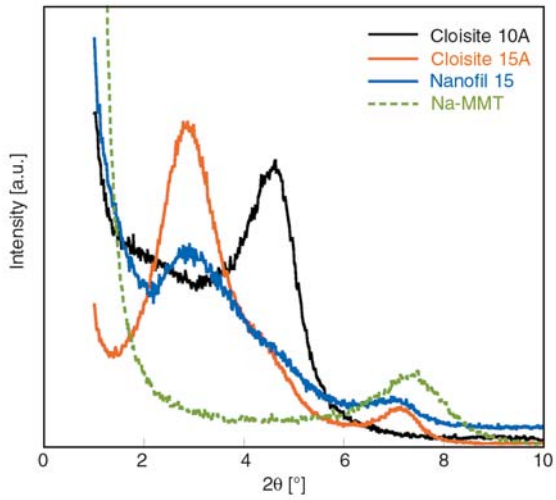

Figure 1. XRD patterns of clays

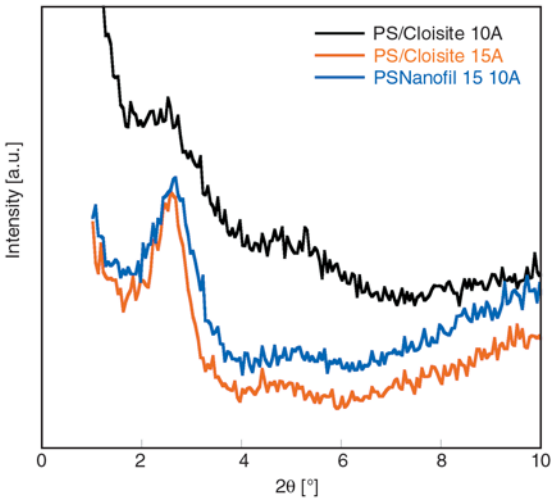

Figure 2. XRD patterns of nanocomposites

The interlamellar layer (d) of the clay was measured by X-ray diffraction (XRD). The d_{001} spacing of clay particles was calculated according to Bragg's law where $d = \lambda/2\sin(\theta)$ at peak positions. The wave-length (λ) of X-ray is 1.5418 Å. In Figure 1 it is possible to observe that all organoclays show sharp peaks and the peak positions shift to lower angles when compared to natural occuring montmorillonite (Na-MMT) which contains exchangeable cations of primarily Na^+. Nanofil 15 and Cloisite 15A presented different diffractograms, although the values of d_{001} spacing (3.03 and 3.07 nm, respectively) were quite similar. The diffractograms of both clays presented a small peak around 1.2 nm that do not correspond to d_{002} spacing and seems to be quite similar to the crystallographic spacing of Na-MMT (1.18 nm). This means that both clays could contain small amounts of tactoids with clays platelets intercalated with cations of Na^+. Cloisite 10A presented just a single peak corresponding to a d_{001} spacing value of 1.91 nm.

In order to determine the effect of the swelling volume of the clay in the monomer, the styrene dispersions were polymerized *in situ*. XRD and TEM were used to characterize the dispersions of the organoclays in polystyrene (PS). The *in situ* incorporation of Na-MMT resulted in a very heterogeneous composite, when the stirring of the reaction medium was stopped the Na-MMT clay sedimented to the bottom of the reaction vessel. No further analysis was performed on this resulting composite. On contrary, the organoclays were very well dispersed in the polystyrene matrix. Figure 2 shows the diffractograms of the resulting nanocomposites. No clearly defined peak can be observed in the curve of PS/Cloisite 10A nanocomposite indicating that the clay could be delaminated. The PS/Cloisite 15A nanocomposite presented the displacement of the peak to 2.58°, corresponding to a basal spacing of 3.42 nm. This means that an increase of the interlayer distance has occurred by PS polymer chains polymerized in the interlayer of clay platelets. A similar diffractogram was observed for PS/Nanofil 15 nanocomposite with a well defined peak at 2θ equal to 2.91° (d_{001} = 3.38 nm) These results indicate that both nanocomposites (PS/Cloisite 15A and PS/Nanofil 15) presented an intercalated structure.

TEM micrographs of the nanocomposites show similar dispersion of all clays in polystyrene. The thin dark lines of Figure 3 suggest that some clay layers of the organophilic clays are exfoliated in polystyrene, while other layers have intercalated structure as it is possible to observe MMT stacks dispersed in polymer matrix. TEM and XRD results suggest that the nanocomposite PS/Cloisite 10A was partially exfoliated whereas the nanocomposites PS/Cloisite 15A and PS/Nanofil 15 presented a predominant intercalated structure.

Thermogravimetric analysis: The TGA data of the samples (Figure 4) showed that the polymer nanocomposites, decompose at higher temperatures compared to virgin PS. The temperature at which 5% degradation occurred, representative of the onset temperature of degradation, and the midpoint degradation temperature, corresponding to the temperature at which the weight loss of the sample

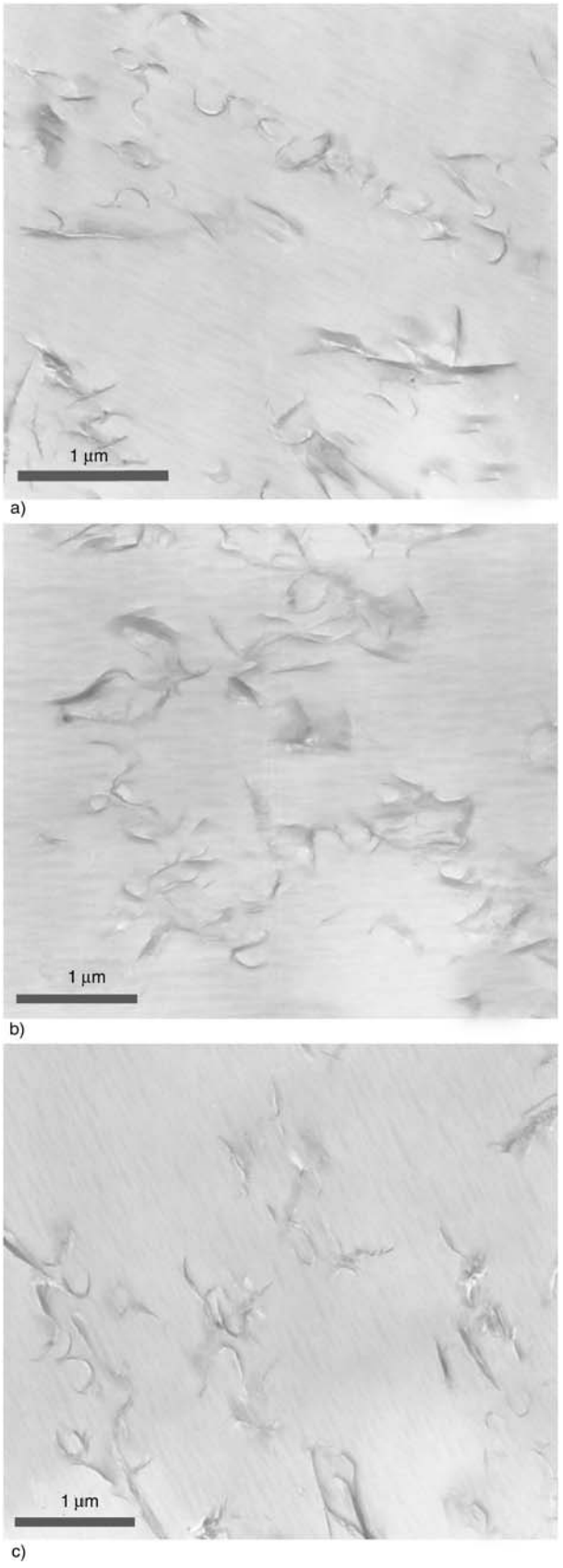

Figure 3. TEM micrographs of the nanocomposites: PS/Cloisite 10A (a), PS/Cloisite 15A (b) and PS/Nanofil 15 (c)

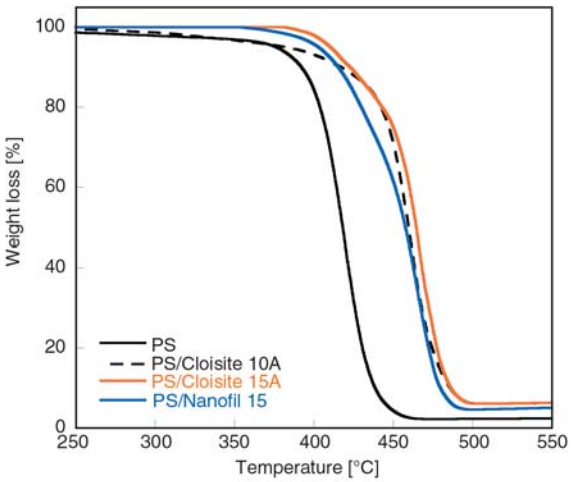

Figure 4. TGA of virgin polystyrene (PS) and of PS/clay nanocomposites

attains 50%, were found to be highest for PS/Cloisite 15A (410.6 and 464.5°C, respectively). The higher degradation temperatures may probably be attributed to extensive interaction of PS with nanodispersed and large surface area organophilic clays that resulted in inhibition of the diffusion of the decomposed product in the polymer matrix. Although all nanocomposites (PS/Cloisite 10A, PS/Cloisite 15A and PS/Nanofil 15) had high mid-point degradation temperatures (459.8, 464.5 and 457.6°C, respectively), when compared to virgin PS (418.1°C), nanocomposite PS/Cloisite 10A lost initial 5% weight at a temperature (382.2°C) just 5.8°C higher than virgin PS (376.4°C).

UL94 test: The results of the flammability analysis assessed by UL94 horizontal burning test are presented in Table 2. These results show that the burning rate was faster for the nanocomposites than for the virgin polystyrene. Similar result was previously reported by other authors that credit the poor UL94 performance of the clay/polymer composite to the presence of the compatibilizers present in the organoclays. These compatibilizers are added to the clay in order to increase the affinity of the clay for the monomer. As UL94 burning test should be regarded primarily as an ignition test and since the

Table 2. Burning rate (UL94)

Sample	Burning rate [mm/min]
PS	12.9
PS/Cloisite 10A	21.2
PS/Cloisite 15A	27.1
PS/Nanofil 15	16.7

organoclays shorten the ignition time they can degrade UL94 performance [27, 28]. Nevertheless, a very different behavior was observed during the burning of virgin PS and PS/organoclay nanocomposites, as during the burning of PS/organoclay nanocomposites, a char structure was formed and no dripping was observed, whereas during the burning of virgin PS specimen dripping of melted polystyrene in flame was constant.

Cone calorimeter: The heat release rates (HRRs) of the virgin polymer (PS) and the nanocomposite (PS/organoclay) during the combustion tests are shown in Figure 5. When the organoclays are present, the ignition time (T_{ig}) decreases from 66 to 52–59 s (see Table 3). Just after ignition, however, the virgin polystyrene heat release rate (HRR) increases much more quickly. The heat release rate of the PS overtakes that of the nanocomposite after 60 s of T_{ig} (HRR = 600 kW/m^2), peaks at 1303 kW/m^2 after 202 s of T_{ig}, and then falls very sharply after 240 s of T_{ig}. The heat release rate of the composite rises regularly to a maximum of 663–704 kW/m^2 after 171–178 s of Tig. Reduction of the peak heat release rate is a typical feature of polymer layered silicate nanocomposites, as reported in the literature [14–18]. The combustion behavior of the nanocomposite is due to a reduction in the mass loss rate, compared to that of the polymer. This greater thermal stability stems from the chemical and physical action of the crystalline layers of the silicate dispersed in the matrix that inhibited the diffusion of the decomposed product in the polymer matrix. Thermal decomposition of the organically modified montmorillonites starts at around 200°C and proceeds according to the Hofmann degradation mechanism [19]. The decomposition products are combustibles that feed the combustion in the flame. Despite a larger heat release rate in the early stage of combustion, the nanocomposite shows an improvement of fire behavior compared to those of the virgin polymer (Table 3). The average heat release rate (Avg. HRR) decreases from 807 kW/m^2 (virgin PS) to 448–475 kW/m^2 (PS/organoclay).

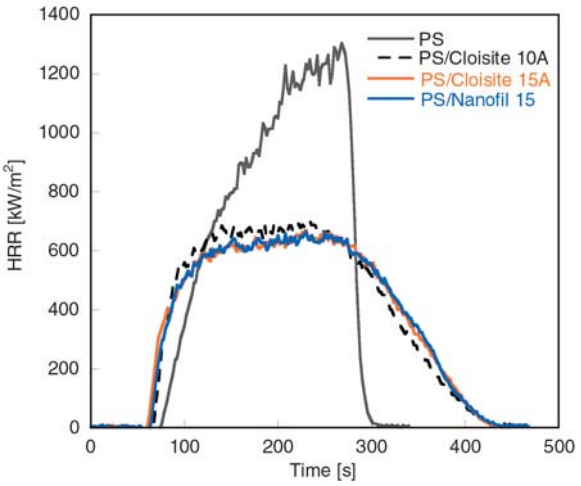

Figure 5. HRR of virgin polystyrene (PS) and of PS/clay nanocomposites

During the cone calorimeter analysis it was observed that once the virgin PS specimen ignited the sample surface did begin to boil rapidly as the polymer burned away, but the flames were steady (not turbulent) as the material burned. After burning no significant char was noted, just some soot and ash in the aluminum sample pan. Whereas for the nanocomposites, once sample ignited the flames were steady and no boiling of polymer underneath the flame front was noted. Formation of condensed phase char was noticeable during the entire burning process. The final char was black and highly cracked, with the aluminum foil clearly seen underneath (see Figure 6). The fire behavior of the nanocomposite PS/Nanofil 15 was identical to that of the others nanocomposites but the char was more pronounced and could be seen sticking up in the flame front area as the sample burned. Char formation is good for fire retardancy purposes as the char prevents the entry of flammable gases into the gas phase and insulates the underlying polymer from the flame [29].

Char formation in cone experiments corroborates the observations during UL94 tests, where a char structure formed during burning was observed for the nanocomposites but not for the virgin PS. The apparently contradictory results of cone calorimeter and UL94 horizontal burning test regarding the

Table 3. Results of the cone calorimeter analysis

Sample	Time to ignition [s]	Time to peak [s]	Peak HRR [kW/m^2]	Avg. HRR [kW/m^2]
PS	66	202	1303	807
PS/Cloisite 10A	59	171	704	475
PS/Cloisite 15A	52	178	669	461
PS/Nanofil 15	55	175	663	448

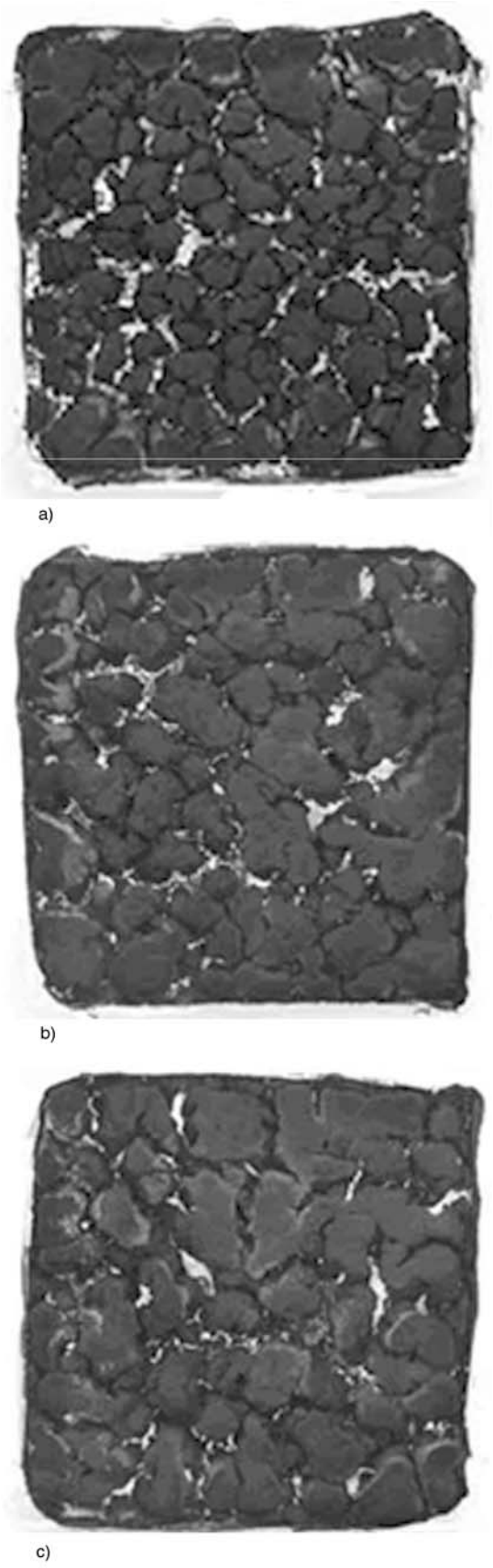

Figure 6. Pictures of the residues of nanocomposites after the cone experiment. a) PS/Cloisite 10A, b) PS/Cloisite 15A, c) PS/Nanofil 15 (pictures size of 75×75 mm)

flammability of the nanocomposites could be explained because UL94 is primarily an ignition test. The thermal degradation of the excess of quaternary ammonium surfactants used to disperse the clays form flammable volatile vapors increasing the probability of early ignition, this behavior was observed in the reduced time to ignition measured by cone calorimeter.

Results indicate that intercalated and partially exfoliated polystyrene/clay nanocomposites presented similar flammability properties assessed by cone calorimeter analysis. These results are in accordance with a recent work of Samyn *et al.* [30] where it was observed that polyamide-6/organoclay nanocomposites exhibit significant reduction of Peak HRR but the nanomorphology (exfoliation, intercalation and presence of tactoids) did not play any significant role. It means that if the nanodispersion is achieved, the polymer/organoclay nanocomposite should exhibit flame retardancy properties, at least in terms of Peak HRR.

4. Conclusions

Results showed that intercalated and partially exfoliated polystyrene/clay nanocomposites were obtained depending on the swelling behavior of the organoclay in styrene. UL94 burning test showed that the burning rate was faster for the nanocomposites than for the virgin polystyrene and that during the burning of PS/organoclay nanocomposites, a char structure was formed and no dripping was observed, whereas during the burning of virgin PS specimen dripping of melted polystyrene in flame was constant.

It was also observed an increase of the higher decomposition temperature and an accentuated decrease on the peak of heat release of the nanocomposites when comparing to the virgin polymer. These results indicate that polystyrene/clay nanocomposite, either intercalated or partially exfoliated, reduced the flammability approximately at the same extent, although reduced the ignition resistance of the polystyrene.

Acknowledgements

The authors thank the financial support from CNPq – Conselho Nacional de Desenvolvimento Científico e Tecnológico, MCT/FNDCT/FINEP (Açoes Transversais: Nanocompósitos, 0.1.05.0547.00) and PETROBRÁS / CENPES (PD-01644).

References

[1] Fu X., Qutubuddin S.: Swelling behavior of organoclays in styrene and exfoliation in nanocomposites. Journal of Colloid Interface Science, **283**, 373–379 (2005).
DOI: 10.1016/j.jcis.2004.09.037

[2] Liauw C. M., Lees G. C., Rothon R. N., Wilkinson A. N., Limpanapittayatorn P.: Evaluation of an alternative modification route for layered silicates and synthesis of poly(styrene) layered silicate nanocomposites by *in-situ* suspension polymerisation. Composites Interfaces, **14**, 361–386 (2007).
DOI: 10.1163/156855407780452896

[3] Arioli R., Gonçalves O. H., Castellares L. G., Costa J. M., Araújo P. H. H., Machado R. A. F., Bolzan A.: Effect of foster swelling degree in polystyrene/clay nanocomposites obtained by in situ incorporation. Macromolecular Symposia, **245–246**, 337–342 (2006).
DOI: 10.1002/masy.200651346

[4] Fu X., Qutubuddin S.: Polymer-clay nanocomposites: Exfoliation of organophilic montmorillonite nanolayers in polystyrene. Polymer, **42**, 807–813 (2001).
DOI: 10.1016/S0032-3861(00)00385-2

[5] Fu X., Qutubuddin S.: Synthesis of polystyrene-clay nanocomposites. Materials Letters, **42**, 12–15 (2000).
DOI: 10.1016/S0167-577X(99)00151-2

[6] Doh J. G., Cho I.: Synthesis and properties of polystyrene-organoammonium montmorillonite hybrid. Polymer Bulletin, **41**, 511–518 (1998).
DOI: 10.1007/s002890050395

[7] Okamoto M., Morita S., Taguchi H., Kim Y. H., Kotaka T., Tateyama H.: Synthesis and structure of smectic clay/poly(methyl methacrylate) and clay/polystyrene nanocomposites via in situ intercalative polymerization. Polymer, **41**, 3887–3890 (2000).
DOI: 10.1016/S0032-3861(99)00655-2

[8] Weimer M. W., Chen H., Giannelis E. P., Sogah D. Y.: Direct synthesis of dispersed nanocomposites by in situ living free radical polymerization using a silicate-anchored initiator. Journal of the American Chemical Society, **121**, 1615–1616 (1999).
DOI: 10.1021/ja983751y

[9] Bottcher H., Hallensleben M. L., Nu S., Wurm H., Bauerb J., Behrens P.: Organic/inorganic hybrids by living/controlled ATRP grafting from layered silicates. Journal of Materials Chemistry, **12**, 1351–1354 (2002).
DOI: 10.1039/b110819k

[10] Zhu J., Morgan A. B., Lamelas F. J., Wilkie C. A.: Fire properties of polystyrene-clay nanocomposites. Chemistry of Materials, **13**, 3774–3780 (2001).
DOI: 10.1021/cm000984r

[11] Sen S., Nugay N., Nugay T.: Effects of the nature and combinations of solvents in the intercalation of clay with block copolymers on the properties of polymer nanocomposites. Journal of Applied Polymer Science, **112**, 52–63 (2009).
DOI: 10.1002/app.29389

[12] Chow W. S., Mohd Ishak Z. A.: Mechanical, morphological and rheological properties of polyamide 6/organo-montmorillonite nanocomposites. Express Polymer Letters, **1**, 77–83 (2007).
DOI: 10.3144/expresspolymlett.2007.14

[13] Sanchez-Olivares G., Sanchez-Solis A., Camino G., Manero O.: Study on the combustion behavior of high impact polystyrene nanocomposites produced by different extrusion processes. Express Polymer Letters, **2**, 569–578 (2008).
DOI: 10.3144/expresspolymlett.2008.69

[14] Gilman J. W., Jackson C. L., Morgan A. B., Harris R., Manias E., Giannelis E. P., Wuthenow M., Hilton D., Phillips S. H.: Flammability properties of polymer-layered-silicate nanocomposites. Polypropylene and polystyrene nanocomposites. Chemistry of Materials, **12**, 1866–1873 (2000).
DOI: 10.1021/cm0001760

[15] Bourbigot S., Vanderhart D. L., Gilman J. W., Bellayer S., Stretz H., Paul D. R.: Solid state NMR characterization and flammability of styrene-acrylonitrile copolymer montmorillonite nanocomposite. Polymer, **45**, 7627–7638 (2004).
DOI: 10.1016/j.polymer.2004.08.057

[16] Morgan A. B., Chu L-L., Harris J. D.: A flammability performance comparison between synthetic and natural clays in polystyrene nanocomposites. Fire and Materials, **29**, 213–229 (2005).
DOI: 10.1002/fam.881

[17] Bourbigot S., Gilman J. W., Wilkie C. A.: Kinetic analysis of the thermal degradation of polystyrene-montmorillonite nanocomposite. Polymer Degradation and Stability, **84**, 483–492 (2004).
DOI: 10.1016/j.polymdegradstab.2004.01.006

[18] Zheng X., Jiang D. D., Wang D., Wilkie C. A.: Flammability of styrenic polymer clay nanocomposites based on a methyl methacrylate oligomerically-modified clay. Polymer Degradation and Stability, **91**, 289–297 (2006).
DOI: 10.1016/j.polymdegradstab.2005.05.007

[19] Levchik S. V., Weil E. D.: New developments in flame retardancy of styrene thermoplastics and foams. Polymer International, **57**, 431–448 (2008).
DOI: 10.1002/pi.2282

[20] Marosi G., Anna P., Márton A., Bertalan G., Bóta A., Tóth A., Mohai M., Rácz I.: Flame-retarded polyolefin systems of controlled interphase. Polymers for Advanced Technologies, **13**, 1103–1111 (2002). DOI: 10.1002/pat.284

[21] Marosi G., Márton A., Szép A., Csontos I., Keszei S., Zimonyi E., Tóth A., Almeras X.: Fire retardancy effect of migration in polypropylene nanocomposites induced by modified interlayer. Polymer Degradation and Stability, **82**, 379–385 (2003). DOI: 10.1016/S0141-3910(03)00223-4

[22] Keszei S., Matkó Sz., Bertalan G., Anna P., Marosi G., Tóth A.: Progress in interface modifications: From compatibilization to adaptive and smart interphases. European Polymer Journal, **41**, 697–705 (2005). DOI: 10.1016/j.eurpolymj.2004.10.039

[23] UL-94: Test for flammability of plastic materials for parts in devices and appliances (2006).

[24] ASTM D635: Standard test method for rate of burning and/or extent and time of burning of plastics in a horizontal position (2006).

[25] ASTM E1354: Standard test method for heat and visible smoke release rates for materials and products using an oxygen consumption calorimeter (2004).

[26] Zanetti M., Camino G., Canavese D., Morgan A. B., Lamelas F. J., Wilkie C. A.: Fire retardant halogen-antimony-clay synergism in polypropylene layered silicate nanocomposites. Chemistry of Materials, **14**, 189–193 (2002). DOI: 10.1021/cm011124t

[27] Si M., Zaitsev V., Goldman M., Frenkel A., Peiffer D. G., Weil E. D., Sokolov J. C., Rafailovich M. H.: Self-extinguishing polymer/organoclay nanocomposites. Polymer Degradation and Stability, **92**, 86–93 (2007). DOI: 10.1016/j.polymdegradstab.2006.08.023

[28] Morgan A. B., Bundy M.: Cone calorimeter analysis of UL-94 V-rated plastics. Fire and Materials, **31**, 257–283 (2007). DOI: 10.1002/fam.937

[29] Manzi-Nshuti C., Hossenlopp J. M., Wilkie C. A.: Comparative study on the flammability of polyethylene modified with commercial fire retardants and a zinc aluminum oleate layered double hydroxide. Polymer Degradation and Stability, **94**, 782–788 (2009). DOI: 10.1016/j.polymdegradstab.2009.02.004

[30] Samyn F., Bourbigot S., Jama C., Bellayer S.: Fire retardancy of polymer clay nanocomposites: Is there an influence of the nanomorphology? Polymer Degradation and Stability, **93**, 2019–2024 (2008). DOI: 10.1016/j.polymdegradstab.2008.02.013

eXPRESS Polymer Letters Vol.4, No.8 (2010) 509–515
Available online at www.expresspolymlett.com
DOI: 10.3144/expresspolymlett.2010.64

A preliminary study of the incorparation of NPK fertilizer into chitosan nanoparticles

E. Corradini[1,3*], *M. R. de Moura*[2,3], *L. H. C. Mattoso*[3]

[1]Depto. de Engenharia de Materiais da UFSCar, CP 676, 13560-905 São Carlos, SP, Brazil
[2]IFSC, Universidade de São Paulo, CP 369, 13560-970, São Carlos SP, Brazil
[3]Laboratório Nacional de Nanotecnologia para o Agronegócio Embrapa/CNPDIA, CP 741, 13560-970, São Carlos, SP, Brazil

Received 10 February 2010; accepted in revised form 30 April 2010

Abstract. The use of slow release fertilizer has become a new trend to save fertilizer consumption and to minimize environmental pollution. Due to its polymeric cationic, biodegradable, bioabsorbable, and bactericidal characteristics, chitosan (CS) nanoparticle is an interesting material for use in controlled release systems. However, there are no attempts to explore the potential of chitosan nanoparticles as controlled release for NPK fertilizers. In this work chitosan nanoparticles were obtained by polymerizing methacrylic acid for the incorporation of NPK fertilizers. The interaction and stability of chitosan nanoparticle suspensions containing nitrogen (N), phosphorus (P) and potassium (K) were evaluated by FTIR spectroscopy, particle size analysis and zeta-potential. The FTIR results indicated the existence of electrostatic interactions between chitosan nanoparticles and the elements N, P and K. The stability of the CS-PMAA colloidal suspension was higher with the addition of nitrogen and potassium than with the addition of phosphorus, due to the higher anion charge from the calcium phosphate than the anion charges from the potassium chloride and urea. The mean diameter increase of the CS-PMAA nanoparticles in suspension with the addition of different compounds indicated that the elements are being aggregated on the surface of the chitosan nanoparticles.

Keywords: *nanomaterials, chitosan, NPK fertilizers, zeta potential*

1. Introduction

Fertilizers are chemical compounds applied to promote plant and fruit growth [1]. Fertilizers are usually applied either through the soil (for uptake by plant roots) or by foliar feeding (for uptake through leaves). Fertilizers can also be applied to aquatic environments, notably ocean fertilization. Artificial fertilizers are inorganic fertilizers formulated in appropriate concentrations and the combinations supply three main nutrients: nitrogen, phosphorus and potassium (N, P and K) for various crops and growing conditions. N (nitrogen) promotes leaf growth and forms proteins and chlorophyll. P (phosphorus) contributes to root, flower and fruit development. K (potassium) contributes to stem and root growth and the synthesis of proteins [2, 3].

However, about 40–70% of nitrogen, 80–90% of phosphorus, and 50–70% of potassium of the applied normal fertilizers is lost to the environment and cannot be absorbed by plants, causing not only substantial economic and resource losses but also very serious environmental pollution [4, 5]. Recently, the use of slow release fertilizers has become a new trend to save fertilizer consumption and to minimize environmental pollution [6, 7]. This brings out the idea of developing encapsulated fertilizers, in which NPK fertilizers are entrapped within nanoparticles [8]. Consequently, the fertiliz-

*Corresponding author, e-mail: elisangela@cnpdia.embrapa.br

ers are protected by the nanoparticles for better survival in inoculated soils, allowing for their controlled release into the soil [5]. Therefore, the method of encapsulation of fertilizers components in polymeric nanoparticles is relatively novel, with potential commercial applications.

Chitosan nanoparticles have been investigated as a carrier for drug delivery, although have been no attempts to explore the potential of chitosan nanoparticles as controlled release for NPK fertilizers. Chitosan (CS) is a polymer of particular interest in this area because it is biodegradable, bioabsorbable, and bactericidal [9, 10]. Due to its polymeric cationic characteristics, chitosan nanoparticles may interact with negatively charged molecules and polymers, showing a favorable interaction. The ability of controlling nanoparticle size is highly desirable for most applications in the field of nanotechnology [11].

In this work chitosan nanoparticles were obtained by polymerizing methacrylic acid for the incorporation of NPK fertilizers. The interaction and stability of chitosan nanoparticle suspensions containing N, P and K were evaluated by FTIR spectroscopy, particle size analysis and zeta-potential.

2. Experimental

2.1. Materials

Chitosan (CS) (MW 71.3 kDa, degree of deacetylation 94%) was purchased from Polymar Ciência e Nutrição S/A (Fortaleza, Brazil).

All reagents were of analytical grade. Potassium persulfate ($K_2S_2O_8$) and methacrylic acid (MAA) were purchased from Sigma-Aldrich Química Brasil Ltda (São Paulo, Brazil). Calcium phosphate $Ca(H_2PO_4)_2{\cdot}H_2O$, urea $CO(NH_2)_2$ and potassium chloride KCl were purchased from Synth-Labsynth Produtos para laboratórios Ltda (Diadema, SP, Brazil).

2.2. Preparation of CS-PMAA nanoparticles

The CS-PMAA nanoparticles were obtained by polymerization of MAA in CS solution in a two-step process [11]. In the first step, chitosan was dissolved in a 0.5% (v/v) methacrylic acid aqueous solution for 12 h under magnetic stirring. The CS concentration used in synthesis was 0.2% (w/v). In the second step, 0.2 mmol of $K_2S_2O_8$ was added to the solution with continued stirring, until the solution became clear. The polymerization was then carried out at 70°C under magnetic stirring for 1 h leading to the formation of CS-PMAA nanoparticles, which was then cooled in an ice bath.

2.3. Characterization of CS-PMAA nanoparticles

The zeta potential measurements and particle size distribution of CS nanoparticules were taken on a Zetasizer NanoZS (Malvern Instruments, Worcestershire, UK). The measurements were carried out after equilibrating the prepared samples at several pH values (2.0–12.0) at 25°C. All analyses were performed in triplicate.

The morphology and size of the CS-PMAA nanoparticles were investigated using a Philips CM200 transmission electron microscope (Philips Electronic Instruments, Mahwah, NJ, USA). CS-PMAA nanoparticle emulsions were sonicated for 2 min to produce better particle dispersion and to prevent the nanoparticle agglomeration on the copper grid. One drop of the nanoparticle emulsion was spread onto a carbon-coated copper grid and was then dried at room temperature for transmission electron microscopy (TEM) analysis. The sizes of the nanoparticles were determined directly from the figure using an Image-Pro Plus 4.5 software. The value is an average size of five parallels.

2.4. Incorporation of NPK fertilizer in chitosan nanoparticles

There are many types of commercial fertilizers that consist of mixing the substances containing nitrogen (N), phosphorus (P) and potassium (K) in different proportions. In this study, the sources of N, P and K used were urea, calcium phosphate, and potassium chloride, respectively. These substances were used separately.

The incorporation of NPK fertilizers in chitosan nanoparticles was obtained by dissolving different amounts of NPK into 50 ml of nanoparticle solution under magnetic stirring for 6 h at 25°C. The resulting solution to incorporate NPK into the nanoparticles presents this final concentration: i) 20, 40, 60, 80, 100, 200, 300, 400 and 500 ppm of N; ii) 10, 20, 30, 40, 50 and 60 ppm of P; iii) 20, 40, 60, 80, 100, 200, 300 and 400 ppm of K. The

maximum P solution concentration was of 60 ppm because the solution will precipitate at higher concentrations. The resulting solutions had a pH between 4.2 and 4.7

2.5. Characterization of the nanoparticles with NPK fertilizers

The zeta potential and particle size distribution measurements of CS-PMAA suspension nanoparticles with entrapment of NPK fertilizers in different concentrations were carried out in a Zetasizer NanoZS (Malvern Instruments, Worcestershire, UK) at pH of the resulting solutions and at 25°C.

2.6. FT-IR analysis

CS-PMAA nanoparticle suspensions with 500, 60 and 500 ppm of N, P and K, respectively were prepared as described in chapter 2.4. The nanoparticle suspensions with/without entrapment of NPK fertilizers were frozen by liquid nitrogen and lyophilized by a freeze drying system in order to obtain dried nanoparticles. FT-IR spectra were taken on a Perkin Elmer Spectrum model Paragon 1000 (Perkin-Elmer Life and Analytical Sciences, Inc., Waltham, MA USA), in the range of 4000 to 400 cm^{-1} to evaluate the chemical interaction between NPK fertilizers and CS nanoparticles. Powdered samples were prepared using KBr to form pellets.

3. Results and discussion

During the synthesis of chitosan nanoparticles, it was observed that the chitosan solution in methacrylic acid (MAA) changed from a clear to an opalescent suspension. This transformation is an evidence of the formation of chitosan nanoparticles with MAA. According to the mechanism proposed by Vasconcelos *et al*. [12], the formation of nanoparticles occurs via inter and intra-molecular linkages between PMAA carboxyl groups and amino groups of chitosan during the polimerization of MAA.

Figure 1 shows a transmission electron microscopy (TEM) image of the chitosan nanoparticles (CS-PMAA). The nanoparticles showed a spherical shape with a homogeneous size distribution. The mean diameter of the chitosan nanoparticles (in the dry state) was of approximately 78 ± 1.5 nm, which is higher in suspension due to the nanoparticles' swelling ability.

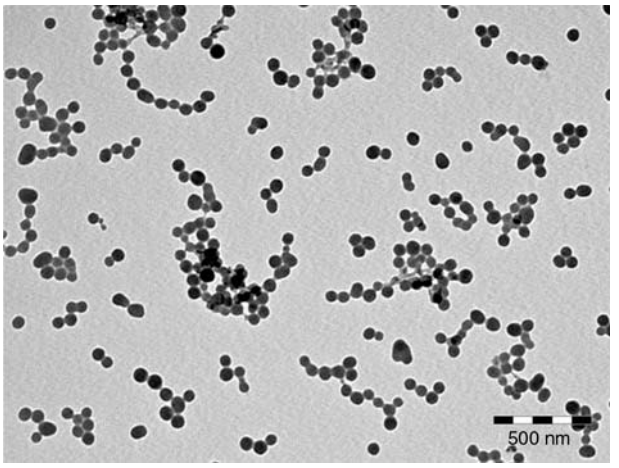

Figure 1. TEM microphotograph obtained for chitosan nanoparticles (CS-PMAA) at pH 4

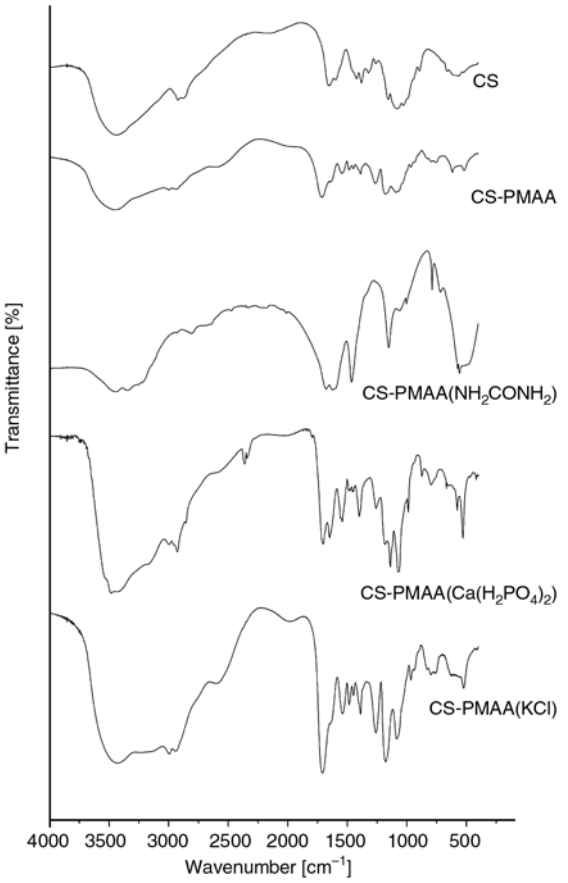

Figure 2. FT-IR transmitance spectra of raw chitosan (CS), chitosan nanopaticles (CS-PMAA) and nanoparticles with urea ($CS\text{-}PMAA(NH_2CONH_2)$), with calcium phosphate ($(CS\text{-}PMAA(Ca(H_2PO_4)_2 \cdot H_2O)$), and potassium chloride (CS-PMAA(KCl))

Figure 2 shows the FTIR spectra of pure chitosan (CS), of the CS-PMAA nanoparticles and of the nanoparticles loaded with urea (CS-PMAA

(NH_2CONH_2)), calcium phosphate (CS-PMAA ($Ca(H_2PO_4)_2{\cdot}H_2O$)) and potassium chloride (CS-PMAA (KCl)). The FTIR spectrum obtained for the chitosan (CS) has characteristic peaks: 3435 cm^{-1} corresponding to the stretching of the NH_2 and OH groups; 1649 cm^{-1} corresponding to the C=O group of amide I; 1083–1020 cm^{-1} due to the stretching of C–O and 620 cm^{-1}, due to vibrations of the pyranosidic rings [13]. It is observed that the band at 1649 cm^{-1}, characteristic of pure chitosan, disappears in the spectrum of the nanoparticles and two new bands appear at 1638 cm^{-1} (group $–COO^-$) and 1545 cm^{-1} (group $–NH_3^+$), indicating the interaction between PMAA and CS. The bands at 1703 and 1264 cm^{-1} (C=O) show the presence of PMAA in the nanoparticles [14].

Comparing the spectrum obtained for CS-PMAA with those obtained for the loaded nanoparticles (CS-PMAA(NH_2CONH_2)), (CS-PMAA($Ca(H_2PO_4)_2{\cdot}H_2O$), (CS-PMAA(KCl)), significant differences can be observed. However, the specific peak of the CS-PMAA nanoparticle appears in the spectra of loaded nanoparticles, hence suggesting that there was no change in the structure of the nanoparticles with the incorporation of N, P and K fertilizers. The main changes observed in the spectrum of the nanoparticles loaded with urea (CS-PMAA(NH_2CONH_2)), when compared to the spectrum of CS-PMAA, occurred at 1400–1500 cm^{-1} region. A strong peak is observed at 1400 cm^{-1} due to deformation of ammonium ions ($–NH_4^+$), which usually occurs at ca. 1500 cm^{-1} [15]. This shifting between the two peaks suggests some interaction between $–NH_4^+$ groups of urea and $–COO^-$ groups of CS-PMMA nanoparticles. For the nanoparticles loaded with calcium phosphate (CS-PMAA$Ca(H_2PO_4)_2{\cdot}H_2O$), the main change in the FTIR spectrum regarding the spectrum of the CS-PMAA nanoparticles, is the increase in the absorption intensity at 1547 cm^{-1}, indicating the interaction between the $–NH_3^+$ group of the chitosan nanoparticles and the $P_2PO_4^-$ and PO_4^{2-} groups of calcium phosphate. The appearance of two intense bands was also noted at about 530 and 1070 cm^{-1}, corresponding to the calcium phosphate grouping [16, 17] that was incorporated into the chitosan nanoparticles. The main change observed in the spectrum of the nanoparticles loaded with KCl occurred at about 1460 cm^{-1}, which is probably due to the interaction of the $–COO^-$ groups of chitosan nanoparticles with the potassium chloride K^+ groups.

Figure 3 illustrates the zeta potential as a function of the pH for the CS-PMAA nanoparticles. The variation of the zeta potential with the pH values is a consequence of the loading density changes on the nanoparticles' surface. The positive values of the zeta potential indicate that the CS-PMAA nanoparticles are positively loaded due to the cationic characteristics of chitosan in the pH range of 2 to 5.5. The isoelectric point of the system is at pH = 5.5, where the positive and negative charges are equal. It is an indication that at this pH the system has certain instability. At a pH greater than 5.5 negative zeta potential values are observed, indicating that the surface of the nanoparticles are negatively charged due to ionization of the carboxyl groups of PMAA and the neutralization of the $–NH_2$ groups of CS.

The stability of a colloidal dispersion is a consequence of the electrical double layer on the surface of the colloidal particles. The addition of an electrolyte to a colloidal dispersion suppresses the diffuse double layer and reduces the zeta potential. This drastically reduces the electrostatic repulsion between the particles and precipitates the colloid. The colloid is extremely sensitive to ions of opposite sign. A positively charged colloidal dispersion is precipitated by negative ions, these ions are incorporated into the fixed portion of the double layer, reducing the total charge of the particle. Similarly, a negatively charged colloidal dispersion will be destabilized by positive ions. The ion with

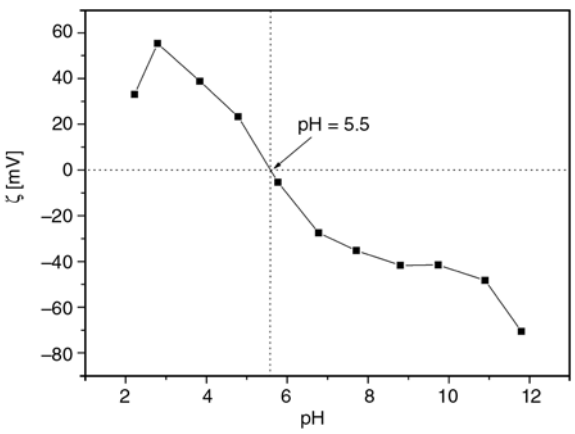

Figure 3. Dependence of zeta potential (ζ) on pH for chitosan nanoparticles (CS-PMAA)

the same charge of the colloidal particle has little effect on precipitation [18].

NPK fertilizer components (urea, calcium phosphate and potassium chloride) that were added to the CS-PMAA suspensions dissociate in aqueous acid solutions according to the reactions (1)–(3) below:

$$CO(NH_2)_{2\,(s)} + 2H^+_{(aq)} + 2H_2O_{(l)} \Leftrightarrow 2NH^+_{4\,(aq)} + H_2CO_{3\,(aq)} \quad (1)$$

$$KCl_{(s)} \Leftrightarrow K^+_{(aq)} + Cl^-_{(aq)} \quad (2)$$

$$Ca(H_2PO_4)_2{\cdot}H_2O_{(s)} \Leftrightarrow Ca^{+2}_{(aq)} + H_2PO^-_{4\,(aq)} + H_2O_{(l)} \quad (3a)$$

$$H_2PO^-_{4\,(aq)} \Leftrightarrow HPO^{-2}_{4\,(aq)} + H^+_{(aq)} \quad (3b)$$

The stability of colloidal suspension of the CS-PMAA nanoparticles at pH values lower than 5.5 is influenced by the presence of positive ions, since the colloidal suspension of CS-PMAA is positively charged. The precipitation of the colloidal suspension of CS-PMAA was observed with the addition of amounts greater than 400 ppm of N and K and amounts greater than 60 ppm of P. This difference is probably related to the greater charge of the anion $H_2PO_4^{2-}$ (from the electrolyte $Ca(H_2PO_4)_2{\cdot}H_2O$) compared to the anion Cl^- (from the electrolyte KCl), because the higher the ion charge, the higher the precipitation efficiency of the colloid.

Figures 4a, 4b and 4c show the zeta potential values and mean particle diameter due to the quantity of phosphorus, nitrogen and potassium, respectively (after 6 hours of mechanical agitation). The mean diameter of the CS-PMAA nanoparticles in suspension was of approximately 142 nm and increased with the addition of the different compounds. The maximum increase in the mean diameter was of 53% with the addition of 60 ppm of phosphorus, of 32% with 400 ppm of nitrogen and of 13% with the addition of 400 ppm of potassium. These values are probably related to the size of the species separated in the colloidal suspension, and the separated species from the KCl have a smaller volume than the separated species from the urea and calcium phosphate. It was found that for the colloidal dispersions of CS-PMAA with phosphorus, the zeta potential values (ζ) were not significantly altered with the addition of up to 60 ppm of phosphorus, indicating the stability of the colloidal system under the conditions studied.

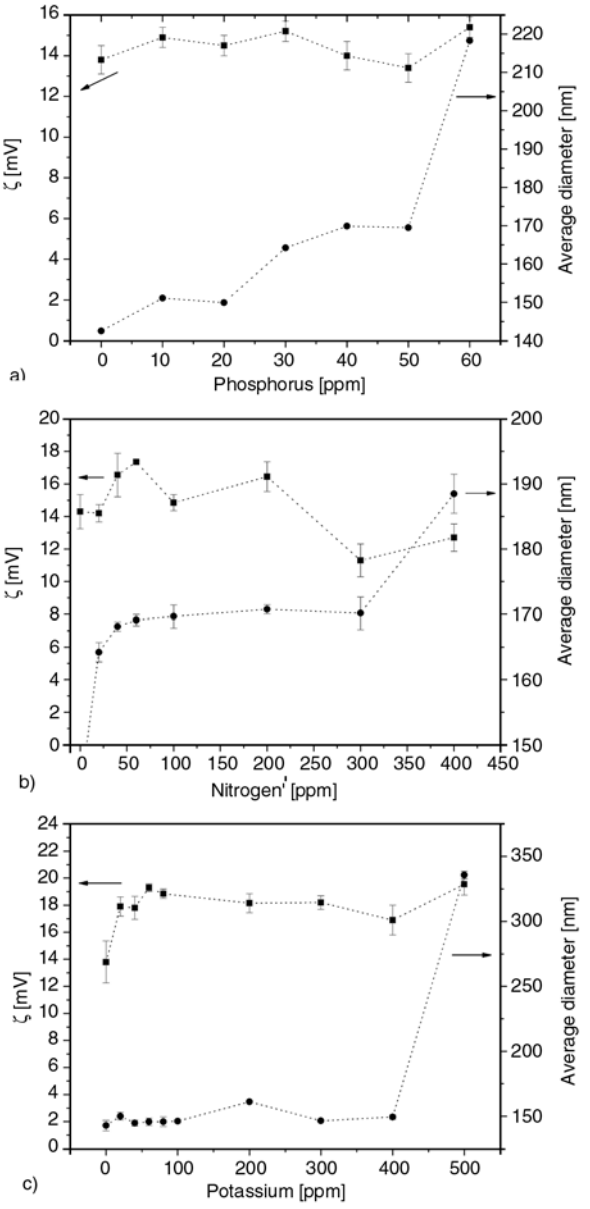

Figure 4. Zeta potencial (ζ) and average diameter [nm] for dispersion of chitosan (CS-PMAA) as a function of the amount of phosphorus (a), nitrogen (b) and potassium (c)

The ζ values of the dispersions of CS-PMAA loaded with up to 200 ppm of N were higher when compared to the ζ value of the dispersion of pure CS-PMAA and for the dispersions with higher amounts of N to 200 ppm, the values of ζ were lower. This indicates that above 200 ppm a suppression of positive charges is occurring in the colloidal dispersion of CS-PMAA, which must be due to the presence of negative groups from the urea molecules (NH_2CONH_2). For dispersions with potassium, the zeta potential showed an increase

with the addition of potassium of 20 to 80 ppm with respect to the dispersion of pure CS-PMAA, indicating an increase of positive charges in the colloidal dispersion and remaining almost constant with the addition of up to 400 ppm. This shows that the presence of the Cl^- ions (from KCl) did not affect the stability of colloidal dispersion with additions of up to 400 ppm and above this amount a decrease of positive charges occurred and consequently, the precipitation of the colloidal system.

4. Conclusions

The chitosan nanoparticles obtained showed spherical shapes and uniform sizes of approximately 78 nm in the TEM micrographs. The stability of the CS-PMAA colloidal suspension was influenced by the presence of the separated species from the urea, potassium chloride and calcium phosphate. The FTIR results indicated the existence of electrostatic interactions between $–COO^-$ and $–NH_3^+$ of the chitosan nanoparticles and the elements N, P and K present in the urea, calcium phosphate, potassium chloride, respectively. The stability of the CS-PMAA colloidal suspension was higher with the addition of nitrogen and potassium than with the addition of phosphorus, due to the higher anion charge from the calcium phosphate than the anion charges from the potassium chloride and urea. The mean diameter increase of the CS-PMAA nanoparticles in suspension with the addition of different compounds indicated that the elements are being aggregated on the surface of the chitosan nanoparticles. Further studies are needed to understand the mechanism and to optimize the incorporation of the N, P and K elements into the CS-PMAA nanoparticles.

Acknowledgements

The authors wish to thank the financial and technical support provided by CNPq, FINEP, FAPESP.

References

[1] Behera S. K., Panda R. K.: Integrated management of irrigation water and fertilizers for wheat crop using field experiments and simulation modeling. Agricultural Water Management, **96**, 1532–1540 (2009). DOI: 10.1016/j.agwat.2009.06.016

[2] Mandal K. G., Hati K. M., Misra A. K.: Biomass yield and energy analysis of soybean production in relation to fertilizer-NPK and organic manure. Biomass and Bioenergy, **33**, 1670–1679 (2009). DOI: 10.1016/j.biombioe.2009.08.010

[3] Gu Y. F., Zhang Z. P., Tu S. H., Lindström K.: Soil microbial biomass, crop yields, and bacterial community structure as affected by long-term fertilizer treatments under wheat-rice cropping. European Journal of Soil Biology, **45**, 239–246 (2009). DOI: 10.1016/j.ejsobi.2009.02.005

[4] Trenkel M. E.: Controlled-release and stabilized fertilizers in agriculture. International Fertilizer Industry Association, Paris (1997).

[5] Saigusa M.: Broadcast application versus band application of polyolefin-coated fertilizer on green peppers grown on andisol. Journal of Plant Nutrition, **23**, 1485–1493 (2000). DOI: 10.1080/01904160009382116

[6] Wu L., Liu M.: Preparation and properties of chitosan-coated NPK compound fertilizer with controlled-release and water-retention. Carbohydrate Polymers, **72**, 240–247 (2008). DOI: 10.1016/j.carbpol.2007.08.020

[7] Guo M. Y., Liu M. Z., Zhan F. L., Wu L.: Preparation and properties of a slow-release membrane-encapsulated urea fertilizer with superabsorbent and moisture preservation. Industrial and Engineering Chemistry Research, **44**, 4206–4211 (2005). DOI: 10.1021/ie0489406

[8] Teodorescu M., Lungu A., Stanescu P. O., Neamtu C.: Preparation and properties of novel slow-release NPK agrochemical formulations based on poly(acrylic acid) hydrogels and liquid fertilizer. Industrial and Engineering Chemistry Research, **48**, 6527–6534 (2009). DOI: 10.1021/ie900254b

[9] Coma V., Martial-Gros A., Garreau S., Copinet A., Salin F., Deschamps A.: Edible antimicrobial films based on chitosan matrix. Journal of Food Science, **67**, 1162–1169 (2002). DOI: 10.1111/j.1365-2621.2002.tb09470.x

[10] No H. K., Meyers S. P., Prinyawiwatkul W., Xu Z.: Applications of chitosan for improvement of quality and shelf life of foods: A review. Journal of Food Science, **72**, 87–100 (2007). DOI: 10.1111/j.1750-3841.2007.00383.x

[11] de Moura M. R., Aouada F. A., Mattoso L. H. C.: Preparation of chitosan nanoparticles using methacrylic acid. Journal of Colloid and Interface Science, **321**, 477–483 (2008). DOI: 10.1016/j.jcis.2008.02.006

[12] de Vasconcelos C. L., Bezerril P. M., dos Santos D. E. S., Dantas T. N. C., Pereira M. R., Fonseca J. L. C.: Effect of molecular weight and ionic strength on the formation of polyelectrolyte complexes based on poly(methacrylic acid) and chitosan. Biomacromolecules, **7**, 1245–1252 (2006). DOI: 10.1021/bm050963w

[13] Tonhi E., Plepis A. M. G.: Preparation and characterization of collagen-chitosan blends (in Portuguese). Química Nova, **25**, 943–948 (2002).
DOI: 10.1590/S0100-40422002000600011

[14] Azhgozhinova G. S., Güven O., Pekel N., Dubolazov A. V., Mun G. A., Nurkeeva Z. S.: Complex formation of linear poly(methacrylic acid) with uranyl ions in aqueous solutions. Journal of Colloid and Interface Science, **278**, 155–159 (2004).
DOI: 10.1016/j.jcis.2004.05.010

[15] Sterne E. J., Reynolds Jr. R. C., Zantop H.: Natural ammonium illites from black shales hosting a stratiform base metal deposit, Delong Montains, Northern Alaska. Clays and Clay Minerals, **30**, 161–166 (1982).

[16] Nordström E. G., Karlsson K. H.: Carbonate-doped hydroxyapatite. Journal of Materials Science: Materials in Medicine, **1**, 182–184 (1990).
DOI: 10.1007/BF00700880

[17] Kandori K., Yasukawa A., Ishikawa T.: Preparation and characterization of spherical calcium hydroxyapatite. Chemistry of Materials, **7**, 26–32 (1995).
DOI: 10.1021/cm00049a007

[18] Castellan G.: Fundamentals of physical-chemistry (in Portuguese). Livros Técnicos e Científicos Editora, Rio de Janeiro (1995).